5/1-1-92 JS(2)

PREPARED FOR THE U.S. DEPARTMENT OF ENERGY,
UNDER CONTRACT DE-AC02-76-CHO-3073

PPPL-2832
UC-426, 427

PPPL-2832

ION BERNSTEIN WAVE HEATING RESEARCH

BY

M. ONO

March, 1992

PRINCETON
PLASMA PHYSICS
LABORATORY

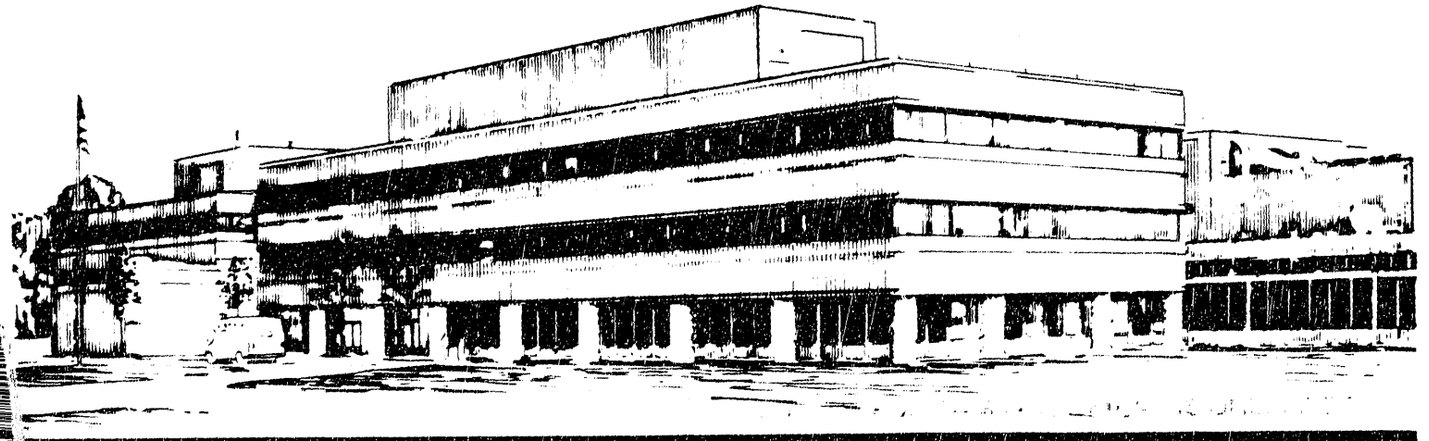

PRINCETON UNIVERSITY, PRINCETON, NEW JERSEY

NOTICE

NOTICE

PPPL--2832
DE92 009392

Ion Bernstein Wave Heating Research

Masayuki Ono

Princeton Plasma Physics Laboratory, Princeton University
Princeton, New Jersey 08543

Abstract

Ion Bernstein wave heating (IBWH) utilizes the ion Bernstein wave (IBW), a hot plasma wave, to carry the radio frequency (rf) power to heat tokamak reactor core. Earlier wave accessibility studies have shown that this finite-Larmor-radius (FLR) mode should penetrate into a hot dense reactor plasma core without significant attenuation. Moreover, the IBW's low phase velocity ($\omega / k_\perp \approx V_{Ti} << V_\alpha$) greatly reduces the otherwise serious wave absorption by the 3.5 MeV fusion α-particles. In addition, the property of IBW's that $k_\perp \rho_i \approx 1$ makes localized bulk ion heating possible at the ion cyclotron harmonic layers. Such bulk ion heating can prove useful in optimizing fusion reactivity. In another vein, with proper selection of parameters, IBW's can be made subject to strong localized electron Landau damping near the major ion cyclotron harmonic resonance layers. This property can be useful, for example, for rf current drive in the reactor plasma core.

IBW's can be excited with loop antennas or with a lower-hybrid like waveguide launcher at the plasma edge, the latter structure being one that is especially compatible with reactor application. In either case, the mode at the plasma edge is an electron plasma wave (EPW). Deeper in the plasma, the EPW is mode-transformed into an IBW. Such launching and mode-transformation of IBW's were first demonstrated in experiments in the ACT-1 plasma torus and in particle simulation calculations. These and other aspects of IBW heating physics have been investigated through a number of experiments performed on ACT-1, JIPPTII-U, TNT, PLT and Alcator-C. In these experiments both linear and nonlinear heating processes have been observed. Interestingly, improvement of plasma confinement was also observed in the PLT, Alcator-C, and JIPPTII-U experiments, opening up the possible use of IBW's for the active control of plasma transport. Two theoretical explanations have been proposed: one based on four-wave-mixing of IBW with low frequency turbulence, the other on the noninear generation of a velocity-shear layer. Both models are consistent with the observed threshold power level of a few hundred kW in the experiments.

Experiments on lower field plasmas on JFTII-M and DIII-D have raised some concern with the IBW wave-launching process. The experiments showed serious impurity release from the walls but little or no core heating, a combination of circumstances strongly suggestive of edge heating. Possible parasitic channels could include the excitation of short wavelength modes by the Faraday shield's fringing fields, antenna sheath-wave excitation, an axial convective loss channel, and nonlinear processes such as parametric instability and ponderomotive effects. Suggested remedies include changes in the antenna phasing, the use of low-Z insulators, operating at higher frequencies, positioning the plasma differently with respect to the antenna, eliminating the Faraday shields, and using a waveguide launcher. The recent JIPPTII-U experiment, employing a 0-π phased antenna array with a higher frequency 130 MHz source, demonstrated that those remedies can indeed work.

Looking to the future, one seeks additional ways in which IBWH can improve tokamak performance. The strong ponderomotive potential of the IBWH antenna may be used to stabilize external kinks and, acting as an rf limiter, to control the plasma edge. Control of the plasma pressure profile with local IBWH heating is already an important part of the PBX-M program in its exploration of the second-stability regime. Association with IBWH can improve the performance of neutral beam heating and also the efficiency and localization of lower hybrid current drive for current profile control. Used with pellet injection, IBWH may also prolong the period of good confinement. The three planned high-power IBWH experiments covering vastly different parameters (f = 40-80 MHz for PBX-M; f = 130 MHz for JIPPT-II-U; and f = 430 MHz for FT-U) appear to be well positioned to explore these possibilities and to clarify other issues including the physics of wave-launching and associated nonlinear processes.

Table of Contents

VII. On-going and Future IBWH experiments

7.1 JIPPT-II-U (130 MHz)

7.2 PBX-M (40-80 MHz)

7.3 FT-U (430 MHz)

7.4 Heating Burning Plasmas (200-250 MHz)

VII. Conclusions

I. INTRODUCTION

The developing of ion Bernstein wave heating(IBWH)[1-3] in the late 1970's owed much to prior research effort in radiofrequency plasma heating, especially ion cyclotron range of frequency heating (ICRF) and lower-hybrid wave heating (LHH). LHH experiments successfully demonstrated an efficient wave coupling using a phased waveguide system.[4,5] Fast wave ICRF heating experiments showed that ions can be heated efficiently at the ion cyclotron resonance layers.[6] The physics of mode-transformation process has become widely accepted, the process whereby a cold plasma wave, propagating through a nonuniform plasma, converts into a hot plasma wave due to the finite-Larmor-radius (FLR) effect.[7,8] Indeed, mode-conversion underlies the idea of launching the ion Bernstein wave (a FLR mode) via mode-transformation process of an externally launched electron plasma wave (the lower-hybrid wave).[1,2] This method for radio frequency plasma heating has been termed *ion Bernstein wave heating*, or IBWH. The three heating schemes (LHH, IBWH and ICRF) are compared in Fig. 1, where wavenumber is plotted as a function of plasma density.

An early question for IBWH concerned wave accessibility to the core of a hot dense reactor plasma. Ray tracing calculations in slab[1] and tokamak[2] geometry showed that the accessibility of IBW to the core can be excellent for a finite range of launched $n_{||}$. Since IBW wave energy is carried mainly by bulk ion motion, electric field related interactions such as electron Landau damping are relatively weak. From such considerations, it was concluded that IBWH possesses a number of features that are attractive for reactor application:

1. The polarization of IB waves at the antenna-plasma interface is similar to that for LHH and a similar waveguide coupler can be employed for IBWH. The waveguide coupler fits neatly between toroidal field coils and is compatible with the requirements for heating tokamak reactors (Fig. 2).

2. Like ICRF, IBWH utilizes efficient and relatively inexpensive rf transmitters operating in the ion cyclotron range of frequencies. And IBW heat is deposited onto the well-defined ion cyclotron harmonic resonance layers in the plasma interior.

3. Characterized by a relatively slow wave phase velocity, $\omega/k_{\perp} \approx V_{Ti}$, IB waves interact with bulk ions and can put rf power directly into the ions without generating runaway ion tails (Sec. 3.3.4). This bulk ion heating property may help in optimizing

fusion reactivity. Similarly, due to its short wavelength nature, $\lambda_\perp \approx \rho_i$, IBWH can heat even at relatively high harmonic resonances (3.3.4).

4. The good accessibility of IBW in hot dense plasmas appears to hold for a range of launched $n_{||}$. Also, calculations indicates that absorption of IB waves by the fusion α-particles can be avoided by using tritium heating scenarios (Sec. 3.3.6). This property may make IBW a good candidate for driving currents in the central region of burning plasmas (Sec. 5.1)

Some concern has been raised with respect to possible deleterious effects on wave accessibility due to impurity harmonic absorption,[3] absorption by fusion alphas,[9] and wave scattering by low frequency turbulence.[10] These effects although not completely negligible, have been shown to be relatively weak for typical reactor parameters.[11,12] To facilitate the analyses of experimental results as well as to plan for the future experiments, tokamak IBWH modeling codes have been also developed.[13-15] These codes combine the tokamak ray-tracing codes with tokamak plasma transport codes.

Another powerful tool for investigating the basic physics of IBWH has been computer particle simulation.[16-18] External launching, mode-transformation, absorption, and ion heating were all investigated, and non-linear heating at $3\Omega_i / 2$ was discovered in this way.[16] From those basic physics investigations, it was concluded that the IBWH concept looked attractive enough to move on to the tokamak heating experiments.

Turning now to pertinent experiments, the first external launching of IBW via mode-transformation process was verified in an ACT-1 hydrogen plasma.[19] In subsequent ACT-1 experiments, external IBW launching at various harmonics,[20] absorption of IBW and bulk ion heating at various ion cyclotron harmonic layers[21] were confirmed. CO_2 laser scattering was used successfully for the first time to detect the launched IBW on ACT-1.[22]

The first tokamak IBWH experiment was carried out on the JIPPT-II-U tokamak device[23]. A B_θ-type ICRF loop antenna, termed Nagoya Type-III antenna,[24] was used to couple the rf power into IBW, and excellent central ion heating was observed at the $3\Omega_H/2$ layers.[23,25] Efficient electron heating regime was also observed.[26] On the Princeton Large Torus (PLT), a series of IBWH experiments were performed where various heating regimes were identified including $5\Omega_D$-minority, 3/2 Ω_D-majority and ^{3}He-minority regimes.[27-31] The efficiency of

IBWH ion heating was found to be comparable to that of ICRF, and the PLT central ions were heated from ≈ 500 eV to 2 keV with IBWH.[30] Under high power IBWH, plasma confinement showed actual improvement which also correlated with a significant reduction in the microturbulence in the half-radius region of the plasma. This improved confinement could be related to the stabilization of microinstabilities by IBWH through non-linear wave interactions.[32,33] On Alcator C, the IBWH was performed in the high density, high field regimes.[34-37] A CO_2 scattering system was used successfully to detect the launched IBW.[34] Good ion heating was observed for various heating regimes.[35,36] Improved particle confinement regime during IBWH was also confirmed.[35] However, above the density of 2 x $10^{14}cm^{-3}$, the efficiency of ion heating was found to drop .[35] This drop has been attributed to the enhanced ion energy loss that appears in the high density regime.[37] On a smaller tokamak, TNT, IBWH was also investigated, yielding detailed informative results on antenna loading, wave fields, and plasma heating. [38,40] More recently, IBWH has been tested in the relatively low field, diverted plasmas of JFT-II-M[41] and DIIID[42]. In these experiments, very little central IBWH heating was observed. On DIIID, the measured antenna loading was much larger than the theoretical value assuming a direct IBW coupling.[43] Moreover, the observed loading was relatively insensitive to the magnetic field. Similar loading behavior was found in the PBX-M experiment.[44] The observed loading can be explained if the antenna is coupling to the electron plasma wave.[44,45] It was noted that in the low frequency IBWH experiment, the antenna rf ponderomotive potential can be quite large that one can expect a significant plasma density reduction in front of the antenna.[46,47] One might note that a similar problem was also investigated for the lower-hybrid wave case.[48,49] Indeed, the effect of ponderomotive density depletion on IBWH antenna coupling was observed previously in ACT-1.[50] The ponderomotive density depletion in DIIID was confirmed by the measurements of the antenna loading as a function of rf power.[51] Therefore, it appears that the measured antenna loading and the calculated values are now in a reasonable agreement.[52,53] Nevertheless, the source of the observed heating inefficiency (parasitic channels) remains to be an important topic for IBWH.

Theoretical models to explain possible parasitic channels include the excitation of short wavelength modes by the Faraday shield's fringing fields,[54] antenna sheath wave excitation,[55] an axial convective loss channel[56] and a variety of non-linear processes such as parametric instabilities and ponderomotive effects.[47,51] Remedies have also been suggested. In general, going toward higher frequency has a beneficial effect on reducing the antenna ponderomotive potential. Higher frequencies also provide better electron plasma wave launching conditions. Antenna changes such as the $n_{||}$-spectrum control (phasing to eliminate long wavelength

component), choice of antenna-limiter materials to reduce impurity problems, etc., should also reduce parasitic effects. Operationally, it has been found that the antenna position relative to the plasma must be carefully controlled in order to optimize the wave launching. IBWH performance is expected to improve as we move toward higher frequency waveguide experiments such as on FT-U[57] and on BPX.[58] The advantage of higher frequency and improved antenna design has been already observed in JIPPT-II-U where $3\Omega_H$ heating at 130 MHz has produced good ion and electron heating results as well as plasma confinement improvements.[59,60] On the other hand, the strong ponderomotive force exerted by the IBWH antenna might be used productively to stabilize the deleterious external modes such as the ballooning modes[61] and the external kinks[62] and to modify the plasma edge to control the power flow into the divertor plates.[63] The multi-megawatt high power IBWH experiment is being prepared on PBX-M to investigate the possibility of pressure profile control by localized heating as well as various non-heating applications of IBWH.[52]

Synergy among various tools has received a considerable interest in recent years. Interesting possibility exists for IBWH as well. JIPPT-II-U, it was shown that an injection IBWH improves the quality of the NBI heated plasmas through confinement improvements.[59,60] Localized electron Landau heating by IBWH can be used to improve lower-hybrid current drive (LHCD) localization and efficiency. The improved particle confinement property of IBWH may be used to improve the performance of pellet injection. These synergistic effects will be tested on JIPPT-II-U, PBX-M and FT-U.

Therefore, the unique wave property of IBW offers many possible applications for improving the tokamak concept. The plan for this review is as follows: In Sec. II, the basic properties and the background of IBWH are reviewed. First, the linear theory of IBWH is summarized including mode-transformation process covering the ACT-1 experiment and particle simulation. In Sec. II, wave power flow, linear and non-linear absorption processes, and wave accessibility question using ray tracing technique are discussed. Tokamak IBWH simulation modelling work are also described. Then the antenna coupling physics are summarized in Sec. IV with an emphasis on the plasma edge conditions. Due to the importance to the high power IBWH experiments, some of the possible deleterious processes which can occur near the plasma edge are discussed in some detail. In Sec V, possible non-heating applications of IBWH such as rf current drive, tokamak plasma confinement improvement, ponderomotive force mode stabilization, and rf limiter concept are also presented. Section VI is devoted to the experimental activities on IBWH starting with the basic physics experiments performed on ACT-1 device, then covering the highlights of high power

IBWH experiments, roughly in a chronological order, including experiments on JIPPT-II-U, TNT, PLT, Alcator C, JFT-II-M, and DIII-D. In Sec. VII, a brief status of the on-going experimental results and future experimental plans is given for JIPPT-II-U (130 MHz), PBX-M, FT-U. A possible experiment on ignition-grade tokamak is also discussed. Finally, a summary is given in Sec. VII for the future IBWH research topics and remaining IBWH related issues.

II. BASIC ION BERNSTEIN WAVE PROPERTIES

2.1 Wave Dispersion Relations

The finite-Larmor-radius IBW wave formalism was established in 1960's by I. Bernstein.[64] The generalized IBW dispersion relation was later given by T.H. Stix.[65] For ion Bernstein wave heating, a relevant wave dispersion relation can be written as,[66]

$$K_{xx} = - \frac{|K_{xy}|^2}{n^2} - \frac{n_{||}^2 K_{zz}}{(n_\perp^2 - K_{zz})} \qquad (2\text{-}1)$$

where K_{xx}, K_{xy}, and K_{zz} are elements of the plasma dielectric tensor which in a non-drifting Maxwellian plasma can be expressed as[65]

$$K_{xx} = 1 + \frac{\omega_{pe}^2}{\Omega_e^2} + \sum_i \frac{\omega_{pi}^2}{\omega k_{||} V_i} \frac{\exp(-b_i)}{b_i} \sum_{n=1}^{\infty} n^2 I_n (Z_n + Z_{-n}),$$

$$K_{xy} = -i \frac{\omega_{pe}^2}{\omega\Omega_e^2} + i \sum_i \frac{\omega_{pi}^2}{\omega k_{||} V_i} \exp(-b_i) \sum_{n=1}^{\infty} n (I_n - I_n')(Z_n - Z_{-n}),$$

$$K_{zz} = 1 + 2\omega_{pe}^2 / k_{||}^2 V_e^2 \ (1 + \xi_{e0} Z_0),$$

where the summation i is over ion species, n is the harmonic number, Z_n is the plasma dispersion function of argument $\xi_{\sigma n} \equiv (\omega + n \Omega_\sigma) / k_{||} V_\sigma$, σ denotes species, $V_\sigma \equiv (T_\sigma/m_\sigma)^{1/2}$ and I_n is the modified Bessel function of argument $b_i \equiv k_\perp^2 T_i / m_i \Omega_i^2$. Here $n_\perp \equiv c\, k_\perp/\omega$ and $n_{||} \equiv ck_{||}/\omega$. In Fig. 3 (a), the perpendicular wavenumber was calculated from the dispersion relation of Eq. (2-1) as a function of the plasma density for various values of the normalized frequency (ω/Ω_i). It is convenient to consider Eq.(2-1) in terms of three different regimes: I - Electron Plasma Wave Regime (EPW); II - Electrostatic Ion Bernstein Wave Regime (ESIBW); and III - Finite-β Ion Bernstein Wave Regime. We shall now consider those three regimes separately. In Fig. 2, those different regimes are shown for a cross section of a reactor-grade plasma.

I. EPW Regime - In a low-β plasma where $n_\perp^2 >> |K_{xy}|^2$, Eq.(2-1) reduces to the usual electrostatic form,

$$n_\perp^2 K_{xx} + (n_{||}^2 - K_{xx}) K_{zz} = 0 . \qquad (2\text{-}2)$$

Equation (2-2) is relevant for describing the physics of the plasma edge region, near the antenna. In a very low density regime where $\omega > \omega_{pi}$ and $K_{zz} \approx 1 - \omega_{pe}^2/\omega^2$, the dispersion relation becomes that of the well-known electron plasma wave,[67]

$$n_\perp^2 = (\omega_{pe}^2/\omega^2 - 1) \ (n_{||}^2 - 1) \ . \qquad (2\text{-}3)$$

This dispersion relation has been investigated in detail for lower-hybrid wave heating and it is relevant for describing the IBW plasma-antenna interface.

II. ESIBW Regime - For the intermediate densities where $\omega \leq \omega_{pi}$, because of the finite-Larmor-radius effect, the wave dispersion becomes that of the electrostatic ion Bernstein wave (ESIBW). As can be seen in Fig. 3(a), the wave is already insensitive to the plasma density. One may note that for $K_{zz} \approx - \omega_{pe}^2/\omega^2$, the only propagating solutions of Eq.(2-2) are when K_{xx} is positive. Equation (2-2) has been investigated theoretically by Swanson.[68] In the limit of $n_{||} \to 0$, the electron term drops from the dispersion relation all together and the wave becomes the so-called "pure" ion Bernstein wave where the wave oscillation is sustained by the ion-Larmor-radius dynamics alone. In this limit the wave dispersion relation is simply $K_{xx} = 0$. J. Schmitt was able to observe this wave in a cesium plasma by using a wire-exciter which was strung carefully along the magnetic field line in order to satisfy the $n_{||} \approx 0$ condition.[69] Using a hydrogen plasma, a detailed IBW dispersion relation of Eq.(2-2) has been measured in the ACT-1 toroidal device. In Fig. 4(a), the measured wave interferogram is shown as a function of the normalized frequency, ω/Ω_H. The wave exhibits a cut-off behavior ($\lambda \to \infty$) for $\omega \to 2\Omega_H$. In Fig. 4(b), the wave interferometer is shown as a function of the phase shift where the wave phase front moves toward the antenna (while the wave packet is moving away from the antenna), confirming the backward propagating nature of IBW. The resulting dispersion relation is plotted in Fig. 4(c). The solid curves are the theoretical values, Eq. (2-2), for various ion temperatures. The agreement is best for the T_i=1.5 eV. This type of measurement could therefore yield the hydrogen bulk ion temperature information.[22] More complete IBW dispersion relation is shown in Fig. 5. The CO_2 scattering data points are shown by the circles which agrees well with the probe data (solid triangles). Due to the

presence of deuterium-like and tritium-like hydrogen molecular ions, the dispersion relation has correspondingly many branches.

III. Finite-β IBW Regime - Moving on to the hotter plasma interior, one must consider the effect of finite β. This occurs when $|K_{zz}|$ becomes larger than $n_\perp^2$, and for a $T_e \approx T_i$ plasma, this condition is equivalent to

$$\beta\,(\%) \; > \; 0.4 \; (b_i / m_i) \tag{2-4}$$

$b_i \equiv k_\perp^2 \rho_i^2$, m_i is the ion mass number, and β is the plasma beta in %. For $|K_{zz}| >> n_\perp^2$, Eq.(2-1) takes on the form,

$$K_{xx} \; = \; n_{||}^2 \; - \; |K_{xy}|^2 / n^2 \, . \tag{2-5}$$

In this regime, the real part of the dispersion relation still remains ESIBW-like, $K_{xx} \approx 0$. However, as we shall discuss it later, due to the absence of the electron term in Eq.(2-5), the electron Landau damping becomes small for IBW in this finite-β limit. This property greatly improves the IBW accessibility to the hot-dense reactor grade plasmas. In Fig. 2, a poloidal cross-sectional view of various wave regimes are shown for a typical reactor-like parameters. One should note here that near the resonance layer, due to increasing $n_\perp$, the wave again regains its electrostatic nature (which also increases electron Landau damping). In the figure, the IBW and fast wave dispersion relations for the mid-plane are shown for comparison.

2.2. Mode-Transformation Process

2.2.1 Basic Theory

Mode-transformation process describes a process where a plasma wave, as it propagates in a non-uniform plasma, due to a change in the plasma parameters (e.g. density or magnetic field gradient), undergoes an intact transition into another type of wave. This process in constrast to the well known mode-conversion processes[7,8], does not have the wave singularities in the transition region. Therefore by utilizing this process, one can excite a desired wave with good efficiency by actually exciting another type of wave which is perhaps easier to be launched by an external antenna. For IBW heating, one can use this mode-transformation process to convert a launched electron plasma wave into the ion Bernstein wave which theoretically has a better wave accessibility property to hot-dense plasma core.[1,2] This smooth transition between the EPW and ESIBW Regimes can be seen in Fig. 1 and 3(a). In

order to illuminate the physics of mode-transformation, it is instructive to expand terms in Eq.(2-2) for small $b_i \equiv (k_\perp \rho_i)^2$, a good approximation for $\omega \approx 2\,\Omega_i$, into the following quadratic form:

$$A\, n_\perp^4 + B\, n_\perp^2 - C = 0 \qquad (2\text{-}6)$$

where

$$A = \Sigma_i\, 3\, \omega_{pi}^2\, (T_i / M_i)\, (4\,\Omega_i^2 - \omega^2)^{-1}\, (\omega^2 - \Omega_i^2)^{-1}$$

$$B = 1 - \Sigma_i\, \omega_{pi}^2 / (\omega^2 - \Omega_i^2)$$

$$C = k_{||}^2\, \omega_{pe}^2 / \omega^2$$

The coefficients A, B, and C represent the finite-Larmour-radius (ion thermal) correction term, the cold ion term, and the cold electron term, respectively. The propagating root of Eq.(2-6) can be written trivially as

$$k_\perp^2 \approx \frac{-B + (B^2 + 4AC)^{1/2}}{2A} \qquad (2\text{-}7)$$

For $\Omega_i < \omega < 2\,\Omega_i$, A is positive, and one can see a continuous evolution of wave dispersion relation ($k_\perp^2 > 0$) from the low density electron plasma wave (EPW) regime where $B \approx 1$ (i.e., $k_\perp^2 \approx C/B$) to the higher density ($\omega < \omega_{pi}$) ion Bernstein wave (IBW) regime where $B << 0$ (i.e., $k_\perp^2 > |B|/A$). This behavior is illustratred in Fig. 6(a) where the wavenumber is plotted as a function of the plasma position in which the density is increasing away from the antenna. The cold plasma resonance disappears for a finite ion temperature (T_i = 1.5 eV in the ACT-1 parameter). The corresponding ray trajectory is shown in Fig. 6(b). One can also show that this mode-transformation occurs even for the higher harmonic launching case provided that ion temperatures are sufficiently high in the transformation region near $\omega \approx \omega_{pi}$. In general, one finds that for the n-th harmonic launching case, due to the increased $k_\perp \rho_i$ values, the required T_i for a smooth transformation goes up as $10^{(n/2-1)}$ in the transformation region.[20] For the lower-hybrid wave ($\omega >> \Omega_i$), the term A in Eq. (2-6) becomes negative which results in the mode-conversion behavior where the double conversion process connects EPW with IBW as illustrated in Fig. 1.

<u>$2\,\Omega_D$ Launching Case</u> - The physics of IBW launching changes significantly for the $2\Omega_D$ launching case, where the presence of even a small concentration of hydrogen could cause a significant change in the deuterium IBW dispersion relation. This case arises for the $\Omega(^3He)$, 2

Ω_T or 3/2 Ω_D heating in deuterium majority and/or deuterium-tritium plasmas. One can illuminate this effect by examining the term 'B' in Eq.(2-6) by writing,

$$B = 1 + \omega_{pH}^2/(\Omega_H^2 - \omega^2) - \Sigma_{i\neq H}\, \omega_{pi}^2 / (\omega^2-\Omega_i^2) \qquad (2\text{-}8)$$

where subscript H denotes the hydrogen. As one can see that the mode-transformation (B≈0) could take place at the ion-ion hybrid resonance frequency Ω_{IH} in addition to the usual ion plasma frequency. Between Ω_H and Ω_{IH}, there is a new mode called the cold electrostatic ion cyclotron wave (CESICW).[70] One should note that the smooth mode-transformation among EPW, CESICW, and IBW could takes place here since the CESICW is also a backward propagating mode, same as EPW and IBW. Therefore, it is also possible to couple directly to CESICW (instead of EPW) and then mode-transform into IBW at the ion-ion hybrid resonance frequency. This type of launching using CESICW might be advantageous particularly for the low-frequency launching regime since the mode is relatively density independent (unlike EPW). The PLT $3/2\Omega_D$ heating was a unique example of IBWH working in this regime.

2.2.2 Mode-Transformation Experiments in ACT-1

The EPW-IBW mode-transformation process has been confirmed and investigated in detail in ACT-1.[19,20] In ACT-1, by changing the neutral pressure, the ion temperature can be varied over a wide range (1/40 eV to 2 eV), and Fig. 7(a) shows the interferogram output for several neutral pressures as labeled. For the high-pressure case, the ions are essentially cold that the excited wave is EPW which stays near the plasma edge, in the low density side of the cold plasma resonance or the lower-hybrid resonance [as shown for the $T_i \approx 0$ case in Fig. 6(b)]. As the neutral pressure is reduced (T_i increased), a gradual transformation into ion Bernstein wave is observed. In Fig.7(b), the measured wave number (shown as dots) is plotted as a function of the radial position in the low-pressure warm-ion plasma. The solid curve is obtained from Eq. (2.2) for $T_i = 1.5$ eV, and the dashed curve is for $T_i = 0$. As expected, no sign of discontinuity near the cold plasma resonance was observed in the experiment as long as the plasma ion temperature was sufficiently high ($T_i \geq 0.5$ eV).

The transition from the electron plasma wave ($\omega > \omega_{pi}$) to ion Bernstein wave ($\omega < \omega_{pi}$) can be also seen clearly in Fig. 8 (a) where the wave packet amplitude (heavier curve) and interferogram output (lighter curve) are shown for various central plasma densities (as labeled).

The higher central density means greater density gradient. In the figure, the radial position of the cold lower-hybrid resonance layer which separates the EPW and IBW regimes is indicated by a dashed curve. One can see that the wave transition between the two regimes is quite smooth. It is also worthwhile to note that in this experiment, the ion Bernstein wave is launched effectively even when the plasma density is raised so that the ω_{pi} layer essentially reaches the limiter radius and approaches within a few millimeters of the antenna surface. In Fig. 8(b), using corresponding plasma parameters, the expected ray positions obtained from ray-tracing calculations are shown for various $\lambda_{||}$ (as labeled). One can see that the wavepacket position follows the ray position for $\lambda_{||} \cong 36$ cm (which is the dominant launched $\lambda_{||}$ in the experiment).

A similar launching at the third ion cyclotron harmonic has been also demonstrated in ACT-1. In Fig. 9(a), the measured wave dispersion relation of the excited IBW is shown by the dots. The calculated values are shown by the solid curves for various values of ion temperature. In Fig. 9(b), the measured wavenumber is plotted as a function of the plasma position (dots). As in Fig. 7(b), the theoretical values for $T_i = 2$ eV and $T_i = 0$ eV are shown. Again, a smooth mode-transformation could be seen across the cold LH resonance layer in a good agreement with theory. In this third harmonic launching case, a higher ion temperature ($T_i \approx 2$ eV) was required for the efficient IBW launching.

2.2.3 Particle Simulation of IBWH

Since IBW is a kinetic wave which propagates due to the ion-Larmor-radius effect and its detailed kinetic properties are difficult to tract mathematically, the particle simulation technique provides a particularly useful tool to investigate the physics of IBWH.[19-21] The physics of wave excitation, mode-transformation, propagation, absorption, and heating are investigated for both a single and muti-ion species plasmas for the $2\Omega_H$ launching with $3/2\Omega_H$ and $3\Omega_D$ heating. A typical wave potential interferograms are shown in Fig. 10(a). The wave is excited (in this case) in a pure hydrogen plasma at $\omega \approx 1.9\ \Omega_H$ by an antenna located at the left side and the wave is absorbed at the right hand side by the cyclotron damping at $\omega \approx \Omega_i$. This strong ion cyclotron absorption region at $\omega \approx \Omega_i$ provides a nice absorption layer to prevent the wave reflections which would considerably complicate the simulation picture. The corresponding perpendicular wave electric field is plotted in Fig. 10 (b). In Fig. 10(c), the measured perpendicular wave number is plotted with the real part as circles and the imaginary part as rhombuses. The calculated linear dispersion relation is indicated with the real part by the solid curve and the imaginary part as the dashed curve, showing an excellent agreement. One

unexpected result is the absorption at 3/2 Ω_H harmonic frequency indicated by the arrow. In simulation, due to the short system scale length, the absorption appears to be small, but when this result is scaled to the tokamak experiments, the absorption can be quite strong (approaching 100%!). This non-linear heating will be discussed in Sec. 3.4.1. Similarly, the $3\Omega_H$ launching case with $5/2\Omega_H$ and $5\Omega_D$ heating case was also investigated with this technique yielding a generally a good agreement with the linear theory.

III. WAVE POWER FLOW, ABSORPTION & ACCESSIBILITY

3.1 Wave Power Flow

Unlike cold plasma waves, the IBW energy flux is mainly carried by the non-electromagnetic energy flux term due to the coherent motion of ions in the wave fields. From Reference 65, one can show that the dominant perpendicular energy flux term T is

$$T = (\omega / k_\perp) \cdot (|E_\perp|^2 / 16\pi) \cdot (k_\perp \partial K_{xx} / \partial k_\perp) . \qquad (3\text{-}1)$$

Since the term, $(k_\perp \partial K_{xx} / \partial k_\perp)$, is typically 10^2 - 10^3, this kinetic term dominates over the usual Poynting flux. Similarly, the energy density is given by

$$W_0 = (|E_\perp|^2 / 16\pi) \cdot (\omega \partial K_{xx} / \partial \omega) . \qquad (3\text{-}2)$$

Again, the term, $(\omega \partial K_{xx} / \partial \omega)$, is typically 10^2 - 10^3 inside fusion plasmas. This makes the IBW energy density rather "dense" compared to other electrostatic waves for a given wave electric field. This kinetic property of IBW makes the wave not as susceptible to processes which could occur through the wave electric fields such as the electron Landau damping, parametric instabilities, wave-wave scattering, etc.

The perpendicular wave group velocity is the ratio of the perpendicular energy flux and the energy density which can be given by

$$V_{g\perp} = T / W_0 = (\omega / k_\perp) (k_\perp \partial K_{xx} / \partial k_\perp) / (\omega \partial K_{xx} / \partial \omega) . \qquad (3.3)$$

From Eq. (3-3), it can be shown that the perpendicular wave group velocity is roughly proportional to the ion thermal velocity, i.e., $V_{g\perp} \approx \omega / k_\perp \approx \Omega_i / k_\perp \approx (\Omega_i \rho_i)/(k_\perp \rho_i) \approx V_{Ti}$.

In calculating the wave packet trajectory (wave power flow direction), it is often convenient to calculate a quantity $V_{g\perp} / V_{g\parallel} \equiv \tan\theta$. Using Eq. (2-1), one can readily find that

$$\tan\theta \approx \frac{k_\parallel}{k_\perp} \frac{\partial K_{xx}}{\partial k_\perp} \frac{k_\perp}{} \frac{n_\perp^2 - K_{zz}}{n_\parallel^2 K_{zz}} \propto \lambda_\parallel V_{Ti} \qquad (3\text{-}4)$$

The wavepacket propagates more directly radially inward for higher ion thermal velocity and parallel wavelength. Therefore, unlike EPW which has the 'resonant cone' behavior (the propagation angle θ is same for all $\lambda_{||}$), the IBW wavepacket is dispersive. This behavior can be readily seen in Fig. 8.

3.2. Linear Absorption Processes of Ion Bernstein Waves

In this section, we shall briefly review various linear absorption processes relevant for IBW in fusion plasmas.

3.2.1 Electron Landau Damping

The electron Landau damping is an important absorption mechanism in hot reactor plasmas, and it could indeed perform a beneficial role of heating electrons. However, an excessive damping could also prevent the wave to reach the hot fusion plasma core. This is a serious problem facing the electrostatic wave based heating schemes such as LHH. Moreover, if the direct ion heating is a desired option, then the electron Landau damping must be minimized. From Eq.(2-1), the damping can be derived as

$$\mathrm{Im}\, k_\perp (\mathrm{ELD}) \approx k_\perp \frac{n_\perp^2 \; n_{||}^2 \; \mathrm{Im}\, K_{zz}}{|n_\perp^2 - K_{zz}|^2 |k_\perp \partial K_{xx} / \partial k_\perp|} \quad . \tag{3-5}$$

In the finite β region ($K_{zz} > n_\perp^2$), $\mathrm{Im}\, k_\perp (\mathrm{ELD}) \propto n_\perp^3 n_e^{-2} T_i^{-1}$. This behavior is illustrated in Fig. 3(b) where the $\mathrm{Im}\, k_\perp$ (ELD) is plotted as a function of n_e showing the n_e^{-2} behavior. The difference in the damping among various values of ω/Ω_D is the $n_\perp^3$ dependence since for IBW, $n_\perp$ is larger for smaller ω/Ω_D value for $\omega < 2\Omega_D$. This damping property greatly improves the IBW wave accessibility of the hot-dense fusion plasma core. The damping increases rapidly near the resonance where $n_\perp \to \infty$. This is the reason that the ESIBW region could again appears near the resonance as shown in Fig. 2.

3.2.2 Collisional Absorptions

The effect of collisions is usually small for IBWH in fusion plasmas due to their relatively low collisionality (compared to the wave frequency). The effect of electron-ion collisions on

the damping is usually negligible. It can be estimated by adding a term (υ_{ei}/ω) Re K_{zz} to Im K_{zz}. Since most of the IBW wave energy is carried by the coherent motion of ions, ion collisions can effectively thermalize the wave energy. One model is given in the Reference 15 as,

$$\text{Im } k_{\perp i} \text{ (collision)} = \Sigma \, (\upsilon_{ij} / 2v_{g\perp}) \, (E_i / W_O) \, [A+B(k_\perp \rho_i)^{-2}]^{-1} \qquad (3\text{-}6)$$

where υ_{ij} is a 90^o collision frequency between i and j ion species, W_O is the wave energy density and E_i is the contribution of i-species to W_O. For the different ion species ($i \neq j$), B is chosen to zero and A =1. For the like ion species (i = j), Halms like model [71] suggests A = 0 and B = 1 where the damping increases with $(k_\perp \rho_i)^2$. In general, the ion collisional damping should be negligible in hot fusion plasmas. However, it may play some role in the lower temperature experimental plasmas particularly near the plasma edge and also near the resonance.

3.2.3 Ion Cyclotron Harmonic Damping

Due to its relatively large $k_\perp \rho_i$, ion Bernstein waves can interact strongly with ion cyclotron harmonic resonances. To calculate for the damping coefficient, we first compute Im $k_\perp$ due to the ion cyclotron resonance. From Eq. (2-1), it can be shown that

$$\text{Im } k_\perp^* = \text{Im } \varepsilon^* / |\partial \varepsilon / \partial k_\perp| \approx \text{Im } K_{xx}^* / |\partial K_{xx} / \partial k_\perp|$$

$$= \frac{\sqrt{\pi}}{|\partial K_{xx} / \partial k_\perp|} \frac{\omega_{pi}^{*2} p^2}{\omega k_{||} V_i^*} Q_p(b_i^*) \exp - \frac{\omega - p\Omega_i^*}{k_{||} V_i^*} \qquad (3\text{-}7)$$

where, $b_i \equiv (k_\perp \rho_i)^2$, K_{xx} is an element of the plasma dielectric tensor, the asterisk denotes resonant ion species, $Q_p(b_i^*) \equiv I_p(b_i^*) / b_i^* \exp (- b_i^*)$, I_p is the modified Bessel function, and p denotes the harmonic number of the ions. The contributions from K_{xy}, K_{zz}, and $n_\perp^2$ terms in Eq. (2-1) may be neglected here since in fusion plasmas their contributions are smaller by an order of m_e/m_i or $n_{||}^2 \omega^2 / \omega_{pi}^2 \approx 10^{-1} - 10^{-2}$. The damping coefficient $\Gamma_{ip}^* \equiv \int \text{Im } k_\perp^* \, dx$ can now be calculated for the p-th harmonic resonance by integrating across the resonance as[12]

$$\Gamma_{ip}^{*} = \frac{k_\perp R\ \pi}{|k_\perp \partial K_{xx} / \partial k_\perp|} \frac{\omega_{pi}^{*2}}{\Omega_i^{*2}} Q_p(b_i^{*}) \qquad (3\text{-}8)$$

where R is the magnetic field gradient scale-length, typically equal to the device major radius. In deriving Eq. (3-8), we have neglected the change in the real part of the wave dispersion relation as we integrate through the absorption layer. If the absorption is sufficiently small, $\Gamma_{ip}^{*} < k_\perp R\pi\ V_i^{*}\ k_{||} / \omega \approx 1$, Eq.(3-8) is a reasonable approximation. For a heavily damped case, one would have to integrate Eq.(3-7) numerically as done in the ray-tracing calculations.

In most cases, the harmonic resonances of the main fusion ions are completely opaque to ion Bernstein waves. For example, for the fifth harmonic damping ($p = 5$), $Q_p(b_i^{*})$ is typically 3×10^{-3}, and one obtains $\Gamma_{ip}^{*} \approx 100$, suggesting a strong absorption. For large p, the asymptotic expansion of the modified Bessel function for large b_i^{*} gives

$$Q_p(b_i^{*}) \approx (2\pi)^{-1/2} (b_i)^{-3/2} \exp(-4p^2 / 8 b_i). \qquad (3\text{-}9)$$

Since $Q_p(b_i^{*})$ is maximum around $4p^2 \approx 8 b_i$, one can estimate $Q_p(b_i^{*}) \approx 0.42\ p^{-3}$. For the damping to be unimportant, Γ_{ip}^{*} must be less than ≈ 0.1, or $Q_p(b_i^{*})$ must be order of 10^{-6}. This requires p to be very large ≈ 100, which is the lower-hybrid frequency range. At this high harmonic frequency range, the wave may be considered unmagnetized and would therefore require different treatment. Therefore, in the ion cyclotron range of frequencies, the ion Bernstein wave can be expected to be strongly absorbed by the majority harmonic resonances. It should be emphasize here that the present calculation is a simple uniform linear theory that a more refined theory might be needed to account, for example, for the particle excursions in the absorption region. In a realistic tokamak heating geometry, the absorption layer becomes quite thin (less that a gyro-radius) particularly at high harmonics that a considerable tunneling may occur.

3.2.4 Quasilinear Diffusion and Bulk Ion Heating

The short wavelength nature ($\lambda_\perp \approx \rho_i$) of the ion Bernstein wave gives a rise to a unique ion heating property for IBWH. The quasilinear rf diffusion coefficient appropriate for IBWH heating is given as,[72]

$$D \propto J_n^2(k_\perp V_\perp / \Omega_i) / (k_\perp V_\perp / \Omega_i)^2 \qquad (3\text{-}10)$$

where J_n is the Bessel function of order n. The rf diffusion coefficient peaks near the $k_\perp V_\perp/\Omega_i \approx n$ which then decreases rapidly for larger energy. Since near the absorption layer, $k_\perp \rho_i \equiv k_\perp V_{Ti}/\Omega_i \approx O(1)$, the ion acceleration decreases for $V_\perp >> V_{Ti}$. For large argument limits, since $J_n(Z) \approx (2/\pi Z)^{1/2} \cos [Z - (2n+1)\pi/4]$, the 'envelope' of the rf diffusion coefficient decreases with $D \propto V_\perp^{-3}$ which indicates that the electron viscosity (which is velocity independent) can easily prevent the further acceleration for $V_\perp \geq 4\ V_{Te}$. One should note that for the fastwave case where $k_\perp \rho_i << 1$, the quasilinear rf diffusion tends to remain large even for $V_\perp >> V_{Ti}$ leading to the well-known quasi-linear ion tail formation for ICRF.[73] This bulk ion heating property of IBWH might make it suitable for heating plasmas with poor high energy ion confinement. Another particularly useful application might be that in reacting plasmas where the fusion reactivity energy cross-section peaks in the energy range of 40-100 keV, the IBWH heating of plasmas of $T_i \approx 10$ keV could enhance the reactivity by heating ions only up to ≈ 150 keV range ($E_i \approx 15\ T_e$).

3.2.5 Harmonic Absorption by Impurity Ions

As the ion Bernstein wave propagates toward the plasma core, it must traverse numerous ion cyclotron harmonic layers stemming from various ionization states of impurity ions.[3] Strong ion cyclotron harmonic damping on those ions could cause a premature absorption of the wave energy and therefore may impede the power flow toward the plasma core. One important difference compared to the majority ion case is that the real part of the dispersion relation is determined mainly by the majority ions not by the impurity ions. Therefore, Eq. (3-8) is much more accurate for the impurity absorption case since the real part can be considered to vary smoothly across the impurity layer. Detailed calculations have been presented in Ref. 12. The effect of damping generally goes down with the mass of impurity ions. The high mass impurity ions such as tungsten should not cause any significant absorption for IBWH. The low-mass impurities such as carbon and oxygen on the other hand are usually fully ionized and assumes a deuterium-like state, and therefore should not cause undesirable absorptions for fusion plasmas. The medium mass impurity ions such titanium can cause a few percent level absorptions, if the impurity concentration is sufficiently high , i.e., $n_{imp} / n_e > 10\%$. Of course, if the plasma temperature becomes sufficiently high that those medium mass impurities also assume the deuterium-like state, the absorption again becomes negligible.

3.2.6 Apha-Particle Absorption

In a reacting plasma, the wave power absorption by the fusion produced alpha-particles may become important. If the α-particle absorption is too strong, the wave accessibility to the plasma core may be impeded.[9] The direct rf heating on the fusion α-s may also affect their confinement characteristics. In addition, the rf power absorbed by the α-particles will generally flow collisionally to bulk electrons which in some cases may not be as desirable as the direct ion heating. This is an important consideration for the ignition experiments as well as for the high-Q fusion reactor operation. For this reason, we shall estimate here the α-particle damping for the case of ion Bernstein waves. We assume an isotropic (non-polarized) α-particle velocity distribution as in Ref. 9. For IBWH, it is a good approximation to assume that $k_\perp V_{\perp\alpha} / \Omega_\alpha$ to be large since $k_\perp V_{\perp i} / \Omega_i$ is already order of one. Therefore, an asymptotic expansion of Bessel function for large argument yields[12]

$$\text{Im } (K_{xx})_\alpha \leq 0.4 \ (\omega_{p\alpha} / \omega)^2 (\Omega_\alpha/\omega) (k_{||} / k_\perp)^3 [\omega / (\omega - p \Omega_\alpha)]^4 \qquad (3\text{-}11)$$

Equation (3-11) shows that the damping can get quite large near the α-particle resonances ($\omega \approx p \Omega_\alpha$). Since for a typical ignition parameters, $k_{||} / k_\perp \approx 10^{-2}$, and $[0.4 \ (\omega_{p\alpha} / \omega)^2 (\Omega_\alpha/\omega)] \approx 1$, that as long as the α-particle resonance is not too close, the absorption can be quite small. For example, the $5\Omega_T$ and $2\ \Omega_T$ heating cases, the launched IBWH at the low field side will encounter the respective tritium resonances without crossing the α-particle resonances. In this tritium heating case, the term in Eq.(3-11) becomes largest at $5\Omega_T$ when $\omega / (\omega - 3\ \Omega_\alpha) = 5\Omega_T / (5\Omega_T - 3\ \Omega_\alpha) = 10$. Even for this case, Im $k_{\perp\alpha} \leq 10^{-2} / | \partial K_{xx} / \partial k_\perp | \leq 10^{-3}$ cm^{-1} which is still quite small. Therefore, it should be still possible to heat tritium ions directly with IBWH without the α-particle absorption.

3.3 Non-linear Absorption Processes

In this section, we discuss the possible non-linear processes for IBWH. In general, non-linear processes are not considered desirable. However, some non-linear processes can provide additional ion heating channels which can be useful. For example, during the JIPPT-II-U IBWH experiment, an efficient ion heating was observed at $3/2\Omega_i$. This type of heating was also observed in the particle simulation calculations as discussed in Secs. 2.3.3. and 3.3.1. There are presently two non-linear heating models, one based on the non-linear particle orbit modification (stochastic heating) and one based on the non-linear ion Landau damping. The non-linear processes which can directly heat the majority bulk ions are attractive for fusion

applications. However, since the required power flux P/A scales as $nT_i^{3/2}$, it still remains to be seen if those processes continue to be important as we move toward ignition parameters where n and T_i are expected to be much higher. In this section, we have also included the wave scattering by low frequency turbulences and parametric instabilities since those processes can also lead to the wave power dissipations.

3.3.1 Stochastic Heating

During the particle simulation investigation of IBWH, an interesting ion heating was observed at $\omega=3/2\Omega_i$.[16] In Fig. 11(a), the energy deposition profile into ions is shown. The resonant layer position, $\omega = 3/2\ \Omega_i + k_{||}\ V_z$, is indicated by the arrow where the heating is maximum. The resulting heated perpendicular ion distribution is shown in Fig. 11(b). The heated ions show relatively bulk ion heating characteristic. The plot of H phase space ($v_\perp^2$, $v_{||}^2$) is shown in Fig. 11(c) for the heated region, $\omega \approx 3/2\Omega_H$. The arrows indicate the upper and lower limits of the parallel resonant velocities $v_{||} = [\omega - 3/2\Omega_H(x)] / k_{||}$. The dashed line indicates the boundary of the initial distribution function which is Maxwellian. In order to understand this result, the motion of ions under the combined influence of the electrostatic wave, $\phi_o \cos (k_\perp x + k_{||}Z - \omega t)$ and an axial magnetic field with cyclotron frequency Ω was examined. The equation of motion is given as

$$\ddot{X} + \Omega^2 x = (q/m)\, k_\perp\, \phi_o \sin (k_\perp x - \omega_d t) \qquad (3\text{-}12)$$

where $\omega_d \equiv \omega - k_{||}\ V_{zo}$. From examining the above equation, it was found that significant trapping in phase space can occur where $w = p/s\ \Omega$ and $\alpha \equiv c\ (E_\perp/B) / (\Omega / k_\perp)$ exceeds certain value. The non-linear quantity α assumes the lowest value for $s = 2$ or $\omega = 3/2\ \Omega$, $5/2\ \Omega$, etc. In the simulation, one finds that the wave single pass absorption becomes significant when $\alpha \approx 0.31$ for $3/2\ \Omega_i$ heating, or in terms of the power flux P(Watt/cm^2),

$$P/A \geq 0.26 \times 10^{-19}\ (\omega/\Omega_i)\ Y\ \alpha^2\ n\ V_i\ T_i\ (k_\perp \rho_i)^{-3} \propto n\ T_i^{3/2} \qquad (3\text{-}13)$$

For the JIPP parameters, $Y = 0.27$, $k_\perp\rho_i = 1.5$, $\omega/\Omega_i = 1.5$, $T_i = 300$ eV, $n_e = 2 \times 10^{13}$cm^{-3}, yielding $P/A \approx 27$ W /cm^2. This value corresponds to $P_{rf} \approx 20$ kW which is well exceeded in the experiment.

The observed stochastic heating may be related to those investigated for the higher frequency (very high harmonic) lower hybrid wave heating.[74] The stochastic ion heating in the neutralized ion Bernstein wave fields (NIBW)[75] has been investigated experimentally using the technique of laser-induced fluorescence (LIF).[76] The LIF was able to detect the perturbed ion velocity distribution function under the wave fields directly. The power threshold of the observed heating was consistent with that expected from the stochastic ion heating.

3.3.2 Non-linear Ion Landau Damping

The importance of non-linear ion Landau damping[77] in the IBWH experiment was pointed out in Ref. 78. Due to the self interaction of IBW when the conditions $2\omega \approx m\Omega_i$ are satisfied, (where $m \geq 3$ corresponds to odd integers), the resulting beat wave (a quasi-mode) at $m\Omega_i$ can provide an effective absorption channel. It should be mentioned that this process has been studied for electron Bernstein waves in laboratory plasmas.[79,80] A condition for significant pump depletion for the tokamak IBW experiment can be given as,[78]

$$P/A \geq (2.75 / \pi)\, 10^{-19} (\omega/\Omega_i)\, (\rho_i/R)\, (Y^2 n T_i V_i)(\, b_i |VI|)^{-1} \propto n\, T_i^{3/2} \rho_i / R \quad (3\text{-}14)$$

where $b_i \equiv (k_\perp \rho_i)^2$, Y is a wave-parameter dependent quantity and $|VI|$ represents a non-linear interaction quantity. For the JIPPT-II-U parameters, $b_i \approx 1.5$, $Y \approx 0.27$, $|VI| \approx 0.02$, $R = 91$ cm, $\omega/\Omega_i = 1.5$, $T_i = 300$ eV, $n_e = 2 \times 10^{13} cm^{-3}$, Eq. (3-14) yields $P/A \approx 35$ W /cm^2. This power level (≈ 20 kW) is well exceeded in the JIPPT-II-U experiment. It is interesting to see that the threshold for the non-linear ion Landau damping which is a collective process is very similar to that of the sub-harmonic heating which is essentially a single particle process.

3.3.3 Scattering by Low-Frequency Turbulences

During IBWH, the heating wave must traverse regions of relatively large low-frequency fluctuations in order to reach the plasma core. Mode-mode coupling of the incident wave with such fluctuations could induce scattering of the incident wave trajectory and could cause significant deviations from the linear-theory predictions.[10] The excessive scattering can cause a diffusion in the $n_{||}$ space which can then enhance electron Landau absorption. At first, one might guess that the scattering of IBW might be significant since the wavelengths of IBW and of the low-frequency fluctuations are similar, $\lambda_\perp \approx \rho_i$. This problem was investigated in Ref. 11, and it was found that the interaction could be weak. One reason is that the IBW power is

carried mainly by the kinetic ion motion. A scaling for the maximum scattering probability was given as,[11]

$$P_s(max) \approx 5 \times 10^{-6}\, T_{i0}^{-1/2}(keV)\, |\tilde{N}(\%)|^2\, a(cm)\, P_c(T) \qquad (3\text{-}15)$$

where a is the plasma minor radius, $\tilde{N}$ is the normalized density fluctuation percentage and the ion temperature profile is assumed to be Gaussian-like with $T_{i0} = 100\, T_i$ (edge). For a PLT-like parameter, $T_{i0} = 1$ keV, $|\tilde{N}(\%)| = 10$ %, a = 40 cm, and $B_o = 2.5$ T, then $P_s(max) \approx 0.05$. For a reactor-like parameter $T_{i0} = 10$ keV, $|\tilde{N}(\%)| = 5$ %, a = 200 cm, and $B_o = 5$ T, then $P_s(max) \approx 0.04$. In either cases, the scattering is relatively small. This result consistent with the ACT-1 experiment where the coherent IBW propagation was observed for $T_i = 1$ eV, $|\tilde{N}(\%)| = 7$ %, a = 8 cm, $B_o = 0.5$ T, and $P_s(max) \approx 0.05$.

3.3.4 Parametric Instabilities

Parametric instability is one of the most extensively studied non-linear wave phenomena in fusion research due to its low power thresholds. Parametric instabilities have been observed in the lower-hybrid experiments[81] and also in the ICRF experiments[82] in certain regimes. This process which tends to occur in the plasma edge region could cause uncontrolled (and generally undesirable) power dissipation (pump depletion) in the plasma edge region. Parametric instability is a three-mode 'decay' process[83] where a pump wave excites two daughter waves or one daughter wave and a quasi-mode pair.[84] The selection rule for the decay process is,

$$\omega_o = \omega_1 + \omega_2 \qquad \text{and} \qquad \mathbf{k}_o = \mathbf{k}_1 + \mathbf{k}_2 \qquad (3\text{-}16)$$

where the subscript o denotes the pump wave and 1 and 2 the decay waves.

The importance of parametric processes depends on many factors including the growth rate, non-linear saturation level, etc., that the actual experimental observations can provide a very valuable information. On ACT-1, parametric instabilities associated with the lower-hybrid[85] and ICRF heating[86] were investigated in detail. For IBW heating, however, very little parametric activity was observed. When the plasma density was lowered so that a significant electron plasma wave(EPW) region exists near the antenna, the well-known decay process, EPW --> EPW + Ion-Quasi-Mode (IQM) was observed.[87]

During the high power IBWH experiment on JIPPT-II-U, PBX-M, and PLT, some attempts were made to look for the instabilities with rf probes in the edge region but no instability activity was thus far observed in these experiments. The parametric instability process was used to explain the puzzling $5/2\Omega_D$ heating results on Alcator-C IBWH experiment although not actually measured in the experiment. Only clear evidence of parametric activities, thus far, comes from the DIII-D IBWH experiments which will be discussed in Sec. 6.7.

3.4 Wave accessibility

In order to make a proper utilization of the rf power, the question of wave accessibility becomes a very important issue. We usually use the word wave accessibility to mean the ability for an externally launched wave to reach the desired plasma core without a significant power attenuation. The wave accessibility can be hampered by various physical processes. If there is a wave singularity (resonances, cut-offs, etc.,) in its path, then the accessibility is questionable since the wave power is either reflected or absorbed (or often it can mode-convert into another type of wave). In addition, if the wave is damped excessively that not much of the original power would reach the desired location, the wave accessibility is considered to be poor. In this section, we shall consider this question of wave accessibility for tokamak plasmas.

3.4.1 Tokamak Ray-tracing Calculation

One of the most important objectives for any rf heating theory is to confirm the wave accessibility and to obtain a realistic rf power deposition profile. For IBW, because of its relatively short perpendicular wavelength, the WKB condition [i.e., $(\partial k_\perp/\partial r) \cdot k_\perp^{-2} \ll 1$] is well satisfied in the most regions that ray-tracing techniques can be used to predict the rf power flow pattern. On ACT-1, the ray tracing calculation was found to predict well the wave packet trajectories of IBW.[19] In actual numerical calculations, the ray trajectory is traced by a series of finite steps. In each step, the linear power absorption (as given in Sec. 3.3) is calculated for both ions and electrons. The ray stops when the original power is decreased to a negligible level (typically 1% of the launched value). In the tokamak ray-tracing code, due to the axisymmetry, the toroidal wavenumber is assumed to be conserved except for a geometric factor [i.e. $k_T(R) = (R_O/R)\, k_T(R_O)$]. Here, the parallel wavenumber $n_{||}$ is a variable since it depends on both the toroidal and poloidal wavenumbers through local rotational transform. To simulate the actual experimental situation, it is necessary to compute a series of launched $n_{||}$

values depending on the antenna geometry and the phasings. For a good approximation, one could represent the launched power spectrum as,

$$P(n_{||}) = A(n_{||}) \cdot F(n_{||}) \qquad (3\text{-}17)$$

where A is a coupling function and F is the antenna Fourier spectrum. The coupling function is a relatively complex physics problem as will be discussed in Sec. IV.

An example of the tokamak IBW ray-tracing calculations is given in Fig. 12 for the JIPPT-II-U 40 MHz IBWH case. In Fig. 12(a), the wavenumber radial profile is shown with the $3\Omega_{He}$ (deuterium-like) resonance in the center of the plasma. The Ω_H and $2\Omega_H$ resonance layers are outside of the plasma. The perpendicular wave electric field is shown in Fig. 12(b). The ray trajectories in the poloidal and toroidal plane are shown in Fig. 12(c) for various launched $n_{||}$ (as labeled). Finally, the normalized power is shown for various launched $n_{||}$ and for the minority concentrations (noting that fully ionized helium and impurity carbon has the same cyclotron frequency as deuterium).

3.4.2 Launching Position Poloidal Dependence

In order to heat the plasma effectively, the placement of the IBWH antenna plays an important role in obtaining good wave accessibility. Normally, the IBWH antennas are placed in the outer mid-plane region since it is the most accessible region of a tokamak. The wave launched from the mid-plane region propagates in an oscillatory trajectory toward the center until it reaches the cyclotron harmonic resonance layer as shown in Fig. 12(c). This can be explained as follows.[12] As the ray propagates poloidally toward higher magnetic field, the poloidal wave number change makes the wave $n_{||}$ to decrease. The wave is reflected poloidally when the $n_{||}$ reaches near zero. The reflected wave then moves poloidally toward lower magnetic field making the $n_{||}$ to increase again. While under going this poloidal oscillation, the wave is constantly moving radially inward such that the trajectory makes an oscillatory motion. The rate of the oscillatory motion increases as the wave approaches the resonance layer due to the radial group velocity slow down. For the case near the mid-plane, the poloidal motion of the ray trajectory (for the weakly damped rays) can be reduced to that of a simple harmonic oscillator. For this reason, the higher launched $n_{||}$ (larger initial velocity) makes larger poloidal (larger oscillation amplitude) excursion. Since the radial group velocity does not depend strongly on $n_{||}$, the rays for all $n_{||}$ therefore tend to converge on the same radial location in the mid-plane as shown in Fig. 12(c).

However, if the antenna is placed significantly away from the mid-plane (poloidal angle $\geq$ 30 °), the launched parallel wave number increases as the wave propagates toward the mid-plane (toward decreasing magnetic field). Ray-tracing calculation indicates that a significant up-shift of the parallel wave number occurs in this situation causing the wave to be absorbed via electron Landau damping not too far from the plasma edge as in the case for the JFT-II-M experiment.[41] Recent independent calculations also confirmed this behavior which were used to explain inefficiencies of IBW heating in some of the experiments.[89] Therefore, according to the ray tracing calculation, the placement of an IBW antenna is optimized when the antenna is placed near the low field mid-plane region.

3.4.3 Possible Relevance to Ion Cyclotron Emission (ICE) Physics

In tokamak experiments, there are observations of radio-frequency emissions from the plasma near and its harmonics of the ion cyclotron frequencies.[90] The observed emission frequency spectra displays features which are peaked for various values of ion cyclotron harmonic frequencies. The observed prominent frequency peaks often correspond to 2Ω, 3Ω, ...$n\Omega$, at the low-field mid-plane magnetic field value. This so-called ion cyclotron emission is believed to be excited by the hot ion population in the plasma interior. This observation may be interpreted as an inverse problem to IBWH. For IBWH, the externally launched radio-frequency electromagnetic wave is transformed into an inward propagating ion Bernstein wave which then heats the plasma interior. As we recall, the most suitable antenna location is for IBWH for heating the plasma core is near the low-field mid-plane region (Sec. 3.5). The suitable frequencies are near (just below) 2Ω, 3Ω, ... at the launching point where the wave could more easily mode convert from the long wavelength electromagnetic wave into a short wavelength IBW. For the ICE, the inverse process should hold true. The excited IBW in the plasma interior should have the most likely 'escape' path along the mid-plane region toward the low field region. Otherwise, the waves must make the long journey in a diffusive manner undergoing series of re-absorptions and re-emissions. Of those outwardly propagating IBW which reach the plasma edge, the ones which could connect on to the vacuum electromagnetic waves would be one near the harmonic frequency, again just below 2Ω, 3Ω, ... , at the point of the conversion (plasma edge) where the IBW wavelegnth increases near the cut-off frequency making it easier to couple to the longer wavelength electromagnetic waves. Therefore, it might be suggested that the tokamak IBW accessibility physics is acting as a filter to connect the externally picked-up electromagnetic signal to the IBW generated in the hot plasma interior. Therefore, the absorbed signal at the ion cyclotron harmonic frequency is

actually generated in the plasma interior one major harmonic below. In a D-H mixture plasma, for example, if the hydrogen ions emit ECH at $1\Omega_H$, $2\Omega_H$, etc, in the plasma interior, the actual emission frequency detected would be at $3\Omega_D$, $5\Omega_D$, etc. at the outer plasma edge. Perhaps, looking another way, the ICE frequency peaks might be correlated with the desirable frequencies for heating the plasma core by IBWH.

3.5 IBWH Tokamak Modelling Codes

The development of appropriate theoretical models to simulate the performance of IBWH in an actual high power tokamak experimental situation is clearly important in order to understand the heating results as well as to be able to extrapolate toward future experiments. As an initial step, the IBWH ray-tracing code was combined with the tokamak transport code BALDUR.[91] As the BALDUR code evolves plasma parameters in time, the IBW ray-tracing code periodically calculates the power deposition profiles in a self-consistent manner. Typically, the transport coefficients are chosen so as to satisfy the ohmic condition prior to the application of IBWH. In Fig. 13, a typical example of the modelling code calculation is shown for the INTOR-type parameters.[13] The corresponding power deposition profiles are shown for $n_{||} = 5$ in Fig. 14 for various time. Initially, the power deposition is primarily into ions [Fig. 14(a)]. As the plasma is heated, the magnetic axis shift toward the larger major radius (Shafranov shift) making the absorption layer closer to the plasma axis [Fig. 14(b)]. Near the ignition, the heating is shifted to electrons [Fig. 14(c)]. The heating profile is central through out the heating phase. It should be mentioned that by launching more well defined spectrum at lower $n_{||} < 5$, it is still possible to heat ions instead of electrons even in the ignited regimes. Another type of IBWH code, MICADO, was developed to account for the multi-ion species plasma with the perpendicular and parallel velocity components for the heated species.[14] These transport analysis codes reproduced many of the IBWH features observed in JIPPT-II-U[15] and PLT[14] which will be discussed in Sec. 6.

IV. IBWH COUPLING PHYSICS

For every rf heating scheme, efficient conversion of rf power into a desired heating wave is clearly a crucial issue. For high frequency waves such as the ones used for electron cyclotron heating (ECH), the heating waves can be considered sufficiently similar to the vacuum electromagnetic waves so that its launching physics is relatively simple. For lower frequency waves, however, the heating plasma waves are usually very different. Therefore, the efficient conversion of rf power into a desired plasma wave is a challenging but worthwhile problem for rf heating. This coupling of rf power into the wave power usually takes place within a few cm of the antenna surface. For ICRF, the coupling into fast magnetosonic waves takes place by means of tunneling through the edge evanescent layer which often requires the antenna surface to be placed relatively close to the main plasma (to minimize the evanescent layer thickness) to maintain a good antenna loading (or high antenna radiation resistance). For LHH, the waveguide position is adjusted to make the waveguide launcher impedance to match the plasma wave impedance (i.e. $\omega_{pe} \approx n_{||}\,\omega$ as described in Ref. 92). For IBWH, since the heating wave is a finite ion temperature mode, IBWH is launched by first exciting electron plasma wave (EPW) as in LHH which then mode-transforms into IBW inside the plasma due to the FLR effect (Sec. 2.2). The preferred edge density for IBWH is generally lower than that of LHH and ICRH. This could be an advantage since the lower coupling density suggests that the launcher can be placed further away from the main plasma thus lowering the plasma heat load onto the launcher. However as will be discussed in Sec. 4.1.1 and 4.3.5, this low edge density could cause coupling problems particularly for the low frequency IBWH experiments.

Because of the relative complexity (and importance) of the wave coupling physics in IBWH experiments, we shall discuss them in a considerable detail in this section. First, the IBW plasma surface impedance models are described and then two types of IBWH launchers used in the experiments, the waveguide launcher and the B_θ-loop antenna, are described. We then discuss the edge plasma conditions for efficient IBW launching. Various deleterious processes due to antenna-plasma interaction are also discussed in Sec. 4.3. We then conclude with a brief summary of IBW coupling.

4.1 Plasma Surface Impedance

To calculate the antenna plasma loading or the waveguide power reflection, it is essential to know the plasma surface impedance for whatever the wave being launched. In a slab model, the surface impedance is determined mainly by the value of plasma impedance at the plasma-

antenna interface which is modified by the reflected waves from the inner gradient region (where WKB is not satisfied).

In considering IBWH launching, we consider three possible coupling regimes. We define the Regime I for the case of low edge density ($\omega_{pi}<<\omega$) that the electron plasma wave (EPW) is launched much the same way as the case for LHH. If the edge density increases such that ω_{pi} approaches ω, the surface impedance is still dominated by a thin but finite thickness EPW layer. We call this intermediate density case, Regime II. When the plasma density at the interface becomes sufficiently high ($\omega_{pi}>\omega$) that IBW is launched directly by the antenna, we call this case Regime III. The EPW region could be neglected if the region thickness L_{EP} is sufficiently thin ($L_{EP} << \lambda_\perp$). In Fig.15, we plot $\omega_{pi} \approx \omega$ density values for various experimental values. This density represents the mode-transformation density (where $\omega_{pi} \equiv \omega$), $n_{trans}(cm^{-3}) = 2.27 \times 10^{11}\ m_i\ f^2(100\ MHz)$, which goes up rapidly with the rf frequency. The dominant plasma species type is indicated in the parenthesis. One should note that the PLT 30 MHz experiment has a unique wave launching physics as discussed in Sec. 2.2.1. For 250 MHz BPX-type DT plasma, n_{trans} is $3.5 \times 10^{12} cm^{-3}$ and for the FT-U 450 MHz high harmonic experiment, it is $5 \times 10^{12}\ cm^{-3}$. These values are compatible with the edge density of the tokamak plasmas. For the lower frequency experiments, the value typically is in the 10^{10} - $10^{11}\ cm^{-3}$ range which is low for a typical tokamak edge density.

4.1.1 WKB Condition

For obtaining the plasma surface impedance, it is important to understand the wave reflection region where the WKB approximation, i.e., $(1/ k_\perp^2)(\partial k_\perp / \partial r) < 1$, is violated. The reflected wave could modify the plasma surface impedance. For this reason, we shall first examine the WKB condition. For a tokamak experiment, the density can vary by a large factor in the antenna coupling region. The WKB condition is usually easier to satisfy for the ion Bernstein wave since the wave dispersion relation mainly depends on the ion temperature and magnetic field but only weakly on the plasma density. The magnetic field variation ($\propto 1/R$) is usually gentle enough for the WKB condition to be well satisfies. The ion temperature gradient is also considered to be relatively mild compared to that of the density. Therefore, the wave reflection is expected mainly from the density gradient in the EPW region. For this reason, if one were to consider Regime I & II, the antenna coupling is mainly determined by the EPW region, and it should not depend very much on the subsequent transformation into IBW.

For EPW, the WKB condition can be obtained from Eq.(2-2) as

$$\frac{1}{k_\perp^2}\frac{\partial k_\perp}{\partial r} \approx \frac{c\,(\omega_{pe}^2/\omega^2)}{2\,\omega\,(\omega_{pe}^2/\omega^2 - 1)^{3/2}}\,\frac{1}{(n_{||}^2 - 1)^{1/2}}\,\frac{\partial n_e}{n_e\,\partial r} < 1 \qquad (4\text{-}1)$$

As one can see from Eq. (4-1), the WKB is violated if $\omega_{pe}^2/\omega^2 = 1$ and $n_{||}^2 = 1$. The $\omega_{pe}^2 = \omega^2$ condition can be easily avoided since the critical density, n_{ec} (cm^{-3}) $= 1.24 \times 10^4 \cdot f^2$(MHz), is quite low for IBWH. For example, n_{ec} is 2×10^7 cm^{-3} for 40 MHz and n_{ec} is 8×10^8 cm^{-3} even for the BPX-like 250 MHz range. The $n_{||}^2 = 1$ condition can be avoided by appropriately phasing the antenna. Therefore assuming that $\omega_{pe}^2/\omega^2 >> 1$ and $n_{||}^2 > 1$, Eq.(4-1) reduces to

$$\frac{1}{k_\perp^2}\frac{\partial k_\perp}{\partial r} \approx \frac{(c/\omega)}{2\,(\omega_{pe}/\omega)\,n_{||}\,L_D} < 1 \qquad (4\text{-}2)$$

where L_D is the density scale length $L_D \equiv n_e / (\partial n_e / \partial r)$. The desired $n_{||}$ is usually determined by the heating requirement. For example, for $L_D \approx 0.5$ cm and $n_{||} \approx 2$, the minimum density n_{min} required to satisfy Eq.(4-2) would be $n_{min} \approx 3.5 \times 10^{10}$ cm^{-3}. Therefore, if one were to avoid excessive reflections, the density in front of the antenna must remain above a certain value as indicated in Eq. (4-2). However, the edge density control becomes somewhat problematic for IBWH in the low frequency regime (f < 100 MHz) due to the large ponderomotive force of the antenna near fields which tends to reduce the plasma density in the coupling region. Due to its importance in the recent IBWH experiments, we shall briefly review the ponderomotive force in the next section.

4.1.2 Ponderomotive Cavity Formation

Charged particles under the influence of an RF field in the magnetic field are subjected to a " ponderomotive potential", ψ_{rf}, given for the ion cyclotron range of frequency by[61-63]

$$\psi_{rf} = \frac{1}{4\,m_i}\,\frac{e^2\,E_\perp^2}{\omega^2 - \Omega_i^2} + \frac{1}{4m_e}\,\frac{e^2\,E_{||}^2}{\omega^2} \qquad (4\text{-}3)$$

where $E_\perp$ and $E_{||}$ are the rf electric fields. Although the perpendicular ion term could become significant near $\omega \approx \Omega_i$, for a given value of electric field, the parallel term is usually dominant due to the light electron mass. Therefore, the ponderomotive force is particularly strong for the ion Bernstein wave coupler where the antenna electric field is predominantly parallel to the ambient magnetic field.

The expected parallel electric field can be estimated from the power flux equation for the EPW and can be given by

$$P/A = (c / 8\pi) (E_Z B_y) = (c / 8\pi) E_Z^2 (\omega_{pe}/\omega)(n_{||}^2-1)^{-1/2} \qquad (4\text{-}4)$$

where A is the effective area of the rf power flow, typically chosen to be the antenna surface area. For the plasma heating applications, P/A is desired to be about 0.5 kW/cm^2. From Eq. (4-4) the magnitude of E_z can be given by

$$|E_z| \text{ (stat-volt/cm)} = 9.2 (\omega/\omega_{pe})^{1/2} (n_{||}^2-1)^{1/4} [P/A \text{ (kW/cm}^2)]^{1/2} \qquad (4\text{-}5)$$

Since the ω_{pe}/ω is 5-10 at the antenna coupling region, one can see that the electric field is typically order of 1 stat-volt/cm in the high power experiment with P/A $\approx$ 0.5 kW/cm^2. As for the ponderomotive potential, from Eq. (4-3), one obtains

$$\psi_{rf} \text{ (eV)} = 10^2 f \text{ (100 MHz)}^{-2} |E_z|^2 \qquad (4\text{-}6)$$

where f is the applied rf frequency and E_z in stat-volt/cm. In Fig. 16, the ponderomotive potential is given for E_z = 1 stat-volt / cm, for the various experimentally relevant rf frequencies. As can be seen from the figure, the ponderomotive potential drops rapidly with the increased rf frequency and it is likely to be small for experimental parameters for FT-U and BPX. However, for the low frequency IBWH experiment, the ponderomotive potential can be substantial; e.g. at F = 30 MHz, and $|E_z| \approx 1$, ψ_{rf} is about 1 keV which is much greater than the edge plasma temperature and therefore one could expect a substantial density modification. The ponderomotive force could therefore, modify the plasma density in front of the coupler and change the antenna loading. This process has been previously investigated for the lower-hybrid wave case.[48,49] The modification of IBWH antenna coupling due to the ponderomotive force has been also observed in the ACT-1[50] and DIIID[51] experiments. This ponderomotive potential if very large can cause a density 'hole' to develop in front of the antenna which then can lead to

further non-linear effects to set in. On the other hand, the ponderomotive density reduction could perhaps help reduce the rf power loss due to the sheath related processes (Secs. 4.3.1 to 4.3.3). For this reason, to maintain an optimum wave launching condition, it may be quite important to adjust the plasma boundary position at a given power level to account for the density profile modification by the ponderomotive force.

4.1.3 Coupling in Regimes I&II

In Regimes I & II, the coupling is dominated by the EPW physics since in both regimes, EPW is excited at the antenna-plasma interface. Also, the wave reflection, if any, should take place mainly in the EPW layer (as discussed in the previous section). For this reason, the antenna coupling theory developed for LHH could be applied directly here.[4,92] A multi-step model was used to simulate arbitrary plasma profiles.[66] In these EPW dominated regimes, the magnetic field dependence for the antenna loading, like LHH case, is therefore relatively weak. In principle, the launching in Regime I or II should be generally more desirable since EPW does not depend on the ion (or electron) temperature (which could be low at the antenna surface). The lower plasma density at the coupling region also makes it more desirable from the heat load and impurity generation point of view.

4.1.4 Coupling in Regime III

There are three theoretical models which have been proposed to treat the Regime III, the direct $2\Omega_i$ IBW launching case. The simplest model was used by W.N.-C. Sy et al., where a step model (with an optional vacuum interface region) where the wave fields were matched at the plasma boundary was used to coupled directly to IBW.[93] Brambilla has used the finite-Larmor-radius expanded wave differential equations to solve for the surface impedance for the $2\Omega_i$ launching case.[43,94] F. Skiff, et. al., have proposed a similar model replacing the vacuum region with a low density plasma ramp region connecting the antenna and the high density plasma again for the $2\Omega_i$ launching case.[95] The model for the higher harmonic launching case has not yet developed in Regime III. The generally low ion temperature expected at the antenna-plasma interface might make the direct coupling to IBW less efficient and could be subjected to the edge collisional absorption (Sec. 3.3.2).

4.2 IBWH Launchers

Development of the IBWH launchers follows somewhat similar logical path as that of LHH. As in the case for LHH, there are three possible options for the IBW couplers; an electrostatic antenna, a B_θ-loop antenna, and a waveguide type launcher. As in the case of the early LHH experiments,[96] in ACT-1 where the plasma density was sufficiently low, an electrostatic antenna was used to excite IBW.[19] However, for high power tokamak experiments, the exposed high voltage rf electrodes is not considered acceptable. It is interesting to note that a B_θ-loop-type antenna was also used in the early LHH tokamak experiment[97] (although the waveguide launcher has quickly become universal for LHH). Therefore, for the tokamak IBWH experiments, a B_θ-loop antenna and a waveguide type launcher are considered to be the two possible IBWH launchers. Although the waveguide launcher appears to be a better long term option, due to the size restrictions, the present day experimental activities are performed using the B_θ-loop type antennas. The first waveguide IBWH experiment is being prepared on FT-U.[57]

4.2.1 Nagoya Type III B_θ-loop Antenna

Since the present day tokamak IBW experiments cannot use the waveguide coupler (because of the size restrictions), a B_θ-loop antenna has been utilized to simulate the waveguide fields. The antenna current strap is placed along the toroidal direction that the antenna generates electric fields along the magnetic field as in the case for the waveguide. This type of antenna (often termed the Nagoya Type III Coil) was used previously for ICRF slow-wave excitation in mirror devices.[24] A schematic of IBW antenna installed in JIPPT-II-U is shown in Fig. 17. In ACT-1, basic physics of IBW loading and excitation by a B_θ-loop antenna was investigated in some detail for the large $n_\parallel$ case.[50,95] In Fig. 18, a two dimensional wave interferogram of the excited IBW excitation is shown. In this experiment, the observed excited IBW power was observed to increase with density consistent with the plasma loading behavior (it should be noted that the plasma loading behavior depends much on the value of $n_\parallel$ that for low $n_\parallel$ case, the loading can actually increase with decreasing density). To understand this IBW loading characteristic, a coupling model based on a local analysis of warm-plasma wave differential equation was developed.[95] A satisfactory agreement between theory and experiment was obtained.

In tokamak experiment, a B_θ-loop antenna was first used in the JIPPT-II-U tokamak and then in the PLT tokamak. A number of IBWH experiment has been since carried out including

Alcator C, TNT, JFT-II-M, DIIID, and PBX-M. More detailed description of the antenna loading is presented in Sec. VI where the experimental results on each device were described. At present, the antenna plasma loading is not fully understood (though a considerable progress has been made in the recent years) partly due to the lack of precise edge plasma diagnostics and partly due to the great variation in the edge plasma densities (often due to the non-linear effects) in the experiments. Most of the tokamak high power IBWH experiments shows loading characteristics of Regime I&II (EPW coupling) which is generally higher than the Regime III (direct IBW coupling) coupling case[94] and in most cases has a weak frequency dependence as expected in Regimes I & II. On Alcator C, some magnetic field dependence was observed over the field independent "background" loading which suggests Regime III coupling is taking place at least partially in the experiment. Some of the loading results from DIIID and PBX-M appear to be consistent with Regime I & II (EPW coupling) which could explain the observed weak frequency dependence and also the larger than expected antenna loading.[44,45] The recent DIIID results[51] suggest that the large ponderomotive potential associated with the Type III antenna operating in the low frequency range (< 100 MHz) causes the density in front of the antenna to drop significantly that the coupling is moves into the lower density EPW regime.

4.2.2 Waveguide Launcher

As in the case for the lower-hybrid waveguide launcher, a waveguide IBWH launcher is a long term attractive engineering option for reactor applications. The coupling physics is relatively simple and it is less prone to the possible complications associated with the lower frequency loop antennas as discussed in Sec. 4.3. Since IBWH waveguide will be operating in the high frequency regime, the coupling physics is very similar to the lower hybrid wave launching[4,5] (it is interesting to note that the FT-U IBWH frequency, 430 MHZ, is only slightly lower than the earlier tokamak LHH experiments). In order to calculate for the waveguide matching, an IBW waveguide coupling code has been developed using multi-slab plasma profiles.[66] Using this code, the waveguide coupling has been investigated for a number of cases which yielded low reflection coefficient (< 10 %) for a wide range of parameters, as shown in Fig. 19. The IBWH waveguide coupler will be tested in the planned FT-U experiment.[57] The schematic view of the FT-U waveguide launcher is shown in Fig. 20. By using hydrogen and high harmonic heating (4 Ω_H heating), one can perform an IBWH waveguide experiment at 430 MHz with an simple vacuum waveguide launcher of less than 40 cm height. For BPX, a 5 Ω_T heating four element waveguide system operating at 250 MHz has been proposed.[58] In this case, the waveguide height of ≈ 70 - 80 cm is quite compatible with the available BPX port height.

4.3 Antenna-Plasma Interaction

In contrast to the case for ICRF, the IBWH antenna current flows predominantly along the ambient magnetic field line that the induced rf electric field has a large parallel electric field component. This parallel electric field in this relatively low frequency operating regime of IBWH (compared to LHH, for example), gives rise to a strong antenna-plasma interaction. In performing a high power IBWH, one must certainly consider the results of this interaction in order to utilize the rf power efficiently for heating or for other purposes. In this section, we shall discuss various parasitic processes related to the antenna-plasma interactions which could cause the rf power to be lost into generally undesirable non-IBW channels. These parasitic processes could drain the rf power and, in many cases, cause undesirable side effects such as the impurity generations.

4.3.1 Antenna Sheath Acceleration

Since the IBW antenna is oriented along the toroidal direction, the rf electric field of as much as ≈ 300V/cm along the toroidal magnetic field is expected at the antenna surface. Analyzing the region between the Faraday shield elements (the gap), the quick electron response to the oscillating parallel electric field shorts out the electric field over most of the gap, leaving a narrow sheath of positive space charge and intense electric field at the shield's surfaces.[98] This sheath electric field could accelerate ions nearly to the gap voltage (≈ 300 V) causing sputtering of the Faraday shield material. If the plasma density between the Faraday shield gap is sufficiently high, $\omega_{pi}^2/\omega^2 \geq 1$ (the gap density of $10^{12}cm^{-3}$), the plasma sheath rectification could cause serious sputtering and impurity generation. The full treatment of the problem requires the presence of plasma in the gap region which would involve the plasma transport and/or the plasma production in the region. This problem could be controlled to some extent by proper choice of the Faraday shield material and by reducing the plasma density in the gap region.

4.3.2 Wave Excitation by Faraday Shield's Fringing Fields.

The rf fringing fields near the antenna Faraday shield could couple into short wavelength electrostatic modes (the modes could be evanescent).[54] The fringing fields of the Faraday shield have a periodicity of the shield element separation, ≈ 1 cm, which is quite short (compared to the desired wavelength).[99] Similar problem was considered for the fastwave ICRF heating case.[100] The Faraday shield elements could act as an phased antenna array of the

periodicity of the Faraday shield elements. For example, for f = 40 MHz, with the element separation of 1cm ($\lambda_{||}$ = 1 cm), the fringing fields could launch waves with parallel phase velocity of 4 x 10^7cm/sec which is similar to the edge electron thermal velocity. Therefore, this excited 'slow wave' is highly dissipative via electron Landau damping and the rf energy is deposited to electrons near the antenna surface. This model predicts the loading to increase with the density and to decrease with the electron temperature, (a) At low densities, $K_{xx} > 0$, $R \propto \sqrt{n_e} / T_e$, and (b) At high density, $K_{xx} < 0$, $R \propto n_e / \sqrt{Te}$. It indeed predicts several ohms of plasma loading for $n_e = 6 \times 10^{11}$ cm^{-3} and T_e = 2.5 eV and the edge electron heating as observed in the DIIID experiment. This process could become particularly important if a high density plasma comes in a direct contact with the Faraday shield (Regime I).

4.3.3 Antenna Sheath Mode Excitation

In order to explain some of the so-called anomalous loading results, the coupling into a class of sheath-plasma waves (SPW) which could be excited in the high-voltage rf sheaths near the antenna has been proposed.[55] These SPW regions arise whenever there is rf flux linkage through a loop consisting of the antenna structure and the magnetic field lines intersecting the antenna surfaces. The analyses reported in Ref. 55 show that SPW antenna loading tends to increase with the plasma density in the sheath region that this could explain the anomalous loading for the directly launched IBW case (Regime III). This model was able to reproduce qualitatively the observed dependence of antenna phasing, plasma density, magnetic field and rf frequency when the plasma was moved toward the antenna surface in the DIIID experiment.[55] The loading into SPW could be reduced by operating in the low density edge region (Regime I or II). This sheath-plasma wave excitation may be reduced by a proper antenna phasing and antenna design (utilizing insulating walls[101], for example).

4.3.4 Plasma Ionization by the Antenna Near Fields.

Electrons in a strong parallel electric field of IBWH antenna near-field could acquire a large thrashing energy which is sufficient to ionize background neutrals. The thrashing energy, $U \equiv e^2 E_{||}^2 / m_e \omega^2$, as for the ponderomotive potential, decreases rapidly with increasing rf frequency. For example, the 300 V/cm parallel electric field (typically expected in a high power IBWH experiment) causes electrons to acquire U = 3 keV at 30 MHz (but only 30 eV for 300 MHz), sufficient energy for causing ionization. Such ionization occuring in front of the antenna is in general not desirable since it is a source for power dissipation, it may cause antenna break down problems, and the creation of plasma near the antenna could lead to the

sheath related problems (Sec. 4.3.1-4.3.3). Fortunately, in a typical tokamak discharge, the neutral pressure is usually sufficiently low ($\approx 10^{-6}$ Torr) that the ionization is likely to be negligible. However, it is also important to minimize the locally enhanced neutral density (such as a nearby limiter and/or a gas feed) near the antenna surface to keep the neutral density to minimum. For example on PLT, a titanium gettering (which is an efficient pump of hydrogen) has been used between plasma discharges on the antenna surface to reduce the gas density. Also to reduce the electron secondary emission, the Faraday shield's surfaces are usually coated with the material with the secondary emission coefficient of less than one, such as carbon or TiC (titanium carbide). One should note that for lower-hybrid waveguide, some effort has been invested in developing the waveguide wall coating to reduce the secondary emission to minimize the rf breakdown problems.

4.3.5 Axial Convective Loss (ACL)

If the WKB condition is violated, the resulting standing wave (due to the reflected wave) in the plasma can result in a significant power loss in the axial direction from the antenna region. This process is important for the EPW region (Regime I & II). Since the EPW wave-packet propagates obliquely to the field (the propagation angle $\theta \approx v_g(\perp)/ v_g(\parallel) \approx k_\parallel / k_\perp << 1$) and it has a large axial group velocity, these multiple reflections can cause the rf power to 'leak' toroidally (axially) out of the antenna region. This process is termed the "Axial-Convective-Loss" or ACL process.[56] A simplified model for the ACL process is shown in Fig. 21. Since this axially lost power will likely to be absorbed at the plasma edge, it could result in the loss of heating efficiency and wall impurity generation.

The rf leakage is likely to be serious only in the electron plasma wave regime, $\omega > \omega_{pi}$ since in this low density regime, the WKB can break down relatively easily and the EPW group velocity is particularly large in the axial direction. The quantity of interest is the ratio of this toroidal leakage power to the useful radially inward rf power, P_{in}/P_{leak}. This factor can be estimated for EPW region as

$$\frac{P_{leak}}{P_{in}} \approx 2 A_{WKB} \frac{\Delta_{ep} V_{g\parallel}}{L_{ant} V_{g\perp}} \approx 2 A_{WKB} \frac{\Delta_{ep} (m_i / m_e)^{0.5}}{L_{ant} [1 - (\omega_{pi} / \omega)^2]^{1/2}} \qquad (4\text{-}7)$$

where $A_{WKB} \propto$ (standing wave ratio)^2 is a factor comes about due to the radial reflections, L_{ant} is the antenna toroidal length and Δ_{ep} is the thickness of the electron plasma wave region. Noting that $(m_i / m_e)^{0.5}$ is about 50, L_{ant} is about 100 cm, and $[\ 1 - (\omega_{pi} / \omega\ )^2]^{1/2}$ might be about 1/2 in average, one obtains a condition that $P_{leak} / P_{in} \approx 2A_{WKB}\ \Delta_{ep}$ (cm). This indicates that it is quite important to minimize both A_{WKB} and Δ_{ep} to obtain efficient IBWH launching. If the edge density is too low such that both quantities to be greater than one, a large fraction of the rf power might be lost through this rf leakage process. A numerical code has been developed to calculate the ACL power loss a multi-slab model.[56] The power efficiency factor defined as $(P_{in} - P_{leak}) / P_{in}$ is plotted in Fig. 22 for the typical experimental parameters for the low frequency experiment such as PBX-M / DIIID and for the high frequency experiment such as FT-U for various density profiles. As can be seen from the figure, the ACL loss is generally greater for the low frequency IBWH experiment. The low $n_{||}$ spectrum range also suffers larger ACL loss since WKB breaks down more easily for lower $n_{||}$ component which would suggests the importance of antenna phasing to reduce the low $n_{||}$ spectrum range.

4.3.6 Antenna Misalignment and Limiter Interference

Another potential problem for IBWH in the low frequency regime is the effect of antenna misalignment and limiter interference.[46] In addition to the plasma sheath problem described in Sec.4.3.3, the antenna misalignment could cause the $n_{||}$ spectrum of the launched wave to change, launching waves with shorter parallel wavelength than the value expected from the antenna geometry. One can estimate the maximum parallel wavelength to be $\lambda_{||}(\max) \approx \lambda_\perp / \theta_m$ where θ_m is the angle of misalignment. This effect is particularly strong for the case of the direct launching of short perpendicular wavelength IBW (Regime III). As we recall that in early IBW excitation experiment,[69] a very careful antenna alignment was essential for a successful IBW wave excitation. The problem tends to be more serious for a low frequency IBWH since the required minimum $\lambda_{||}$ for a good central heating tends to be larger and the alignment of the relatively long IBWH antenna is somewhat more difficult. The alignment problem is less severe for the electron plasma wave launching scheme due to the longer $\lambda_\perp$ (Regime I or II) and for the future higher frequency waveguide IBWH experiments[57,58]. Another potential problem might be the interference by the antenna protective limiters if they protrude significantly into the plasma since the relatively shallow initial propagation angle of the launched wave packet could cause it to hit the side limiters. If the limiters are made out of a resistive material such as graphite, significant fractions of the power might be absorbed by the limiter and such a

reflection may also introduce a change in the wave number spectrum. Calculations indicate that the protrusion length also should be no more than 1 cm, preferably only a few millimeters beyond the Faraday shield surface.

4.4 IBW Coupling Physics Summary

In this section, three coupling regimes I, II, and III have been discussed. The Regime III (direct IBW launching regime) may not be a good operating regime for high power experiment due the stronger antenna-plasma interaction as discussed in Sec. 4.3.1-4.3.3 which could cause anomalous antenna loading and impurity generation. In addition, launching IBW directly might be hampered by the generally low ion temperature expected at the antenna surface where the IBW excitation takes place. The Regime I would be quite acceptable for the high frequency waveguide experiment where the experience of lower hybrid waveguide coupling could be used. For the low frequency IBWH experiments with loop antenna, in order to avoid excessive reflection and the axial-convective-loss (ACL), the desired edge density might be that of Regime II where $\omega \approx \omega_{pi}$. Also due to the large ponderomotive force for the low frequency experiments, the edge plasma density might require some fine adjustment for a given rf power level. The antenna phasing appears to be important to reduce the ACL effect. The recent utilization of boron nitride antenna plates around the fastwave ICRF antenna has successfully reduced the rf induced edge currents and related edge rf power dissipation and impurity production.[101] This technique might provide a solution for reducing the edge sheath related problems even for the IBW B_θ-loop antenna.

V. "NON-HEATING" APPLICATIONS OF IBWH

In addition to plasma heating, the radio-frequency power might be used in some situations to enhance the performance of tokamak reactor. The rf current drive is a very good example (though strictly speaking, the rf current drive is a type of rf heating).[102] The feasibility of current drive by IBWH is discussed in Sec. 5.1. Application of large rf power inevitably leads to a major perturbation to tokamak plasmas that, in some cases, the effects may serve a useful function such as the plasma confinement improvements. In this section, we discuss the following possible "non-heating" applications of IBWHP: 1. Driving tokamak core currents; 2. Plasma confinement improvements as already observed in many of the IBWH experiments; 3. Stabilization of potentially deleterious external MHD modes such as the external kinks by the antenna ponderomotive force; and 4. Control of the plasma edge by the ponderomotive force to reduce, for example, the divertor plate heat load density and to modify the plasma potential for confinement improvement.

5.1 IBW Current Drive

Thus far, IBW has not been an obvious choice for driving the tokamak current for two reasons. The electron Landau interaction is much weaker than LHH as discussed in Sec. 3.3.1, although it is still large compared to the ICRF fastwaves. The oscillatory ray trajectory of IBW (Sec. 3.4) also makes it unsuitable for creating an asymmetric velocity distribution required for current drive. However, IBW may serve a useful function for driving tokamak currents in the high temperature burning reactor plasma situation. The wave penetration to the plasma core is quite excellent. As shown in Fig. 14, at the high temperature burning phase, it is still possible to put much of the rf power into the electrons in the plasma core. The enhanced electron Landau damping near the resonance [since $\mathrm{Im}k_\perp(\mathrm{ELD}) \propto n_\perp^3$, see Sec. 3.3.1] could give the desired current drive localization. The α-absorption which is deleterious for current drive should be avoidable (Sec. 3.2.6). For reactor size devices, a phased waveguide should be easily constructed for IBWH as in the case for the lower-hybrid current drive (LHCD). In Fig.23, the ray tracing calculation is shown for a reactor grade plasma at a relatively high central electron temperature of 20 keV. In this case, the electron absorption is central (near the plasma resonance). Moreover, the absorption in one direction is about 90 % indicating that the unidirectionality of absorption can be achieved for IBWH in a very high temperature plasmas. For lower temperature plasmas, what one would need is a target plasma with an asymmetric velocity distribution for IBW to damp preferentially in one direction. This might be achieved, for example, by using LHCD to produce a target plasma with an asymmetric velocity

distribution and such a distribution then might be maintained by IBWH. This synergy with LHCD might be investigated in FT-U and PBX-M where the sufficient amount of LHCD power will be available along with the IBWH power.

5.2 Plasma Confinement Improvements

During IBWH, the plasma confinement has shown a significant improvements (e.g., PLT[31], Alcator-C[36], and JIPPT-II-U[60]). The observed improvements usually are in the plasma core in contrast to the H-mode related edge improvements. On PLT, the microwave scattering diagnostic has measured a strong modification in the turbulence spectrum in the half-radius region.[30] These results suggest that IBW might be effective in reducing the low-frequency turbulences. This might be related to the fact that the IBW wavelength is similar to that of the turbulences or due to its strong non-linear ponderomotive force. Two theoretical models one based on a four-wave-mixing process and one based on the poloidal velocity shear generation are proposed for the turbulence suppression.

5.2.1 Stabilization of Microturbulences through Four-Wave-Mixing

In Sec. 3.4.3, we discussed the interaction of IBW with the low-frequency turbulences. With a finite amount of rf power, the side-bands ($\omega_0 \pm \omega$, $\mathbf{k}_0 \pm \mathbf{k}$) are generated by the beating of the incident IBW (ω_0 , $\mathbf{k}_0$) and the ambient low-frequency turbulences (ω, $\mathbf{k}$). The side-band disturbances then in turn beat with the primary IBW to produce low-frequency currents that can modify the stability of the low-frequency mode. This is a four wave mixing problem and in a weak turbulence condition, a nonlinear dispersion relation for the low-frequency mode has been derived yielding the frequency shift and the growth rate change of the low-frequency modes.[32] For IBWH, the stabilization of the tokamak dissipative trapped electron modes (DTEM) has been investigated. The analysis shows that the IBW with $k_\perp \rho_i > 1$, $\mathbf{k}_0 > \mathbf{k}$ could stabilize DTEM giving a relatively large stabilization parameter space. Relatively low required power for the stability is encouraging, e.g. the estimate of 100 kW for the PLT experimental parameters and 5 MW for the BPX parameters for the stabilization.

5.2.2 Turbulence Suppression by Non-Linear Velocity Shear

The suppression of edge turbulence by sheared plasma flow has been proposed to explain the improvement of confinement in the L- to H-mode transition.[103] The recent observations of locally reduced turbulence in the vicinity of shear layer even in non-H-mode discharges[104]

suggest that this mechanisms is not limited to the H-mode discharges. For IBWH, the nonlinearly-generated, ponderomotive ion poloidal flow was calculated and shown that the sufficient poloidal flow shear layer required for turbulence suppression can be created near the wave absorption layer.[33] The calculated required power for the PLT parameter is order of 100 kW which is consistent with the experimentally observed value. Since, this IBWH generated flow shear layer has a very good radial localization (order of the power absorption width), it might provide an active knob to control tokamak transport.

5.3 Utilization of Antenna Ponderomotive Force

As discussed in Sec. 4.3.4, the strong $E_{||}$ fields of high power IBWH antenna could create a region of large ponderomotive potential. Although, such large ponderomotive potential can cause difficulties for wave launching, some theoretical predictions were made to use the potential for tokamak performance improvements. One recalls that in the early days of fusion research, the ponderomotive potential was considered as a tool for providing plasma confinement (e.g. rf-plugging). This idea was largely abandoned due to the excessively large required power. However, the use of ponderomotive force might still be useful for aiding the plasma stability or for modifying the plasma edge region where the required power may be more reasonable. In a typical IBWH antenna situation, the near fields of the IBWH B_θ-loop antenna $E_{||}$ is maximum at the antenna surface and decays radially away from the antenna (into the plasma). This electric field gradient can give a rise to the ponderomotive force, $F_{pond} \approx 1/16\pi (\omega_{pe}^2/\omega^2)\partial|E_{||}|^2/\partial r$, where F_{pond} exerts a radially inward force onto the plasma electrons. The force could in fact become quite large that it might be used to stabilize the plasma external modes and to modify the plasma edge.

5.3.1 Stabilization of External MHD Modes

The stabilization of external modes have its root in the mirror experiments.[105] The theoretical analyses for tokamak plasmas suggest that the ponderomotive stabilization may be effective in stabilizing the external modes which causes the plasma boundary to move such as the external kink and the edge localized ballooning modes.[61,62] As the instability moves the plasma boundary closer to the antenna, it encounters a repelling force of the ponderomotive potential from the antenna fields. The analysis for the mode stability uses the modified energy principle,[61,62]

$$\delta W = \delta W_{MHD} + \delta W_{rf} \qquad (5.1)$$

where the term δW_{rf} which describes the change in plasma potential energy due to the work done against the ponderomotive force of the applied rf fields, was added to the usual energy principle for a tokamak plasma. The result suggests for PBX-M type experiments, the relatively low required power of 2 MW for stabilizing the edge localized ballooning modes with $n > 8$.[61] For the external kink, the required power would be larger, in the 10 MW range for the PBX-M parameters.[62] If the merit of stabilization is demonstrated, since the required power for the kink stabilization goes up with f^2B^2, the efficiency of the method must be improved considerably to extend this technique toward larger and higher field devices. To reduce the power requirement, it is advantageous to go down in frequency as much as possible. A suitable frequency appears to be near the lowest ion cyclotron frequency and for fusion plasmas, the frequency would be that of the tritium. One interesting possibility for reducing the power requirement significantly may be to modulate the rf power to 'feed-back stabilize' the modes. A simple estimate suggests that the rf modulation could reduce the required power by a factor of 10^{-1} to 10^{-2} from the steady-state value which would make the technique attractive even for the ITER size devices.[106]

5.3.2 RF Limiter Concept

The strong ponderomotive force of the IBWH antenna could also be used to modify the plasma edge region.[63] If it is possible to control the edge scrape-off layer distances, it can be used to control the power density of plasma impinging upon divertor plates. This is a critical technical issue for designing long pulse and/or steady-state reactor grade devices such as ITER.[107] The ability to repel most of the electrons in the antenna surface region and to form a positive ambipolar potential could be used to control the plasma transport near the edge such as in the case of H-mode study. This rf limiter concept was demonstrated in PISCES, a small scale test linear device.[63] In the experiment, the ponderomotive potential barrier, ponderomotive density depletion, positive edge potential formation and the F_{pond} x B drift velocity were measured. Some reduction in the edge turbulences has been also observed. Extension of this experimental technique to tokamak experiments such as on PBX-M is of the near term interest. If proven successful, the power scaling toward ITER size device will be the key issue.

VI ION BERNSTEIN WAVE HEATING EXPERIMENTS

Ion Bernstein wave heating experiments have been performed in the ACT-1 toroidal device and subsequently in several fusion devices in the past years. By utilizing already available ICRF transmitters and other rf hardwares, a series of high power IBWH experiments have been performed with a relatively modest investment of building the IBWH antennas. Many of the IBWH experiments were in fact performed as an extension of the ICRF heating program. In this section, the IBWH heating experiments which are concluded at the present time are reviewed in an approximately chronological order. On-going and planned experiments are reviewed in Sec. VII. Interested readers are referred to the original published papers for more detail.

6.1 ACT-1 (12-18 MHz)

The first IBW heating experiment was conducted in the ACT-1 toroidal device.[22] In this device, with an advantage of probe diagnostic, the physics of IBWH was investigated for all phases of the wave heating; IBW launching, propagation, absorption and heating.[19-22] In a hydrogen plasma ($T_e \approx 2.5$ eV, $T_i \approx 1.5$ eV, and $n_o \leq 10^{11}$ cm^{-3}), detailed measurements of wave absorption and of the ion temperature profiles have identified the heating layers near the ion-cylotron harmonics of deuterium-like (H_2^+) and tritum-like ions (H_2^+) where the dominant absorption resonances were $5\Omega_D$ and $5\Omega_T$. In Fig. 24, the ion temperature increase is shown as a function of frequency, confirming that the heating peaks near the heating layer. In this experiment, the antenna phase was chosen to avoid the electron Landau damping of the wave. Interestingly, as shown in Fig. 25, the central ion heating efficiency actually improves with the rf power as the higher ion temperature resulting from heating further improves the wave penetration. In the lower temperature range, the IBW power was initially absorbed partially near the plasma edge by the collisional absorption. As the ions are heated, the higher ion temperature increases the wave group velocity (since $V_g \propto V_{Ti}$, Eq. 3-3) and reduces the collisional absorptions (Im $k_\perp \propto V_{Ti}^{-4}$, Eq. 3-6). In the best case, the power balance estimates suggest that the ion heating is quite efficient (nearly 100%) for IBWH. Moreover, the ion heating was very much bulk ion heating without any significant ion tail production as monitored by the ion energy analyzer. This bulk ion heating nature of the IBWH could be explained by the quasilinear diffusion theory + collisions as described in Sec.4.3.3. The B_θ-loop was also tested on ACT-1 where the physics of IBWH wave loop-excitation and the antenna loading has been investigated in a considerable detail as discussed in Sec. 4.1.3.[50,95]

6.2 JIPPT-II-U (40 MHz)

The first tokamak IBWH heating experiments were carried out in the JIPPT-II-U tokamak device (R = 91-93cm, a = 21-23 cm, a circular plasma, $B_T \leq 3T$, $I_p \leq 100$-200 kA, and $\overline{n_e}$ = 1 - 3 x $10^{13}cm^{-3}$).[23] The IBW was launched by the Bθ-loop Nagoya Type III antenna.[24] The transmitter frequency was 40 MHz. Two important heating regimes, Mode-I [23] and Mode-II,[26] were identified.

6.2.1 Ion Heating Regime : Mode-I

An efficient central ion heating regime was observed near 1.8 T in a majority hydrogen plasma (H-He or H-D) which corresponds to $3\Omega_D$ (or $3/2\ \Omega_H$) layer located near the center of the plasma (Fig. 12).[23,25] Due to the relatively high aspect-ratio nature of JIPPT-II-U (R/a ≈ 4), other major resonances such as Ω_H, $2\Omega_D$, $2\Omega_H$ and $4\Omega_D$ layers are outside of the plasma in this experiment. In a hydrogen-deuterium mixture plasma, both hydrogen and deuterium ion heating was observed. The observed ion heating has a strong magnetic field dependence as shown in Fig. 26. The maximum heating was observed when the resonance layer is placed near the center of the plasma axis. This central heating of hydrogen ions was also measured directly by a spectroscopic technique.[25] From the measured $T_\perp > T_{||}$, it was concluded that the hydrogen ions are directly heated by a non-linear heating process at the $3/2\ \Omega_H$ resonance in addition to the $3\ \Omega_D$ deuterium ion heating. The experimental data was analyzed by a tokamak IBW heating modelling code.[15] This code was developed by combining a tokamak transport code[91] with an ion Bernstein wave tokamak ray tracing code.[2] This modelling code was able to reproduce many of the observed heating features such as the temporal ion temperature evolution as well as the strong heating dependence on the magnetic field (the curve in Fig. 26) which comes about due to the relatively well localized power deposition profile of IBWH (Fig 12d). Qualitatively speaking, $n_i(r)\ \Delta T(r) \approx (P/V)\ \tau_i\ (r)$ where P/V is the deposited power density and τ_i (r) is the local ion energy confinement time. The central ion heating is effective due mainly to the reduced heating volume or larger heating power density.

6.2.2 Electron Heating Regime : Mode-II

An interesting electron heating regime (termed 'Mode-II' in contrast to the ion heating regime of previous Mode-I) was observed at 2.76 T with 40 MHz. This experiment was carried out in a mostly deuterium plasma. It is a third harmonic Ω_D launching and second Ω_D

or fundamental Ω_H heating regime, quite similar to the fastwave hydrogen minority experiment. The electron temperature increases rapidly after the rf turn-on in the central region of the plasma ($r/a < 0.5$). While ion temperature increases more gradually with the time constant of about 10 ms which is roughly equal to the collision time between electrons and ions. The charge-exchange spectra show that the velocity distribution functions for both hydrogen and deuterium are nearly Maxwellian with a slight high-energy tail for the hydrogen (this might be due to a presence of small amount of fastwave component launched by the antenna[29]). This heating regime is clearly different from the Mode-I IBWH ion heating regime and also from the fastwave hydrogen-minority heating regime. The power balance analysis retaining electron ohmic confinement indicates that the best agreement with the experimental observation is obtained assuming most of the rf power ≈ 80% is absorbed by the electrons. The bulk ion temperature rise is consistent with the collisional heating from electrons in terms of its magnitude and temporal behavior. The main physics reason for the electron heating can be understood from the wave accessibility point of view. The heating resonance in this case is majority deuterium second harmonic and the minority hydrogen fundamental. From IBW wave dispersion relation, one should note that as the wave approaches this major resonance layer, the wave number increases and the group velocity slows down considerably both of which contribute to the enhanced electron Landau damping. In the experiment, the higher ohmic central electron temperatures (resulting from the 2.7 T operation for Mode II compared to the 1.8T operation for Mode-I) are also expected to aid the electron absorption. Therefore, most of the IBW power could be expected to be absorbed through electron Landau damping before it reaches the ion cyclotron absorption layer. This result is a meaningful demonstration of the electron Landau absorption by IBWH which might lead for example to the utilization of IBWH for the rf current drive (Sec. 5.1).

6.3 PLT (30, 90 MHz)

Following the JIPPT-II-U IBWH experiment, IBWH was investigated in the Princeton Large Torus (PLT), R = 132cm, a = 40cm, $B_T \leq 3T$, $Ip \leq 400$ kA, $\overline{n_e} \leq 5 \times 10^{13}cm^{-3}$.[27-31] Two new heating regimes were investigated: $5\Omega_D$-minority heating with a 90MHz source and 3/2 Ω_D majority heating with a high power 30 MHz source. The 3/2 Ω_D heating has heated deuterium bulk ions to 2 keV from 500 eV and the IBWH power in excess of the ohmic power was applied to the plasma for the first time.

6.3.1 Fifth-Harmonic Ω_D Minority Heating

Utilizing the 90 MHz transmitter, the fifth harmonic Ω_D minority heating was investigated in a hydrogen majority plasma.[27] In Fig. 27, the heating configuration and IBW wave trajectories are shown. Due to the off-axis antenna configuration, the ray-tracing was performed starting from the antenna current maxima for various launched $n_{||}$. In this experiment, most of the wave power is expected to be absorbed by the deuterium ions at the 5 Ω_D layer. In Fig. 28 , the observed ion temperature evolution for $P_{rf} \approx 100$ kW at a line average density $\overline{n_e} = 1.5 \times 10^{13}$ cm^{-3} at $B_T = 27$ kG is shown. The perpendicular component of the deuterium velocity distribution is heated rapidly to ≈ 1.5 keV which then comes down as the plasma density increases. The parallel component of the deuterium temperature as well as the bulk hydrogen temperature increases at slower rate as expected from the collisional power transfer from the heated component. It is interesting to note that the even the heated ion species retains near Maxwellian energy distribution function as might be expected from the quasi-linear rf diffusion characteristics of IBWH.

6.3.2 3/2 Ω_D and ^{3}He-minority Heating Regime

The 3/2Ω_D heating was investigated since the high power 30 MHz ICRF rf transmitter was already available on PLT. From the wave launching physics point of view, this regime is somewhat unique in that the IBW frequency is now operating below the hydrogen fundamental frequency which can modify the wave launching physics (as discussed in Sec. 2.2). In Fig. 29(a), the temporal evolution of the charge-exchange deuterium ion temperature during 3/2 Ω_D heating at 150 kW level is shown. The ion temperature goes up relatively quickly in the time scale of the ion energy confinement time. The measured perpendicular energy distribution is near Maxwellian without noticeable ion tail as expected. The parallel ion temperature is similar to the perpendicular temperature which is consistent with the fusion neutron based ion temperature. In PLT, due to the longer ion energy confinement compared to the JIPPT-II-U case, the ion temperature isotropization is expected. The heating was observed to peak near 28 kG which corresponds to the heating layer being near the plasma axis as in the case of the JIPPT-II-U case.

High Power Heating - The 3/2Ω_D heating was extended toward higher power level utilizing the 30 MHz high power transmitters for the ICRF fastwave heating experiment.[27] This is the 3/2 Ω_D heating regime with optional ^{3}He resonance. The temporal evolution of the ion temperature

is shown in Fig. 30(a) with the power level of 500 kW at $\overline{n_e} = 3 \times 10^{13} cm^{-3}$. The central Doppler broadening ion temperature reaches 2 keV exceeding that of the TVTS central electron temperature (≈ 1.6 keV). In Fig. 30(b), the measured ion temperature profile from the Doppler broadening measurements of various ion lines are shown indicating that the heating is central. No strong ion tail was observed by the charge-exchange diagnostic as expected for the majority bulk ion heating. This measured ion temperature profile is similar to the calculated profiles assuming ohmic like ion transport [the curves in Fig. 30(b)], an indication of no ion transport deterioration during IBWH. The ion heating efficiency was found to be nearly constant up to a 650 kW level, with a heating quality factor of $\Delta T_i(0)\ \overline{n_e} / P_{rf} = 6\text{-}7 \times 10^{13} eV\ cm^{-3}/kW$ which is comparable to the PLT fastwave ^{3}He-minority heating results. The global energy confinement shows a gradual degradation with increase rf power . The degradation could be attributed solely to the enhanced radiative losses in the electron channel during IBWH.

Particle Confinement Improvement - With application of IBWH, the plasma density was observed to increase by more than a factor of three as shown in Fig. 31(a). This occurs without active gas puffing and without increasing particle recycling, as indicated by the drop in the D_α emission particularly near the antenna. From the D_α emission measurements around the device, it was concluded that the density rise was due mainly to the particle confinement improvement. From fusion neutron, spectroscopic, Bremsstrahlung, and bolometric measurements, it was concluded that the incremental density rise is due in most part to the increase of deuterium ions. Similar factor of 2-3 confinement improvements were observed for helium (low Z) by a helium gas-puff and selenium (high Z) by the impurity injection technique. This Z-independent confinement improvement suggests non-classical particle transport behavior.

Low-Frequency Turbulence Modification - An interesting change in the low-frequency turbulence activity was observed during PLT IBWH. Microwave scattering technique was used to detect the waves in the half radius region of the plasma.[108] As shown in Fig. 32, the scattered turbulence signal amplitude has gone down by an order of magnitude (from the ohmic discharge with similar density) and the frequency has up-shifted indicating an increasing poloidal plasma rotation in the electron diamagnetic drift direction. This observed poloidal drift velocity of 5×10^4 cm/sec corresponds to an effective increase of the radial electric field of 15 volt/cm in the radially inward direction. The relationship between microturbulence (and plasma transport) and IBWH is a very interesting puzzle, suggesting that the processes such as the

ones proposed in Refs. 32,33 might be indeed occuring. An understanding of this problem could lead to a development of an active technique for improving tokamak plasma confinement.

Impurity Generation - During high power IBWH, an increase in the influx of metallic impurities (predominantly iron) was observed. This high-Z impurity influx could result in non-negligible central radiative losses during high power (high density) IBWH and could limit the rf power which can be applied to the plasma. By using carbon coated Faraday shields, it was possible to reduce the ion flux which lead us to conclude that the much of the iron influx has originated from the antenna Faraday shields in this experiment.[109] The carbon coating has allowed the IBWH experiment to go toward higher power. This finding demonstrates that the Faraday shield design is an important element for the future IBWH antenna development.

6.4 Alcator-C (184MHz)

Paralleling the PLT IBWH experiments, IBWH heating in the high density regime was investigated in Alcator C under the following conditions: R = 64cm; a = 11.5 - 12.5 cm; f = 183.6 MHz; B_T = 4.8 T - 11T; Ip = 160 - 260 kA; $\overline{n_e}$ = 0.5 - 4.0 x 10^{14} cm^{-3}; $P_{rf} \leq 180$ kW; hydrogen majority plasma with deuterium minority, n_D / n_e = 0.1% - 20% ; and Z_{eff} = 2-3. Three heating regimes were investigated: $\omega = 5/2\ \Omega_H$ (5.1T); $\omega = 3/2\ \Omega_H$ (7.6T); $\omega = 5/2\ \Omega_D$(9.3T). As shown in Fig. 33, the observed heating efficiency improves with the magnetic field and the best heating efficiency is observed at 9.3T. At $\overline{n_e} = 10^{14}$ cm^{-3}, an excellent ion heating of $\Delta T_i \approx 350$ eV has been observed at $5/2\ \Omega_D$ with the IBWH power of 100 kW. In terms of usual heating quality factor $\Delta T_i\ \overline{n_e} / P_{rf}$, this heating represents a phenomenal ≈ 40 x 10^{13}eV cm^{-3}/kW. Scanning charge-exchange analyzer measurements show that the observed ion heating is central with a superthermal deuterium component at T_D = 2 keV which is expected for the $5/2\Omega_D$ heating. The heating exhibited a non-linear behavior with a threshold power of ≈ 30 kW which is similar to the value expected for the non-linear absorption.[78] In this heating regime, the $\omega = 3\ \Omega_D$ layer is located at 2 cm in front of the antenna. From the linear theory (Sec. 3.2.3), the IBW absorption across the $\omega = 3\ \Omega_D$ layer should be complete that the central heating should not be possible. There are several possible explanations. First, the field ripple of 2-4% expected near the Alcator C access port could move the $3\omega_D$ resonance layer behind the antenna surface at the both ends of the antenna allowing the wave to penetrate there. Second, since the deuterium is a minority species (≈ 2%), the rf power deposited to the deuterium minority ions in the ripple region could deplete (pump out) the deuterium concentration sufficiently to allow for the power penetration. In this case, the power threshold

should also exists. Thirdly, the density at the 3 Ω_D deuterium layer might be depleted (perhaps by the ponderomotive force) sufficiently to be in the EPW regime (which is not expected have much interaction with the ion cyclotron harmonic resonances) to allow the power transmission. In addition, it was also suggested that the parametric instability could cause the decay waves to penetrate further into the plasma.[107]

Improved Particle Confinement Regimes - Improvements in the particle confinement time τ_p, of up to 3 times that of the ohmically heated plasma was observed for $\overline{n_e} < 2 \times 10^{14} cm^{-3}$. The hydrogenic species confinement improvement was estimated from the increased density and the H_α measurements. The improvements were also seen for the impurity ions by injection of trace amounts of silicon using the laser blow-off technique. Under the best condition, the decay rate was slowed by a factor of 3. The Z_{eff} is typically constant or decreasing during the rf injection. Those particle confinement improvements are quite similar to the PLT IBWH results.

CO_2 Laser Scattering - In the Alcator C IBWH experiment, the CO_2 laser scattering was used successfully to directly detect the launched IBW for $k_\perp$ = 10 - 140 cm^{-1}.[34] The IBW was identified from the wave dispersion relation obtained from the measured $k_\perp$ spectrum as shown in Fig. 34. The optimum detected IBW signal was obtained when the ion cyclotron harmonic layer is located just behind the antenna as expected from the IBW launching theory. The absorption at 3/2 Ω_H was observed by monitoring the IBW signal across the absorption layer. In relation to the 5/2Ω_D heating, a strong radial attenuation of the scattered signal was observed across the 3Ω_D layer suggesting a strong absorption of IBW at the layer. The observed scattered signal also had the inverse relationship to the low-frequency plasma turbulence level that the detected signal decreased with the plasma density.

High Density Regime - As the plasma density was raised above 1.1 x $10^{14} cm^{-3}$, the heating and particle confinement improvements show a rapid drop, and for the target density above 2.5 x 10^{14} cm^{-3}, no observable heating (Fig. 35) nor the confinement improvements (Fig. 36) were seen. A suggestive explanation is that the increasing low-frequency turbulence in the high density regime could scattered the wave power to prevent the wave penetration to the plasma core. The CO_2 scattering experiment appears to support this mechanism. However, the detailed analysis of the ray-tracing code with Monte Carlo calculation (to include the scattering effect) indicates that the actual power scattering may not be large enough to account for the observed lack of heating. It should be mentioned that the CO2 layer scattering (which

has very little vertical resolution) is rather sensitive to the phase coherence of IBW that the detected signal could drop significantly just due to the wave coherence destruction (not power dissipation) by the scattering. The lack of heating may also come from the enhanced plasma transport behavior observed in the high density regime. A detailed power balance analyses of the Alcator-C discharge indicate that the increased ion thermal conduction from the Chang-Hinton neoclassical value at $\overline{n_e} = 10^{14}$ cm^{-3} to 5-8 time the value at $\overline{n_e} = 2 \times 10^{14}$ cm^{-3} is sufficient to explain the lack of observable heating.[37] The future test of IBWH in this regime may require higher rf power and/or other tools to improve the transport in this regime .

6.5 TNT (5-8MHz)

Physics of tokamak ion Bernstein wave coupling, propagation, and heating was investigated in the TNT-A tokamak, a small research tokamak with R = 40 cm, a = 8.8cm, elongation of 1.2, and Ip = 4-6 kA.[38-40] The TNT experiment has shown in detail the loading characteristics of the IBWH antenna.[39] In this experiment, T-shaped rotatable antenna was used for comparison between B_θ (IBW-type) and B_z (fastwave-type) couplings. The frequency of 5 - 8 MHz used in the experiment means that the mode-transformation density is near 10^9 cm^{-3} (Sec. 4.2.4). Since the tokamak plasma density is still quite high ($n_{eo} \approx 10^{13}$ cm^{-3}), the coupling physics in this experiment can be considered to be fully in Regime I where IBW is directly launched. The small antenna (7 cm) and the low wave frequency (5.6 MHz) makes the antenna $n_{||}$ spectrum rather wide (extending up to a few hundred). The antenna loading decreases for the phased case (high $n_{||}$ phasing where $\omega/k_{||} \approx 1 \times 10^8$ cm/sec << V_{Te}). Therefore, a considerable fraction of the wave spectrum might be heavily electron Landau damped near the antenna in this experiment. The loading only weakly depends on the magnetic field. The loading generally increases with the rf frequency and also with the plasma density. This loading behavior is consistent with the high $n_{||}$ loading case.[95] The loading decreases with the rf power which is likely to be attributable to the density drop expected due to the ponderomotive potential. In addition to the antenna loading, the wave propagation was also studies in TNT where the magnetic probe has detected the magnetic field dependent features as expected from the ray tracing calculations. During the IBWH experiment, the electron heating[38] as well as ion heating[40] was observed.

6.6 JFT-II-M (27MHz)

The IBWH was first attempted in a diverted plasma in the JFT-II-M tokamak. In this experiment, the antenna was installed significantly off the mid-plane (placed about 45° poloidally from the mid-plane). The rf frequency was 27 MHz and the $3\Omega_D$ or $3/2\Omega_H$ heating was investigated around 1.2T magnetic field. The stored energy increase has a magnetic field dependence which appeared to be optimized around 1.2T where the heating layer is near the plasma center. However, the application of rf power produced significant impurity generation (the large radiative loss up to three times the applied rf power) that the maximum rf power injected was only about 150kW. Strong metallic impurity influx, Ti (Faraday shield material) and Fe (the vacuum vessel material) was observed. The radiative loss caused the electron temperature to decrease and together with the impurity contamination, the loop-voltage likewise increased. With the NBI heating(570 kW), this radiative collapse could be avoided up to the rf power of 300 kW. However, due to the strong edge cooling, the IBWH quenched the H-mode even with a relatively low power. The wall impurity influx in addition to that from the Faraday shield suggests a significant power deposition in the plasma surface region. The off-axis placement of the IBWH antenna may be causing the edge heating and subsequent impurity generation in the JFT-II-M IBWH experiment as described in Sec. 3.4.2.

6.7 DIII-D (30-60MHz)

The IBWH research was carried out in the DIII-D tokamak, which is a large size D-shaped tokamak with a divertor.[42,45,51] The DIII-D IBWH experiment had two phases. The first phase of experiment concentrated on a systematic search for central ion heating in the $\omega = 3/2\Omega_H$ ($3\Omega_D$) regime in hydrogen plasmas with a deuterium minority species. An extensive search for the central IBW heating under a wide range of plasma conditions failed to produced evidence of significant increases in the core ion temperature. For this reason, the second part of the effort was devoted to evaluate a large number of possible explanations for the phenomena observed during high-power IBWH injection. The edge ion heating which is well-correlated with parametric decay activity was observed. Other effects not predicted by the standard linear theory of IBWH were also observed and studies: power dependence of the antenna loading, particularly of the reactive component, the magnetic field independent antenna loading, and electron heating in the plasma scrape-off layer. Toward the end of the investigation, a possible explanation for many of the observed phenomena was developed, centered around the importance of the ponderomotive force near the antenna.

Plasma Impurity Control - The high-Z impurity influx problem was observed during IBWH in most conditions studies in DIII-D, resulted in a substantial increase in radiated power. The increment in radiated power was usually observed to be between 50 to 100 % of the injected rf power. From the sheath physics point of view, the antenna surfaces particularly the Faraday shields would be subjected to severe ion bombardment causing severe impurity problem. However, the radiation increase was shown to be predominantly from the nickel line; this finding is significant since the IBW antenna has no exposed Ni-bearing surfaces, while the vacuum vessel walls and protective tiles near the outer midplane are composed of stainless steel and inconel. This observation suggests the sheath related problem on the antenna Faraday shield may not be the dominant process, and this observation may be consistent with the ponderomotive density depletion near the antenna surfaces, reducing the antenna-sheath interaction. The Ni levels were reduced by more than two orders of magnitude just after the carbonization compared to just before. The radiated power was reduced to only one-third of the rf power, essentially solving the impurity problem during IBWH. Under freshly carbonized wall conditions, I MW of net rf power was coupled for 0.1 second, a world record for the B_θ-type antenna.

Antenna Loadings - An extensive antenna loading measurements were taken during IBWH. The measurements have clearly shown that the antenna loading has no strong magnetic field dependence for all the edge conditions looked. For the diverted discharge, the edge density is expected to be small that the antenna loading is dominated by the electron plasma wave (Regime I or II) and thus, the weak dependence is not surprising. On the other hand, in limiter discharges, the measured edge density is sufficiently high that $\omega < \omega_{pi}$ condition should be satisfied at the antenna surface. Under these high edge density conditions, the antenna loading is predicted to be highly toroidal magnetic field dependent. The measured loading however showed no hint of the expected resonant dependence on B_T. A very informative finding came from the power dependence of the reactive component of the antenna loading. It was found that raising the rf power level has the same effect as moving the plasma away from the antenna; the reactive loading decreases in both cases, as shown in Fig.37. This may be interpreted as an evidence of ponderomotive density depletion in front of the antenna. This ponderomotive force which is quite strong for the low frequency experiment (as discussed in Sec. 4.3.4) may be always strong enough to reduce the density in front of the antenna to bring it into Regime I or II. If the strong density hall is developed in front of the antenna, the axial-convective-loss (ACL) may prevent the coupling into IBW. This would results in the wall impurity influx as well as the electron heating in the scrape-off region as observed in the experiment.

Parametric Instabilities - The DIII-D IBWH experiments provided the first clear evidence of parametric activities during IBWH. Under conditions where efficient coupling to IBW was theoretically predicted, heating of ions in the edge plasma was observed. The edge ion heating was well-correlated with parametric decay activity, detected with rf probes in the scrape-off layer. The decay waves were identified as an ion cyclotron quasimode (ω_1) and an IBW (ω_2). From the qasimode frequency where ω_1 is expected to be near Ω_i, the location of the decay was identified to be near the low-field side of the plasma, i.e., near the antenna. A typical parametric decay spectrum is shown in Fig. 38(a), along with the hydrogen neutral particle charge exchange spectrum observed during the same discharge. Both hydrogen and deuterium ions showed high-energy perpendicular tail formation [shown in Fig. 38(b)]; no parallel heating was observed. The time behavior of of the charge exchange signal indicates that the confinement time of the high-energy ions is much less than 1 msec, indicating that the high energy ions were generated near the plasma edge. In some cases, estimates of the fraction of the applied rf power which is required to account for the observed edge heating suggest that the parametric decay channel could indeed drain a significant fraction of the applied rf power.

VII ON-GOING AND FUTURE IBWH EXPERIMENTS

As described in Sec. V, there are a number of possible utilization of the high power IBWH in addition to the conventional plasma heating. Those applications of high power rf aim to improve the tokamak performances; the rf current drive, the plasma confinement improvements, the plasma external mode-stabilization, and plasma scrape-off layer (SOL) control. The on-going and future IBWH experiments are addressing some of those research topics. On JIPPT-II-U, the physics of plasma confinement improvement by IBWH is being investigated. On PBX-M, using the variable frequency high power transmitters (40-80 MHz), the pressure profile control to aid the access to the second stability region will be investigated. Use of the non-linear effects to improve plasma confinements, mode stability and control of SOL will be also considered. With the FT-U waveguide IBWH experiment, the IBWH is moving for the first time into an exciting regime where one can test the reactor relevant waveguide launchers which can demonstrate the viability of IBWH for future ignition and/or steady-state experiments. Possible synergistic effects current drive with LHCD can be also explored on PBX-M & FT-U.

7.1 JIPPT-II-U (130 MHz)

The IBWH experiment was conducted with the 130 MHz RF system in JIPPT-II-U at 3T field.[59,60] The JIPPT-II-U 130 MHz experiment has some features which are significant for the IBWH research. First, the three element center-fed antenna design has permitted the launching of a relatively well defined $n_{\parallel}$ spectrum for the first time. In terms of the power handling capability, the radiated antenna power of 400 kW was achieved limited only by the transmitter output power. The relatively high frequency of 130 MHz increased the mode-transformation density to $4 \times 10^{11} cm^{-3}$ (an order of magnitude increase from the previous JIPPT-II-U 40 MHz experiments)which is more consistent with the JIPPT-II-U edge plasma density. Lastly, this frequency has permitted for the first time (at a reasonable magnetic field of 3T), the investigation of $3\Omega_H$ heating (with $4\Omega_H$ launching which is the highest hydrogen harmonic frequency thus far). This mode of heating is similar to the one being planned for FT-U.

Heating Results - During IBWH, the ion heating has been observed by both the charge exchange diagnostic as well as the Doppler spectroscopy. With neutral beam heating, the ion temperature profile has been also measured using the charge-exchange recombination spectroscopy (CXRS).[59] The ion heating result is shown in Fig. 39. With about 350 kW of injected IBWH power, the central ion temperature increased from about 600 eV with 350 kW of NBI alone at the central density of $4 \times 10^{13} cm^{-3}$ to about 900 eV at the central density of $8 \times 10^{13} cm^{-3}$ which is a quite

respectable heating efficiency. The central electron temperature increased from the ohmic values of the similar density plasmas. Due to the central density rise, the net energy increase in the central region of the plasma is quite significant.

Observation of the Peaked Density Profile during IBWH - During the JIPPT-II-U IBWH experiment, the peaking of the density profile was observed by the multi-channel FIR laser interferometer system. In Fig. 40, time evolution of the density profile peaking factor k defined as $n_e = n_{e0} (1 - (r/a)^2)^k$ and the central density is shown. The density peaking during IBWH is quite evident. The steepening of a strong density gradient at about the half-radius region during IBWH can be seen. This observation may be related to the previous particle confinement improvements observed in PLT and Alcator-C.

Plasma Transport Analysis During IBWH - Using the measured density and temperature profiles, some plasma transport analyses have been performed.[60] The particle confinement during NBI alone deteriorates roughly by a factor of two from the ohmic value. With an addition of IBWH, the confinement improves to the level of the OH alone case. The particle confinement improves further by a factor of two when the NBI is turned off. The electron and ion energy diffusivities were calculated using the measured profiles and the calculated energy deposition profiles. As shown in Fig. 41, compared to the NBI alone case, the ion energy diffusivity decreases in the plasma core region where the IBW power is deposited. On the other hand, the electron energy diffusivity appears to decrease more broadly with the addition of IBWH. This is an encouraging result since in this experiment, the total heating power is already roughly three times the ohmic power.

Future JIPPT-II-U IBWH Topics - Due to the importance of tokamak transport for the future fusion program, it would be of interest to investigate the cause of the plasma transport improvement during IBWH. Several profile diagnostics on JIPPT-II-U including the multi-channel FIR laser scattering system, and the 0.5 MeV-Heavy-Ion-Beam for the fluctuation and potential diagnostics are being prepared. Also the present stainless steel Faraday shields are being coated with a thin carbon layer to reduce the metallic impurity influx as in PLT which should further reduce the radiative losses during IBWH.

7.3 PBX-M (40-80MHz)

A multi-megawatt level IBWH experiment is under preparation on PBX-M.[52] The goal of the experiment is to contribute to the attainment of the high beta, second regime of stability. The high power IBWH will be used as an additional heating power source (up to 6 MW) to supplement the

existing 6 MW of NBI power to achieve higher β values in PBX-M. Bulk ion heating with localized, off-axis IBWH power deposition may provide a tool to modify the pressure profile for improved plasma stability at high β. The high power off-axis heating in principle can generate a significant bootstrap current (≈ 30 %) in the high β_{pol} PBX-M plasma, complementing LHCD for broadening the current profiles (reducing the central q) which is desired for the access to the second stability. The confinement improvements of the strongly NBI heated plasmas (as observed in the JIPPT-II-U 130 MHz experiment) would be of a practical interest to PBX-M. It is also worthwhile to note that the available rf power (multi-megawatt) is comparable to the predicted power levels required to slow down the growth rate of pressure driven modes (such as the high-n ballooning[61]) and the external kink modes[62] in the presence of the closely fitted stabilizing shell configuration of PBX-M. The high power IBWH antenna could be also used as an rf limiter. The localized electron heating capability of IBWH may be used in conjunction with LHCD to yield a desirable synergistic effects on current drive and current profile control. In addition, the PBX-M IBWH experiments could provide important reactor relevant information on IBWH performance in the diverted high-β plasmas.

Prototype High Power IBWH Antenna Test. A prototype 1 MW IBWH antenna was tested on PBX-M.[52] The IBWH antennas is placed in the PBX-M outer midplane region at R = 200 cm. The antenna is a center-fed design to eliminate the low-$n_{||}$ spectrum. The magnetic field was around 13 kG putting the 4 Ω_D layer near the center of the plasma for the 41 MHz rf frequency. In a relatively short time, the applied power was increased to 660 kW steady-state and(900 kW transiently which was near the arc-limit of the transmission line). The power was limited only by the transmitter output power.

Some Observed Features - Throughout the experiment, parametric instability activities were monitored by an rf probe placed a few port away from the antenna, placed poloidally near the outer mid-plane. Both electrostatic and magnetic signals showed no sign of parametric instability activities for 50 db down from the pump. During IBHW, no sign of serious impurity problem was observed with the plasma Z-effective remain relatively unchanged. There is some indication of increased titanium level during IBWH suggesting an influx from the Faraday shield rods which are TiC coated. A second antenna with a carbon coated Faraday shield has been installed for a comparison test. IBWH was also added to a significantly (2 MW) NBI heated plasma. The incremental stored energy increase was similar to that of the NBI heating. The main stored energy increase could be accounted by the electrons. In this regime with $2\Omega_H$ (and $4\Omega_D$) heating, with the phased antenna ($n_{||} \approx 8$), most of the rf power is expected to flow into electrons. The application

of IBWH also had a moderating influence on the sawtoothing behavior in a strongly NBI heated discharge.

7.4 FT-U (430 MHz)

The FT-U experiment is the first IBWH experiment to test the IBWH waveguide launcher.[57] A schematic of the launcher is shown in Fig 20. It is a two waveguide system capable of being phased. There will be three waveguide launchers of this type for the 1.5 MW experiment. The 430 MHz frequency was chosen for the $4\Omega_H$ heating at 70 kG field. At this frequency, a simple vacuum waveguide could fit within the 40 cm high port on FT-U. The waveguide width is 2 cm each. As discussed in Sec. 4, the FT-U IBWH frequency of 430 MHz is approaching that of the lower-hybrid wave frequency (e.g. earlier LH heating experiments has been in the 600-800 MHz frequency range). For this reason, the coupling physics should be considerably simplified compared to the antenna with Faraday shields. The ponderomotive force is also greatly reduced which could simply the waveguide placement. With the large available lower hybrid power on FT-U, synergistic effects of IBWH and LHCD could also be explored.

7.4 Heating of Burning Plasmas (200-250 MHz)

If the FT-U waveguide IBWH experiments works well for heating plasmas in high density regime, similar waveguide launcher could be used in the high field burning plasmas such as BPX.[58] Possible heating regimes are shown in Fig. 42. The preferred frequency is $5\Omega_T$ for D-T operation at the full field and $4\Omega_D$ or $5\Omega_D$ for the lower field deuterium or hydrogen operation. The rf frequency of 200-275 MHz should permit the waveguide launcher with $\approx$ 1m height which should fit nicely in the BPX size port space. Sine the available port width is relatively wide, a four-element phased waveguide launcher could be used to control the wave $n_{\parallel}$ spectrum. As discussed in Sec.3.3.6, IBWH is attractive for directly heating the tritium without being affected by the fusion α-particles. In addition, the shorter wavelength of IBWH could be used to directly heat the tritium ions without producing high energy tail ions, perhaps optimizing the fusion reactivity by keeping the heated tritium population in the range of 40 -100 keV where the fusion cross section assumes maximum.

VIII. CONCLUSIONS

As we look toward future IBWH experiments, it is clearly important to develop and establish reliable and efficient IBW launching techniques. This would involve identification of the root cause of power draining parasitic channels and coming up with acceptable remedial measures. This may involve antenna improvements as well as identifying the acceptable operational parameter range for IBWH. The on-going efforts on PBX-M, JIPPT-II-U and FT-U should provide additional important experimental data for the large plasma and operational parameter space. If this can be accomplished, IBWH offers many interesting possibilities due to its unique wave characteristics. For reactor situation, it could offer an option for heating fusion ions directly ($5\Omega_T$ or $2\Omega_T$) without being affected by the fusion α-s (Sec. 3.3.6). The quasilinear diffusions of ions in the intense IBWH fields is certainly of interest for maximizing the fusion yields. The tendency for the ion acceleration to stop at some reasonable energy ($E_i \approx 15\ T_e$) is a potentially useful property of IBWH. This suppression of run away ion acceleration should be a meaningful experimental and theoretical research topic. Furthermore, it should be of considerable interest to investigate IBWH in a plasma with a significant α-population (or high energy ions) to verify the theoretical prediction of negligible α-damping for the direct tritium heating scenarios. The current drive possibility might be also explored due to the potential importance for driving current in burning plasmas.

The IBWH heating experiments are moving toward high frequency range in order to expand the data base toward ignition experiments. The JIPPT-II-U 130 MHz and FT-U 430 MHz experiments are excellent forerunners of this trend. The FT-U experiment offers for the first time, the capability to launch ion Bernstein waves via a reactor relevant waveguide launcher. As demonstrated by the LHH experiments, the coupling physics of phased waveguide launcher is considerably more well understood than that of the B_θ loop antenna with Faraday shields. The higher frequency also should make the IBWH much less susceptible to the non-linear effects such as the ponderomotive potential. Assessment of the waveguide launcher compared to a B_θ loop antenna with Faraday shields is an important future topic for the IBWH.

At present, it is not clear what process is causing the confinement improvements during IBWH as observed in PLT, Alcator-C and JIPPT-II-U. This process (or processes) does not appear to be a simple edge potential modification as caused by the ponderomotive potential since the changes are taking place well inside the plasma interior. Also since this improvement was observed in the high density and high frequency experiments such as in Alcator-C and JIPPT-II-U, the prospect of confinement improvement may still be good for FT-U and high field ignition experiments. If the improvement is due to the microturbulence suppression such as the ones proposed in Refs. 32-33,

the power required might still be acceptable. The high power IBWH experiments should yield further data particularly with high power NBI heating in the high beta regime.

For heating non-tokamak helical plasmas such as LHS, IBWH might be attractive since it does not produce run-away ion tails. However, some fundamental conditions might need to be satisfied. One of the important requirement is to launch sufficiently fast wave so as to avoid electron Landau damping. The parallel phase velocity, $f\,\lambda_{||}$ must be large compare to electron thermal velocity, V_{Te}. For a helical plasma, due to a relatively large magnetic field variation the toroidal direction, the maximum effective $\lambda_{||}$ which could be excited might be some fraction of the helical distance (here one can no longer assume the toroidal wavenumber conservation). For LHS, if $\lambda_{||} \approx 100$ cm $<<$ $2\pi R/10 = 250$ cm and $f = 130$ MHz ($3\Omega_H$ at 3T), then $f\,\lambda_{||} \approx 1.3 \times 10^{10}$ cm/sec ($n_{||} \approx 2.5$) which could be fast enough for heating high temperature plasmas. Therefore, as in tokamak, the IBWH tends to become more attractive as the device size and magnetic field value increase, and it might become quite feasible for heating large size helical devices such as LHS. The larger size also would make the ray-tracing calculations to be more valid even in the helical geometry.

As for the ponderomotive force application of IBWH, if the experiments on PBX-M are successful, the crucial question would be the required power scaling toward future devices. A simple estimate might suggest prohibitively high required power for the high field, large devices. Therefore, it would be important to work on the required power optimization. Since the ponderomotive effects tend to increase with the lowering of rf-frequency, the power optimization might lead to lower frequency regimes. Naturally, the antenna design and placement must also be considered with such applications in mind. Both the mode-stabilization and the plasma edge control are certainly extremely important areas of fusion research for tokamak improvements. Therefore the future ponderomotive based concept development might take an independent path from the IBW heating experiments (which tend to move toward higher frequency antenna/waveguide direction).

ACKNOWLEDGEMENTS

The author acknowledges contributions from a large number of researchers whose paper are being refereed here. In particular, he thanks members of ACT-1, JIPPTII-U, PLT, Alcator C, and TNT, JFT-II-U, DIII-D and PBX-M for providing experimental data for this paper. He also thanks Dr. T.H. Stix for his valuable comments on the manuscript.

REFERENCES

[1] M. Ono, Princeton Plasma Physics Laboratory Report, PPPL-1593 (1979).

[2] M. Ono, T.H. Stix, K.L. Wong, T. Horton, 8th Conference on Plasma Physics and Controlled Nuclear Research, Brussels, T-1-2(B), (1980)

[3] S. Puri, Phys. Fluids 22, 1716 (1979).

[4] M. Brambilla, Nucl. Fusion 16, 47 (1976)

[5] S. Bernabei, et al., Nucl. Fusion 17, 929 (1977).

[6] J. Hosea et. al., 8th Conf. on Plasma Physics and Controlled Nuclear Fusion Research, Brussels (1980), D-5-1.

[7] T. H. Stix, Phys. Rev. Letters 15, 878 (1965).

[8] D. G. Swanson and Y. C. Nygan, Phys. Rev. Letters 35, 517 (1975).

[9] F. W. Perkins, in ORNL/FEDC-8311, Oak Ridge National Laboratory, Oak Ridge, TN (1983); K. L. Wong and M. Ono, Nuclear Fusion 24, 615 (1984).

[10] E. Ott, Phys. Fluids 22, 1732 (1979).

[11] M. Ono, Phys. Fluids 25, 990 (1982).

[12] M. Ono, in Course and Workshop on Application of RF Waves to Tokamak Plasmas, Varenna, Vol. I, 184 (1985).

[13] P. Colestock et. al., U.S. Cont. to INTOR Workshop, Phase II, Part IIa, INTOR Design Group, IAEA, Vienna (1985).

[14] M. Ono et al., AIP Conference Proceedings of Sixth Topical Conference on RF Plasma Heating, Callaway Gardens, Georgia, 1985, P. 83.

[15] M. Okamoto and M. Ono, Nuclear Fusion 28, 1385 (1988)

[16] H. Abe, H. Okada, et al., Phys. Rev. Lett. 53, 1153 (1984).

[17] H. Okada, H. Abe, R. Itatani, and M. Ono, Phys. Fluids 29, 489 (1986)

[18] H. Okada, H. Abe, R. Itatani, and M. Ono, Plasma Physics and Controlled Fusion 29, 743 (1987)

[19] M. Ono, K. L. Wong, Phys. Rev. Lett. 45, 1105 (1980).

[20] M. Ono, K. L. Wong, and G. A. Wurden, Phys. Fluids 26, 298 (1983).

[21] M. Ono, G.A. Wurden, and K. L. Wong, Phys. Rev. Lett. 52, 37 (1984).

[22] G. A. Wurden, M Ono, and K. L. Wong, Phys. Rev. A 26, 2297 (1982).

[23] M. Ono, T. Watari, R. Ando, J. Fujita, Y. Hirokura, K. Ida, E. Kato, K. Kawahata, Y. Kawasumi, K. Matsuoka, A. Nishizawa, N. Noda, I. Ogawa, K. Ohkubo, M. Okamoto, K. Sato, S. Tanahashi, Y. Taniguchi, T. Tetsuka, K. Toi, and K. Yamazaki, Phys. Rev. Lett. 54 , 2339 (1985).

[24] T. Watari, et al., Phys. Fluids 21, 2076 (1978); T. Watari et al., Nucl. Fusion 22, 1359 (1983).

[25] K. Sato, M. Mimura, M. Otsuka, T. Watari, K. Kawahata, Phys. Rev. Lett. 56, 151 (1986).

[26] Y. Ogawa, K. Kawahata, R. Ando, E. Kako, T. Watari, S. Hirokura, Y. Kawasumi, S. Morita, K. Sakai, K. Sato, S. Tanahashi, Y. Taniguchi, K. Toi, Nuclear Fusion 27, 1379 (1987); also K. Kawahata, R. Ando, E. Kako, T. Watari, S. Hirokura, Y. Kawasumi, S. Morita, Y. Ogawa, K. Sato, S. Tanahashi, Y. Taniguchi, K. Toi, in Proc. 13th Europ. Conf., Shriesee II, 169 (1986).

[27] J. R. Wilson et al, AIP Conference Proceedings of Sixth Topical Conference on RF Plasma Heating, Callaway Gardens, Georgia, 1985, P. 8.

[28] J. C. Hosea et al., Plasma Physics and Controlled Fusion 28, 1241(1986).

[29] J. R. Wilson, R. Bell, A. Cavallo, P. O. Colestock, S.A. Cohen, J. Hosea, G.J. Greene, R. Kaita, D. McNeill, E. Mazzucato, M. Ono, K. Sato, S. Suckewer, and A.W. Wouters, J. Nucl. Matt. 145-146, 616 (1987).

[30] M. Ono, P. Beiersdorfer, R. Bell, S. Bernabei, A. Cavallo, A. Chmyga, S.A. Cohen, P. Colestock, G. Gammel, G.J. Greene, J. Hosea, R. Kaita, I. Lehrman, G. Mazzitelli, E. Mazzucato, D. McNeill, M. Mori, K. Sato, J. Stevens, S. Suckewer, J. Timberlake, V. Vershkov, J.R. Wilson, and A. Wouters, in Plasma Physics and Controlled Nuclear Fusion Research 1986 (Proc. 11th Int. Conf. Kyoto, 1986), Vol.1., IAEA, Vienna (1987) 477.

[31] M. Ono, P. Beiersdorfer, R. Bell, S. Bernabei, A. Cavallo, A. Chmyga, S. Cohen, P. Colestock, G. Gammel, G.J. Greene, J. Hosea, R. Kaita, I. Lehrman, G. Mazzitelli, E. Mazzucato, D. McNeill, K. Sato, J. Stevens, J. Timberlake, J.R. Wilson, and A. Wouters, Phys. Rev. Letters 60, 294 (1988).

[32] J. B. McBride, Phys. Fluids 31, 129 (1988).

[33] H. Biglari, M. Ono, P.H. Diamond, G.G. Craddock, AIP Conference Proceedings, Ninth Topical Conference on Radio-Frequency Power in Plasmas, Charleston, SC 1991.

[34] Y. Takase, J. D. Moody, C.L. Fiore, F.S. McDermott, M. Porkolab, and J. Squire, Phys. Rev. Letters, 59, 1201 (1987).

[35] M. Porkolab, P. Bonoli, K. Chen, C. Fiore, G. Granetz, D. Griffin, D. Gwinn, S. Knowlton, B. Lipschultz, S.C. Luckhardt, E. Marmar, M. Mayberry, F.S. McDermott, J. Moody, R. Parker, J. Rice, Y. Takase, J. Terry, S. Texter, and S.M. Wolfe, in Plasma Physics and Controlled Nuclear Fusion Research 1986 (Proc. 11th Int. Conf. Kyoto, 1986), Vol.1., IAEA, Vienna (1987) 509.

[36] J.D. Moody, M. Porkolab, C.L. Fiore, F.S. McDermott, Y. Takase, J. Terry, and S.M. Wolfe, Phys. Rev. Letters 60, 298 (1988).

[37] J.D. Moody and M. Porkolab, Phys. Fluids B1, 1675 (1989).

[38] S. Shinohara, O. Naito, Y. Ueda, H. Toyama and K. Miyamoto, J. Phys. Soc. Jpn. 55, 2648 (1986).

[39] S. Shinohara, O. Naito, K. Miyamoto, Nuclear Fusion 26, 1097 (1986).

[40] S. Shinohara, O. Naito, H. Toyama and K. Miyamoto, AIP Conference Proceedings 159, Seventh Topical Conference on Applications of Radio-Frequency Power to Plasmas, Kissimmee, Fl (1987) pp. 330 - 333.

[41] H. Tamai, T. Ogawa, H. Matsumoto and K. Odajima, Eighth Topical Conference on Radio-Frequency Power in Plasmas, Irvine, CA 1989 (American Institute of Physics, New York, 1989), p. 350.

[42] R.I. Pinsker, M.J. Mayberry, M. Porkolab, and R. Prater, Eighth Topical Conference on Radio-Frequency Power in Plasmas, Irvine, CA 1989 (American Institute of Physics, New York, 1989), p. 314.

[43] M. Brambilla, Nucl. Fusion 28, 549 (1988).

[44] T-W. Jiang and M. Ono, Bull. of American Phys. Society, the Thirty-Second Annual Meeting of the Division of Plasma Physics, Cincinnati, Oct. 1990.

[45] R. Pinsker, M. Mayberry, C.C. Petty, M. Porkolab, S.C. Chiu, M. Ono, Bull. of American Phys. Society, the Thirty-Second Annual Meeting of the Division of Plasma Physics, Cincinnati, Oct. 1990.

[46] M. Ono, Eighth Topical Conference on Radio-Frequency Power in Plasmas, Irvine, CA 1989 (American Institute of Physics, New York, 1989), p. 306.

[47] M. Porkolab, S. Coda, M. Mayberry, C. Petty, R. Pinsker, Bull. of American Phys. Society, the Thirty-Second Annual Meeting of the Division of Plasma Physics, Cincinnati, Oct. 1990.

[48] G.J. Morales, Phys. Fluids 20, 1164 (1977).

[49] J.R. Wilson and K.L. Wong, Phys. Fludis 25, 675 (1982).

[50] F. Skiff, Ph.D. thesis, Princeton University, 1985.

[51] R.I. Pinsker, M.J. Mayberry, M. Porkolab, S.C. Chiu, and R. Prater, Ninth Topical Conference on Radio-Frequency Power in Plasmas, Charleston, SC 1991 (AIP Conference Proceedings).

[52] T-W Jiang, G. Greene, M. Ono, et al., Ninth Topical Conference on Radio-Frequency Power in Plasmas, Charleston, SC 1991 (AIP Conference Proceedings).

[53] S.C. Chiu, Ninth Topical Conference on Radio-Frequency Power in Plasmas, Charleston, SC 1991 (AIP Conference Proceedings).

[54] S.C. Chiu, V.S. Chan, F.W. Perkins, and S. Puri, Physics of Fluids B3, 159 (1991).

[55] J.R. Myra, D.A. D'Ippolito, D.W. Forslund, and J.U. Brackbill, Phys. Rev. Letters 66, 1173 (1991)

[56] M. Ono, AIP Conference Proceedings, Ninth Topical Conference on Radio-Frequency Power in Plasmas, Charleston, SC 1991.

[57] A. Cardinali, R. Cesario, F. DeMarco, M. Ono, 16th European Conference on Controlled Fusion and Plasma Physics, Venice, Italy (March 1989).

[58] D.W. Ignat and M. Ono, Princeton Plasma Physics Laboratory Report PPPL-2583 (1989).

[59] R. Kumazawa, M. Ono, T. Seki, et al., 18th European Conference on Controlled Fusion and Plasma Physics, Berlin, Part III 325 (1991).

[60] T. Seki, K. Kawahata, M. Ono, et al., AIP Conference Proceedings, Ninth Topical Conference on Radio-Frequency Power in Plasmas, Charleston, SC 1991.

[61] D. A. D'Ippolito, J. R. Myra, G. L. Francis, Phys. Rev. Letters 58, 2216 (1987).

[62] D. A. D'Ippolito, Phys. Fluids 31, 340 (1988). J. P. Goedbloed and D. A. D'Ippolito, Phys. Fluids B2, 2366 (1990).

[63] T.Shoji, A. Grossman, R. Conn, Y. Hirooka, R. Lehmer, W. Leung, L. Schmitz and G. Tynan, Journal of Nuclear Materials, 176 -177, 830 (1990)

[64] I. B. Bernstein, Phys. Rev. Lett. 109, 10 (1958)

[65] T. H. Stix, Theory of Plasma Waves (McGraw-Hill, New York 1962).

[66] M. Ono, et al., in Heating in Toroidal Plasma II, ed. E. Canobbio, et al., (Pergamen, New York 1981) Vol. I, p. 593.

[67] A.W. Trivelpiece and R.W. Gould, J. Appl. Phys. 14, 1784 (1959).

[68] D .G. Swanson, Phys. Fluids 10, 1531 (1975).

[69] J. P. M. Schmitt, Phys. Rev. Lett. 31, 982 (1973).

[70] M. Ono, Phys. Rev. Letters 42, 1267 (1979).

[71] K.D. Harms, Nucl. Fusion 16, 753 (1976).

[72] C. F. Kennel and F. Engelmann, Phys. Fluids 9, 2377 (1966).

[73] T. H. Stix, Nucl. Fusion 15, 737 (1975).

[74] C. F. F. Karney and A. Bers, Phys. Rev. Letters 39, 550 (1977).

[75] F. Skiff, F. Anderegg, and M. Q. Tran, Phys. Rev. Letters 58, 1430 (1987).

[76] J. Goree, M. Ono, and K. L. Wong, Phys. Fluids 28, 2345 (1985).

[77] M. N. Rosenbluth, et a., Ann. Phys. (NY) 55, 248 (1969).

[78] M. Porkolab, Phys. Rev. Letters 54, 434 (1985).

[79] R.P.H. Chang and M. Porkolab, Phys Fluids 15, 297 (1972).

[80] M. Sugawa, Phys Rev Letters 61, 543 (1988).

[81] M. Porkolab, S. Bernabei, W. M. Hooke, R. W. Motley, and T. Nagashima, Phys. Rev. Letters 38, 230 (1977).

[82] R. Van Nieuwenhove, G. Van Ooast, J.-M. Beuken, et al., on Controlled Fusion and Plasma Heating (Proc. 15th Eur. Conf. Dubrovnik, 1988) Vol. 12B, Part II, European Physics Society 889 (1988).

[83] Y. M. Aliev, V. P. Silin and C. Watson, JETP 23, 626 (1966), T. Amano and M. Okamoto, J. Phys. Soc. Japan 24, 916 (1968).

[84] M. Porkolab, Phys. Fluids 17, 1432 (1974).

[85] K. L. Wong and M. Ono., Phys. Rev. Letters 47, 842 (1981).

[86] M. Ono, M. Porkolab, R.P.H. Chang, Phys. Fluids 13, 1656 (1980).

[87] F. N. Skiff, M. Ono, K. L. Wong, Phys. Fluids 27, 1051 (1984).

[88] F. N. Skiff, K. L. Wong, M. Ono, Phys. Fluids 27, 2205 (1984).

[89] A. Cardinali and F. Romanelli, Submitted to Phys. Fluids.

[90] D. Buchenauer, et al., in Proc. 4th Int. Symp. on Heating in Toroidal Plasmas (Rome, 1984), pp.111, Greene, et al., in Proc. 17th European Conference on Controlled Fusion and Plasma Physics, (1990).

[91] C. Singer, D. E. Post, D. R. Mikkelsen, et al., BALDUR: A One-Dimensional Plasma Transport Code, Rep. PPPL-2073, Princeton Plasma Physics Laboratory (1983).

[92] J. E. Stevens, M. Ono, R. Horton, and J. R. Wilson, Nucl. Fusion 21, 1259 (1981).

[93] W. N.-C. Sy, T. Amano, R. Ando, A. Fukuyama, T. Watari, Nucl. Fusion 25, 795 (1985).

[94] M. Brambilla, in Proceedings of Seventh Topical Conference on RF Plasma Heating, Kissimmee, Florida, 1987.

[95] F. Skiff, M. Ono, and K. L. Wong, Phys. Fluids 31, 2030 (1988).

[96] R. J. Briggs, P. R. Parker, Phys. Rev. Letters 29, 852 (1972), P. M. Bellan, M. Porkolab, Phys. Fluids 17, 1592 (1974).

[97] G. Gormezano, P. Blanc, M. Durvaux, et al., in Proceedings of the Third Topical Conference on Radio Frequency Plasma Heating, California Institute of Technology, Pasadena, paper A3, (1978).

[98] F. W. Perkins, Nucl. Fusion 29, 583 (1989).

[99] Y. Sato, K. Sawaya, and S. Adachi, IEEE Transactions on Plasma Science 15, 574 (1988).

[100] S. Puri, Phys. Rev. Letters 61, 959 (1988).

[101] R. Majeski, P. Robert, T. Tanaka, D. Diebold, G. McKee, and R. Breun, Bull. Am. Phys. Soc. 36, 2419 (1991).

[102] N. J. Fisch, Rev. Mod. Phys. 59, 175 (1987).

[103] H. Biglari, P.H. Diamond, P. Terry, Phys. Fludis B 2, 1 (1990).

[104] Ch. O. Ritz et al., Phys. Rev. Lett. 63, 2543 (1990).

[105] J. R. Ferron, N. Hershkowitz, R. A. Breun, S. N. Golovato, and R. Goulding, Phys. Rev. Lett. 51, 1955 (1983); Y. Yasaka and R. Itatani, Phys. Rev. Lett. 56, 2811 (1986).

[106] M.Ono, D. A. D'Ippolito et al., Bull. Am. Phys. Soc. 36, 2315 (1991).

[107] S. Cohen, et al., in Plasma Physics and Controlled Nuclear Fusion Research (Proc. 13th Int. Conf. Washington, 1990)

[108] E. Mazzucato, Phys. Fluids 21, 1063 (1978); Phys. Rev. Lett. 48, 1828 (1982).

[109] J. Timberlake et al., Bull. Am. Phys. Soc. 31, 1467 (1986).

[110] M. Porkolab and J.D. Moody, Bull. Am. Phys. Soc. 32, 1939 (1987).

Figure Captions

Fig. 1. Comparison of wave number as a function of plasma density for LHH, IBW, and ICRF fastwave.

Fig. 2. IBW heating configuration in a typical tokamak parameters.

Fig. 3. Wave number as a function of plasma density for various values of ω/Ω_i, as labeled.

Fig. 4. Ion Bernstein wave identification. (a) Wave interferometer traces for various values of ω/Ω_H (r=2cm), as labeled. (b) Interferometer traces for various phase delays, $\omega\Delta t/2\pi$. (c) Wave dispersion relation. Dots are experimental points and solid curves are the theoretical values.

Fig. 5. A complete IBW dispersion relation in ACT-1 hydrogen plasma. Solid triangles are probe values, open circles are the CO_2 laser points and lines are theoretical curves. The corresponding wave interferometry data are shown in the right. Deuterium-like and tritium-like resonances are due to the H_2^+ and H_3^+ ions.

Fig. 6. EPW-IBW mode-transformation. (a) Wave number vs radial position in a hydrogen plasma with a linear rise in density for a cold ($T_i = 0$) case and a finite ion temperature ($T_i = 1.5$ eV) case. $f = 12$ MHz, $\omega/\Omega_H(r=0) = 1.9$, $\lambda_{||} = 34$ cm, $n_e(res) \equiv 2.5 \times 10^9$ cm^{-3}. (b) Wave trajectories for the case shown in (a).

Fig. 7. Observation of EPW-IBW mode-transformation. (a) Interferometer traces for various neutral pressures. (b) Wave number vs radial position. Dots are experimental points and curves are theoretical values. $\omega/\Omega_H(r=0) = 1.92$; $p_H = 7 \times 10^{-6}$ Torr.

Fig. 8. Wave packet trajectory vs. plasma density. (a) Radial wave packet amplitude profiles (thicker curves) and interferogram traces (finer curves) for various central densities (as labeled). (b) Corresponding wave packet positions as predicted from ray-tracing calculation for various $\lambda_{||}$. The dashed line, $\omega \equiv \omega_{pi}$, separates IBW and EPW regions.

Fig. 9. Third harmonic launching of IBW. (a) IBW dispersion relation. (b) Wave number vs. radial distance from the antenna. Dots are measured and solid curves are theoretical values. Lower-hybrid resonance is indicated by the dashed lines.

Fig. 10. IBW wave propagation characteristics in particle simulation. (a) Wave potential contours. (b) $E_\perp$ vs. x. (c) $k_\perp$ vs. x. Solid and dashed curves are the real and imaginary parts of $k_\perp$ calculated from the linear dispersion relation.

Fig. 11. IBW heating in particle simulation. (a) Radial power deposition into hydrogen. The arrow indicates the location of $3/2\Omega_H$ resonance. (b) Time evolution of perpendicular velocity distribution at the resonance. (c) H phase space ($v_\perp^2$, $v_{||}^2$) in the resonance region. The arrows indicate the upper and lower limits of the parallel resonant velocities, $v_{||} = [\ \omega - 3/2\Omega_H(x)] / k_{||}$. The dashed curve indicates the boundary of the initial Maxwellian distribution function.

Fig. 12. Typical example of tokamak ray tracing calculation (JIPPT-II-U 40 MHz parameters). (a) Wave number vs. radial position. (b) Wave phase amplitude vs. radial position. (c) Poloidal and toroidal rays for various values of launched $n_{||}$. (d) Normalized power vs radial position for various values of launched $n_{||}$ and minority species concentration.

Fig. 13. IBW heating simulation of INTOR like parameters. (a) Input power to the plasma. (b) Volume averaged density and ohmic current evolution. (c) Volume-averaged T_e and T_i evolution. (d) Volume-averaged β evolution.

Fig. 14. IBW power deposition profiles for the case shown in Fig. 13. (a) at t = 1.625 sec representing the beginning of the discharge, (b) at t = 2.593 sec when the α-heating is becoming significant, and (c) at t = 3.815 sec end of the rf heating phase. Note that the heating shifts from ions to electrons as T_e increases toward ignition temperature.

Fig. 15. EPW-IBW mode-transformation density for various IBWH experimental parameters. The dominant plasma species are indicated in the parenthesis.

Fig. 16. Ponderomotive potential for the antenna $E_{||}$ = 1 stat-volt/cm for various IBWH experimental parameters.

Fig. 17. A schematic view of the JIPPT-II-U 40 MHz IBWH experiment. (a) Top view of the device. (b) An enlarged view of the IBWH antenna region.

Fig. 18. Two dimensional interferometry traces of IBW excited by a B_θ-loop antenna in ACT-1.

Fig. 19. Power reflection coefficient vs. the density gradient scale length L for a two-waveguide phased launcher. $\Delta\phi$ is the relative phase between the guide. L is an exponentiating distance in which the density increases by a factor of 10.

Fig. 20. A schematic view of the waveguide launcher for the 430 MHz FT-U IBWH experiment.

Fig. 21. A simplified model for the axial convective loss (ACL).

Fig. 22. Power efficiency factor as a function of $n_{||}$ for various values of density steepness factor y as labeled[where $n_e(x) \propto x^y$]. (a) for the DIII-D, PBX-M type parameters with f = 43 MHz. (b) for the FT-U type parameters with f = 430 MHz.

Fig. 23. Ray tracing calculation for a reactor-grade plasma. (a) Poloidal ray trajectory for the launched $n_{||} = 2$. (b) Variation in $n_{||}$ along the trajectory. (c) Wave parallel phase velocity normalized to the local electron thermal velocity. (d) Normalized wave power.

Fig. 24. Ion temperature vs. rf frequency in the ACT-1 IBW heating. (a) $\omega/\Omega_H = 1.6 - 1.9$; (b) $\omega/\Omega_H = 2.4 - 2.75$. $P_{rf} = 10$W, r = 3 cm, $B_0 = 4.75$ kG, and $n_0 = 2.5 \times 10^{10}$ cm^{-3}.

Fig. 25. ACT-1 IBWH. (a) Ion temperature profiles for various rf power levels (as labeled). (b) Peak ion temperature vs. rf power. f = 11.6 MHz, $B_0 = 4.75$ kG, $n_0 = 2.5 \times 10^{10}$ cm^{-3}.

Fig. 26. JIPPT-II-U 40 MHz IBWH. (a) Dependence of ion heating quality factor on magnetic field strength, B_0 (R = 91cm). He minority (as labeled) in a predominantly hydrogen plasma. f = 40 MHz, $\overline{n_e} = 1.5 \times 10^{13}$ cm^{-3}, and P_{rf} (loaded) = 60-80 kW.

The points are experimental measurements. The solid line is the calculation result. (b) Dependence of ΔT_i on P_{rf}. The solid line is the calculated value with a Shafranov shift Δ_S= 1.3 cm. Broken line is for Δ_S = 0.

Fig. 27. PLT 90 MHz 5 Ω_D minority (hydrogen majority) heating configuration. Lines are IBW ray trajectories for $n_{||} = \pm$ 1, 3, and 5.

Fig. 28. PLT 5 Ω_D heating experiment. (a) Ion temperature evolution for various temperature components. (b) Energy distributions for perpendicular and parallel components. P_{rf} = 100 kW, f = 90 MHz, B_T = 2.4T, and $\overline{n_e}$ = 1.5 x $10^{13}cm^{-3}$.

Fig. 29. PLT 3/2 Ω_D heating in pure deuterium plasma. (a) Deuterium temperature evolution for with and without rf. (b) Deuterium energy distribution, $T_\perp \cong T_{||}$. P_{rf} = 150 kW, f = 30 MHz, B_T = 2.8T, and $\overline{n_e}$ = 1.7 x $10^{13}cm^{-3}$.

Fig. 30. PLT high power IBWH experiment. (a) A typical time evolution of ion temperatures in 3/2 Ω_D heating. P_{rf} = 500 kW, f = 30 MHz, B_T = 2.9T, and $\overline{n_e}$ = 3 x $10^{13}cm^3$. (b) Temperature profiles at t = 600 msec. Open circles are Doppler T_i with rf and solid circles are without rf for a simulated density rise. The curves are calculated values.

Fig. 31. PLT IBWH particle confinement behavior. (a) Density time evolution for IBWH case (solid curve) shown in Fig. 30 and an ohmic case (dashed curve), in which the gas puffing was used to simulate the density rise with IBWH. $\langle Z_{eff} \rangle$ evolution during IBWH is shown by the broken curve. (b) Time evolution of D_α emission for IBWH and ohmic cases taken near the antenna-limiter region.

Fig. 32. PLT IBWH particle transport physics. (a) Time evolution of the selenium XXV resonance line intensity for the IBWH case and the simulated ohmic case. The selenium was injected at t = 550 ms. (b) Time evolution of the integrated low frequency turbulence level at 100 kHz for the two cases; k (scatt) = 6-8 cm^{-1} at r = 25 $\pm$ 10 cm. Inset: Frequency spectrum of the scattered signal at t = 700 ms for the two cases.

Fig. 33. ΔT_i versus P_{rf} for three values of magnetic fields for f = 184 MHz in Alcator-C. At B = 9.3T, $\omega/\Omega_H(0) = 1.25$; at B=7.5T, $\omega/\Omega_H(0) = 1.5$; at B = 5T, $\omega/\Omega_H(0) = 2.5$, $\overline{n_e} \cong (0.7\text{-}1.1) \times 10^{20} cm^{-3}$.

Fig. 34. IBW dispersion relation determined from CO_2 laser scattering data in Alcator-C.

Fig. 35. Normalized ΔT_i versus $\overline{n_e}$ for B = 7.6 T in Alcator C; hydrogen ions.

Fig. 36. Particle confinement improvement in Alcator C with and without IBW injection versus density. B = 9.4 T.

Fig. 37. Measured reactive component of IBW antenna loading in DIIID.

Fig. 38. (a) Parametric decay spectrum observed during 0.8 MW power applied to the DIIID IBW antenna. The peak at 36 MHZ generator frequency is saturated to facilitate display of the decay wave peaks. (b) Charge exchange H spectrum showing perpendicular tail formation during IBW. (I_p = 0.9 MA, $\overline{n_e} = 2 \times 10^{13} cm^{-3}$).

Fig. 39. JIPPT-II-U ion temperature profiles as measured by the charge-exchange recombination spectroscopy. Central ion temperature measured by the FNA is shown. The central density with NBI is $4 \times 10^{13} cm^{-3}$ and with NBI + IBWH is $8 \times 10^{13} cm^{-3}$ due to improved confinement.

Fig. 40. Particle confinement during JIPPT-II-U IBWH. (a) Temporal evolution of the central density and the profile peaking factor k. (similar discharges to Fig. 39).

Fig. 41. Calculated ion and electron energy diffusivity profiles for NBI + IBWH compared to NBI alone.

Fig. 42. IBW heating resonance frequency as a function of the magnetic field in the BPX type operating regimes.

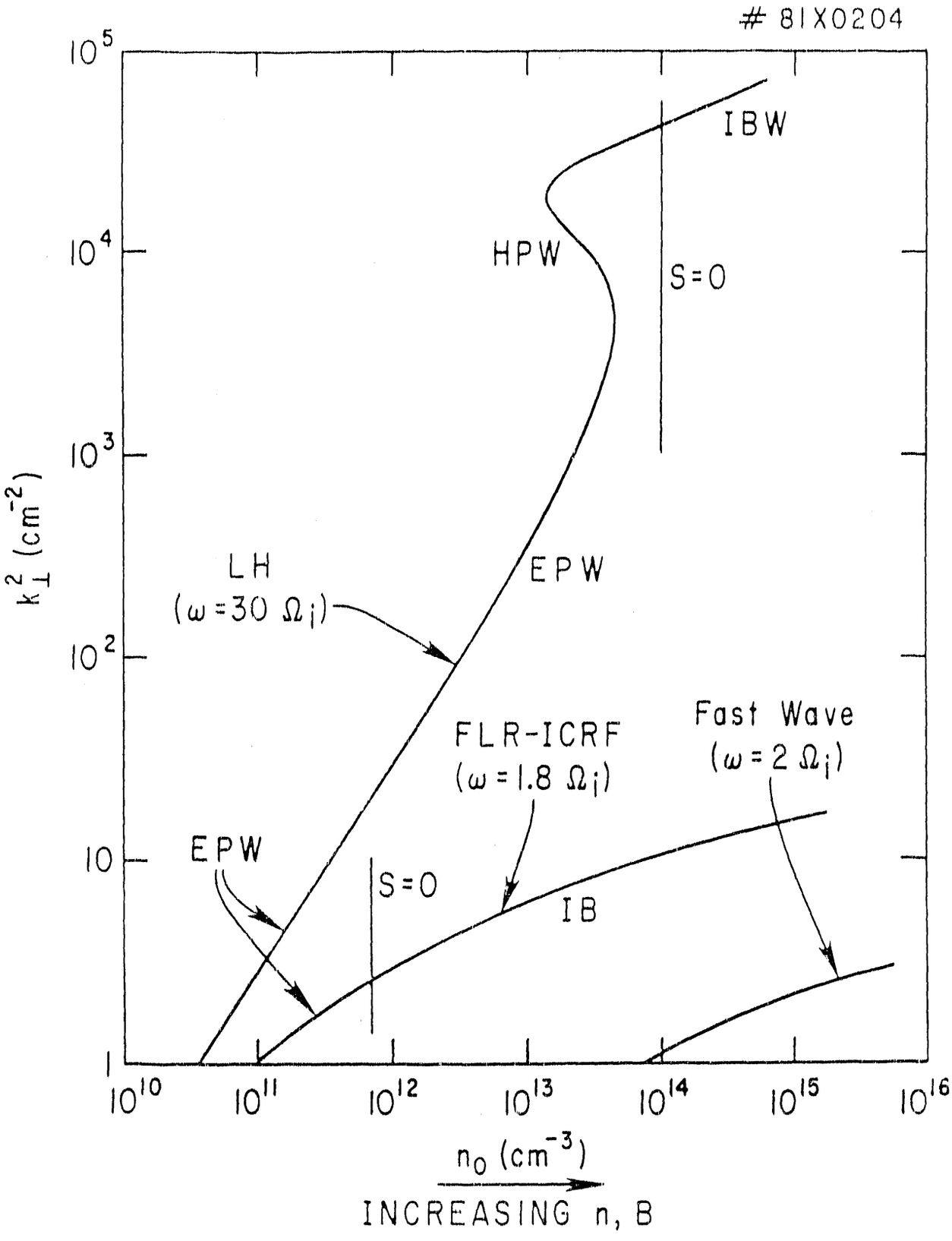
81X0204
10^5
10^4
10^3
10^2
10
1
$k_\perp^2$ (cm^{-2})
IBW
HPW
S=0
LH
(ω = 30 Ω_i)
EPW
FLR-ICRF
(ω = 1.8 Ω_i)
Fast Wave
(ω = 2 Ω_i)
EPW
S=0
IB
10^{10}
10^{11}
10^{12}
10^{13}
10^{14}
10^{15}
10^{16}
n_0 (cm^{-3})
INCREASING n, B

Fig. 1

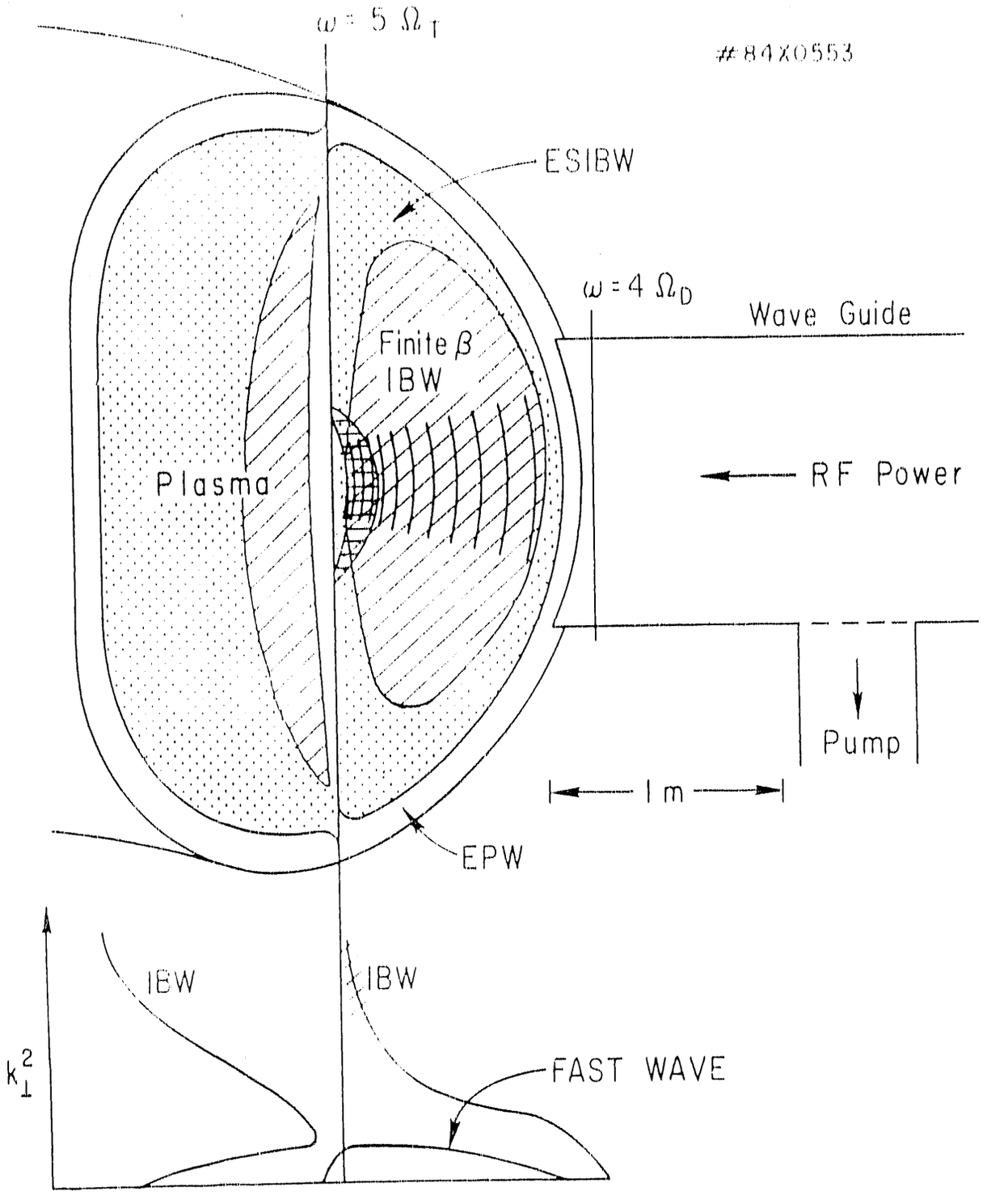
ω = 5 Ω_I
#84X0553
ESIBW
ω = 4 Ω_D
Wave Guide
Finite β
IBW
Plasma
RF Power
Pump
1 m
EPW
IBW
IBW
FAST WAVE
k⊥²

Fig. 2

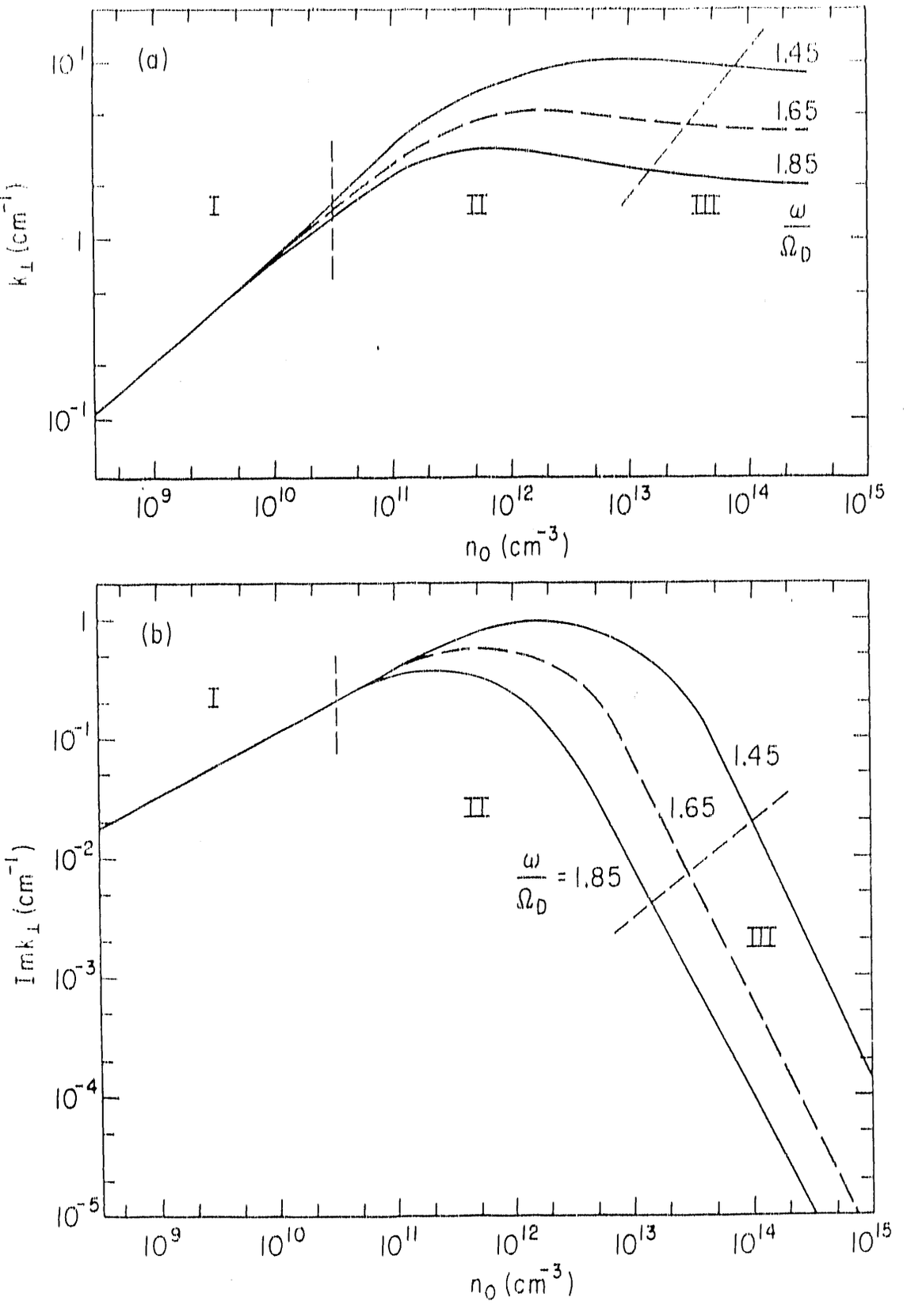
(a)
1.45
1.65
1.85
I
II
III
$\frac{\omega}{\Omega_D}$
$k_\perp$ (cm^{-1})
10^1
1
10^{-1}
10^9
10^{10}
10^{11}
10^{12}
10^{13}
10^{14}
10^{15}
n_0 (cm^{-3})
(b)
I
II
III
1.45
1.65
$\frac{\omega}{\Omega_D}$ = 1.85
Im$k_\perp$ (cm^{-1})
1
10^{-1}
10^{-2}
10^{-3}
10^{-4}
10^{-5}
10^9
10^{10}
10^{11}
10^{12}
10^{13}
10^{14}
10^{15}
n_0 (cm^{-3})

Fig. 3

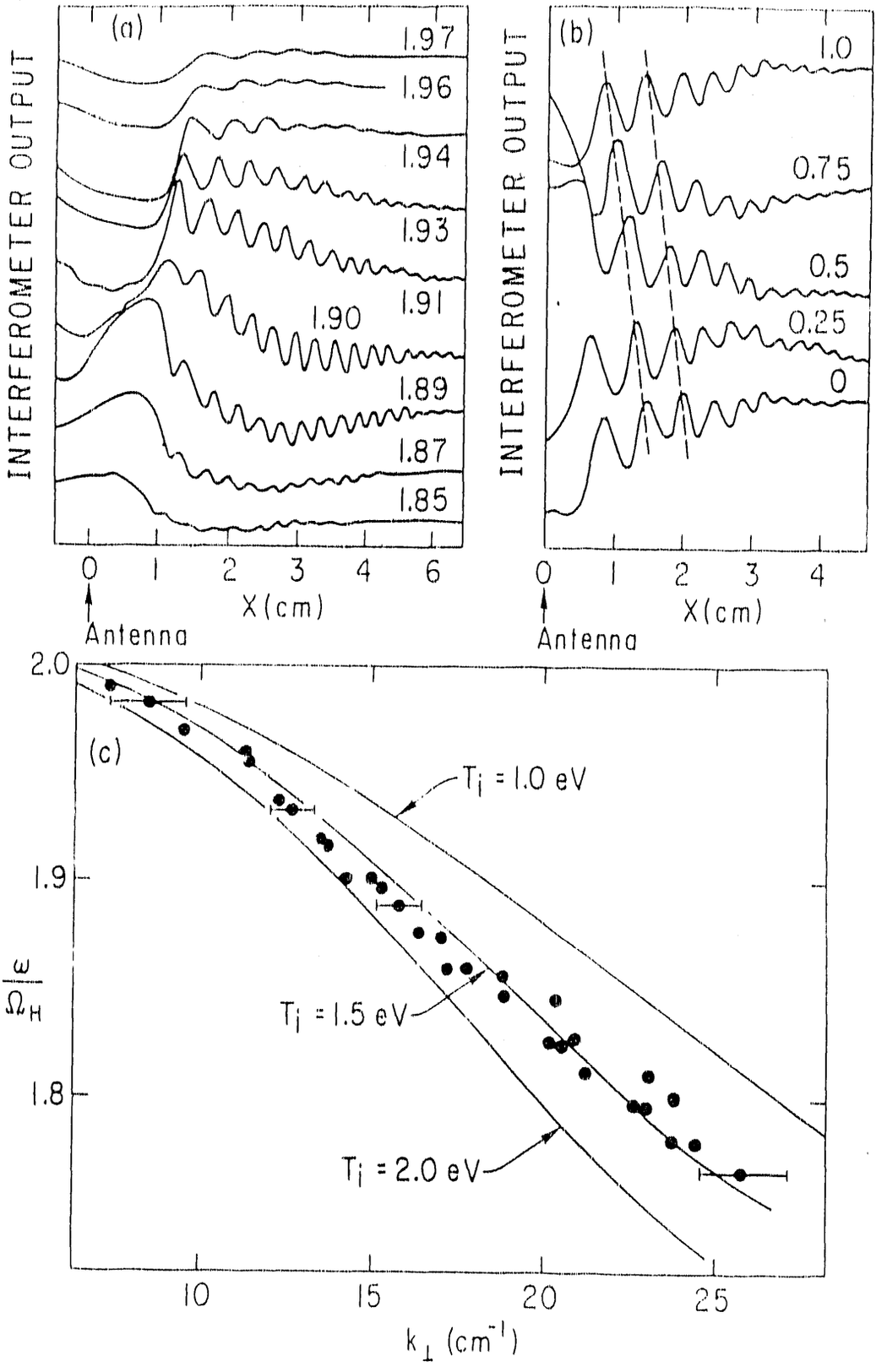
(a)
1.97
1.96
1.94
1.93
1.91
1.90
1.89
1.87
1.85
INTERFEROMETER OUTPUT
0 1 2 3 4 6
X(cm)
Antenna
(b)
1.0
0.75
0.5
0.25
0
INTERFEROMETER OUTPUT
0 1 2 3 4
X(cm)
Antenna
(c)
T_i = 1.0 eV
T_i = 1.5 eV
T_i = 2.0 eV
$\frac{\omega}{\Omega_H}$
2.0
1.9
1.8
10 15 20 25
$k_\perp$ (cm^{-1})

Fig. 4

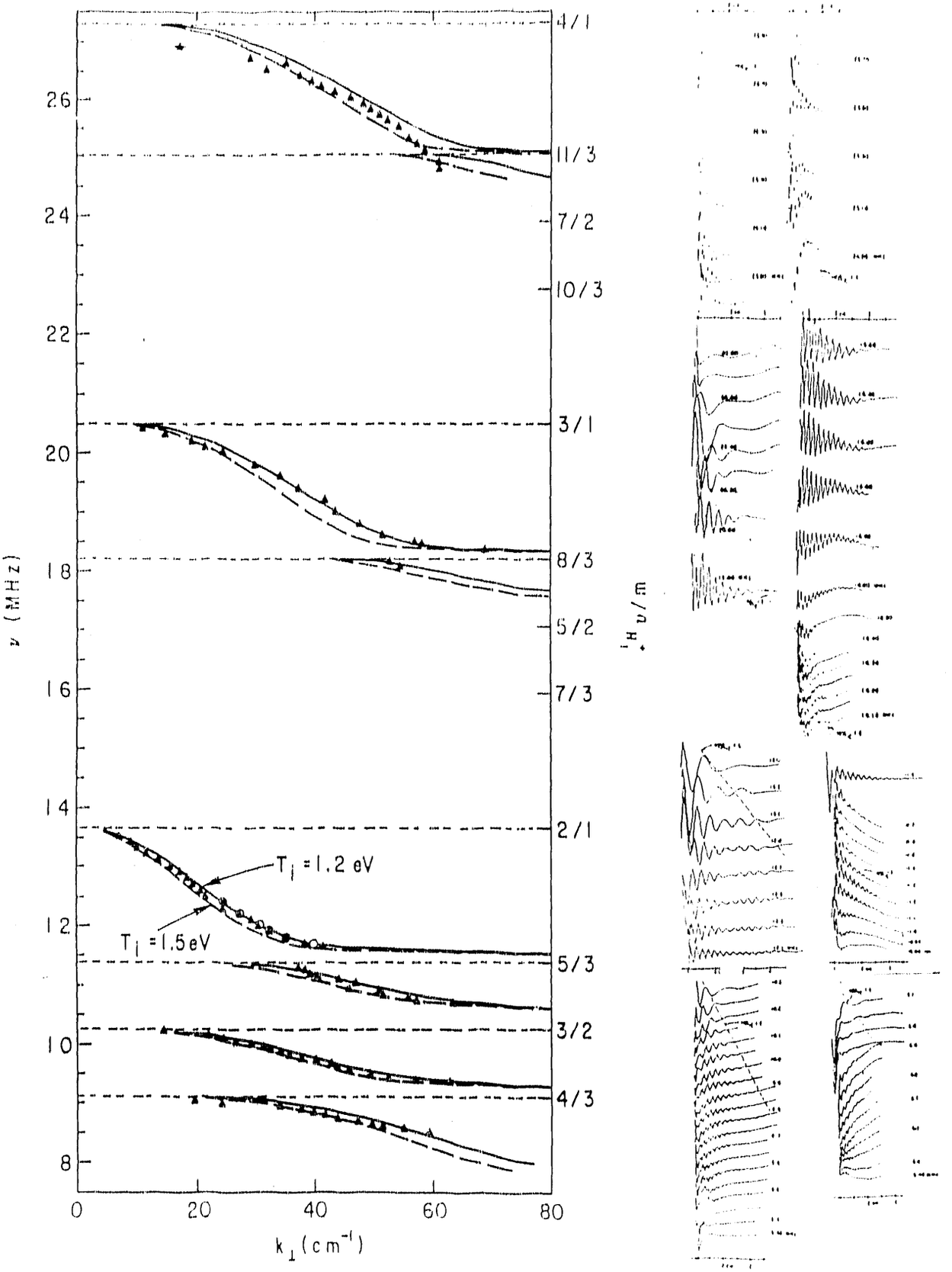
4/1
11/3
7/2
10/3
3/1
8/3
5/2
7/3
2/1
5/3
3/2
4/3
T_i = 1.2 eV
T_i = 1.5 eV
ν (MHz)
$k_\perp$ (cm^{-1})
i_H υ/m

Fig. 5

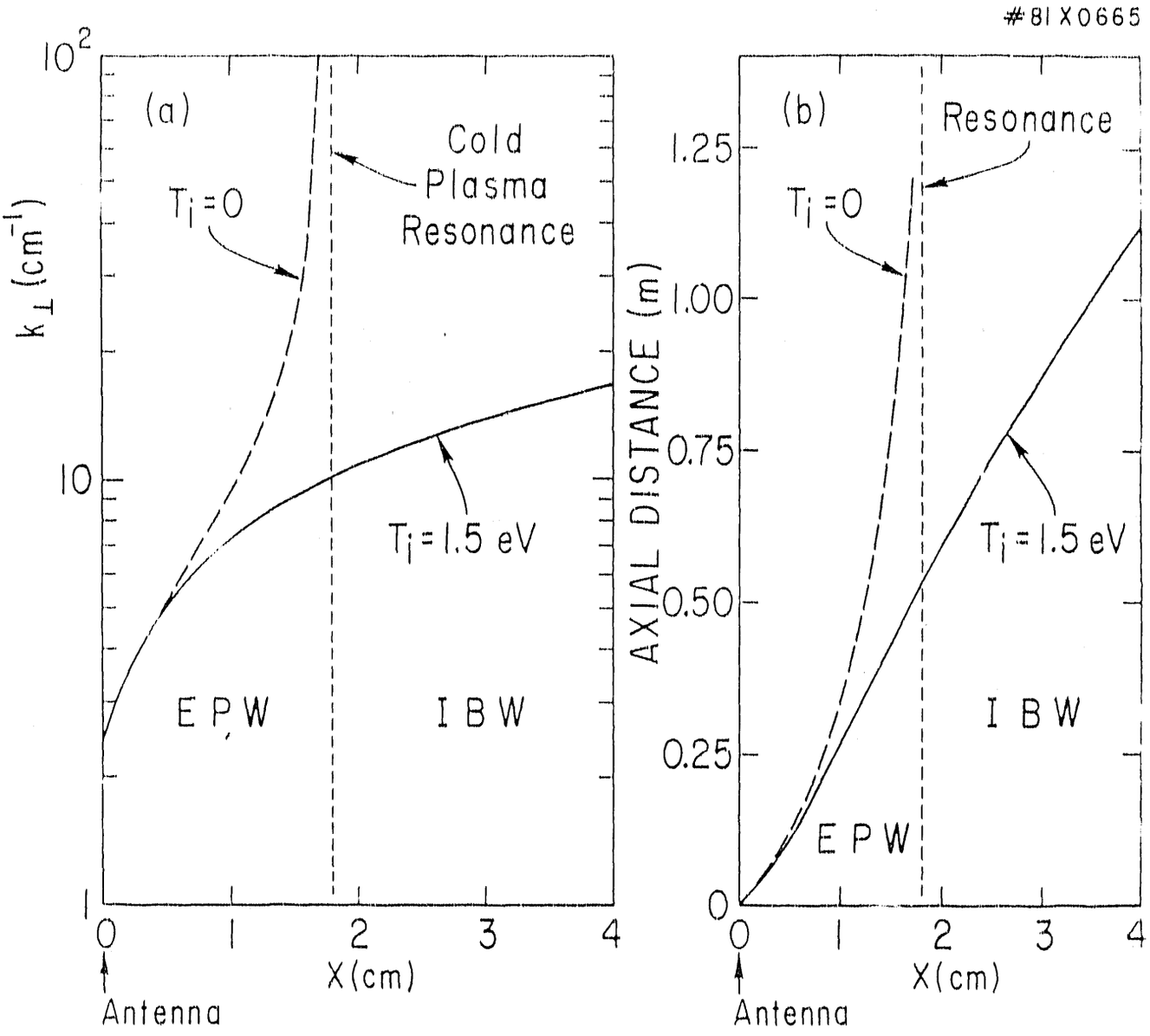
#81X0665
(a)
Cold
Plasma
Resonance
$T_i = 0$
$T_i = 1.5$ eV
E P W
I B W
$k_\perp$ (cm^{-1})
10^2
10
1
0
1
2
3
4
X(cm)
Antenna
(b)
Resonance
$T_i = 0$
$T_i = 1.5$ eV
E P W
I B W
AXIAL DISTANCE (m)
1.25
1.00
0.75
0.50
0.25
0
0
1
2
3
4
X(cm)
Antenna

Fig. 6

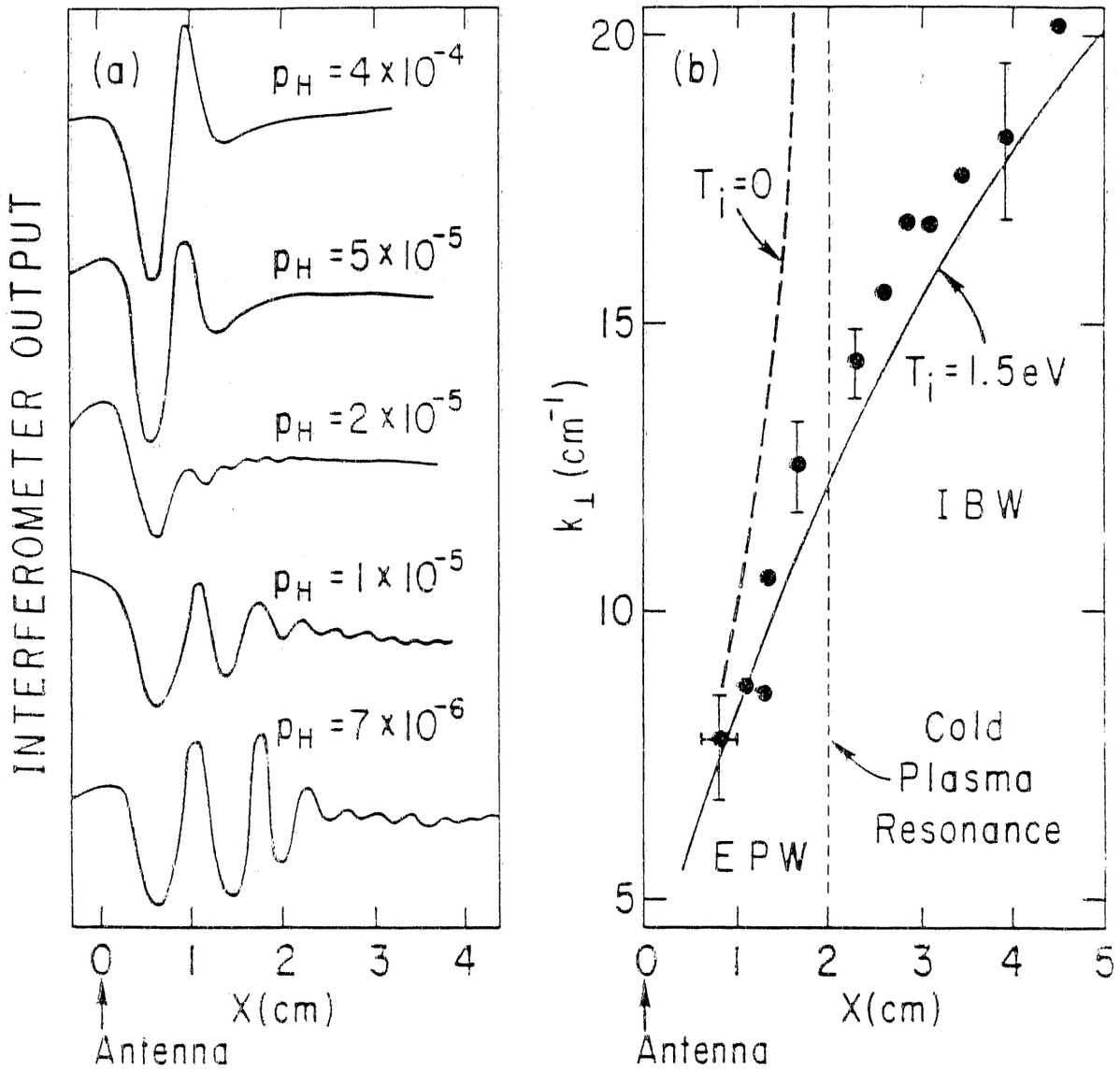
(a)
$p_H = 4 \times 10^{-4}$
$p_H = 5 \times 10^{-5}$
$p_H = 2 \times 10^{-5}$
$p_H = 1 \times 10^{-5}$
$p_H = 7 \times 10^{-6}$
INTERFEROMETER OUTPUT
0 1 2 3 4
X(cm)
Antenna
(b)
$T_i = 0$
$T_i = 1.5$ eV
IBW
Cold
Plasma
Resonance
EPW
$k_\perp$ (cm^{-1})
20
15
10
5
0 1 2 3 4 5
X(cm)
Antenna

Fig. 7

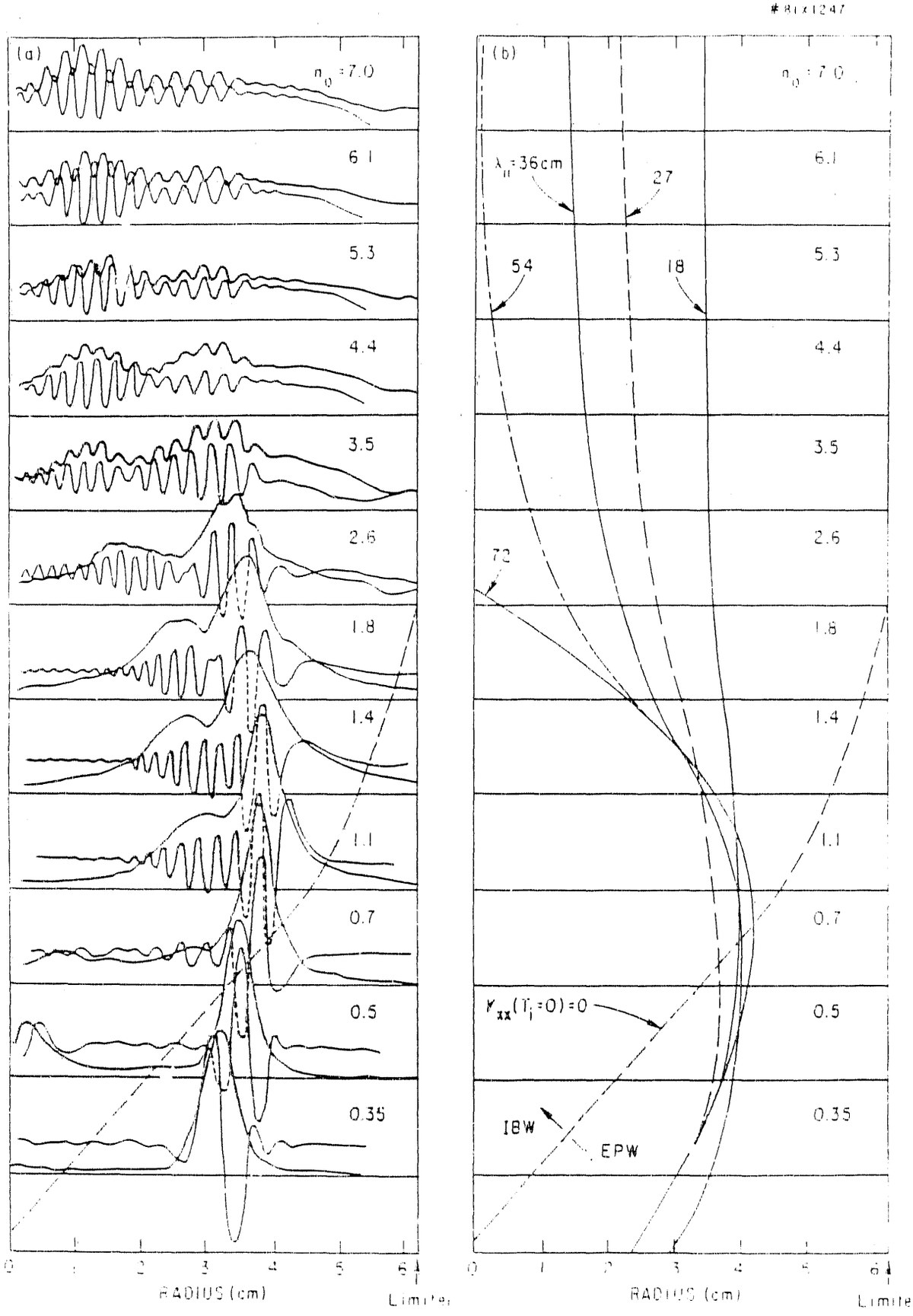
#81x1247
(a)
n_0 = 7.0
6.1
5.3
4.4
3.5
2.6
1.8
1.4
1.1
0.7
0.5
0.35
0
1
2
3
4
5
6
RADIUS (cm)
Limiter
(b)
n_0 = 7.0
$\lambda_{\parallel}$ = 36cm
27
54
18
72
$K_{xx}(T_i=0)=0$
IBW
EPW
6.1
5.3
4.4
3.5
2.6
1.8
1.4
1.1
0.7
0.5
0.35
0
1
2
3
4
5
6
RADIUS (cm)
Limiter

Fig. 8

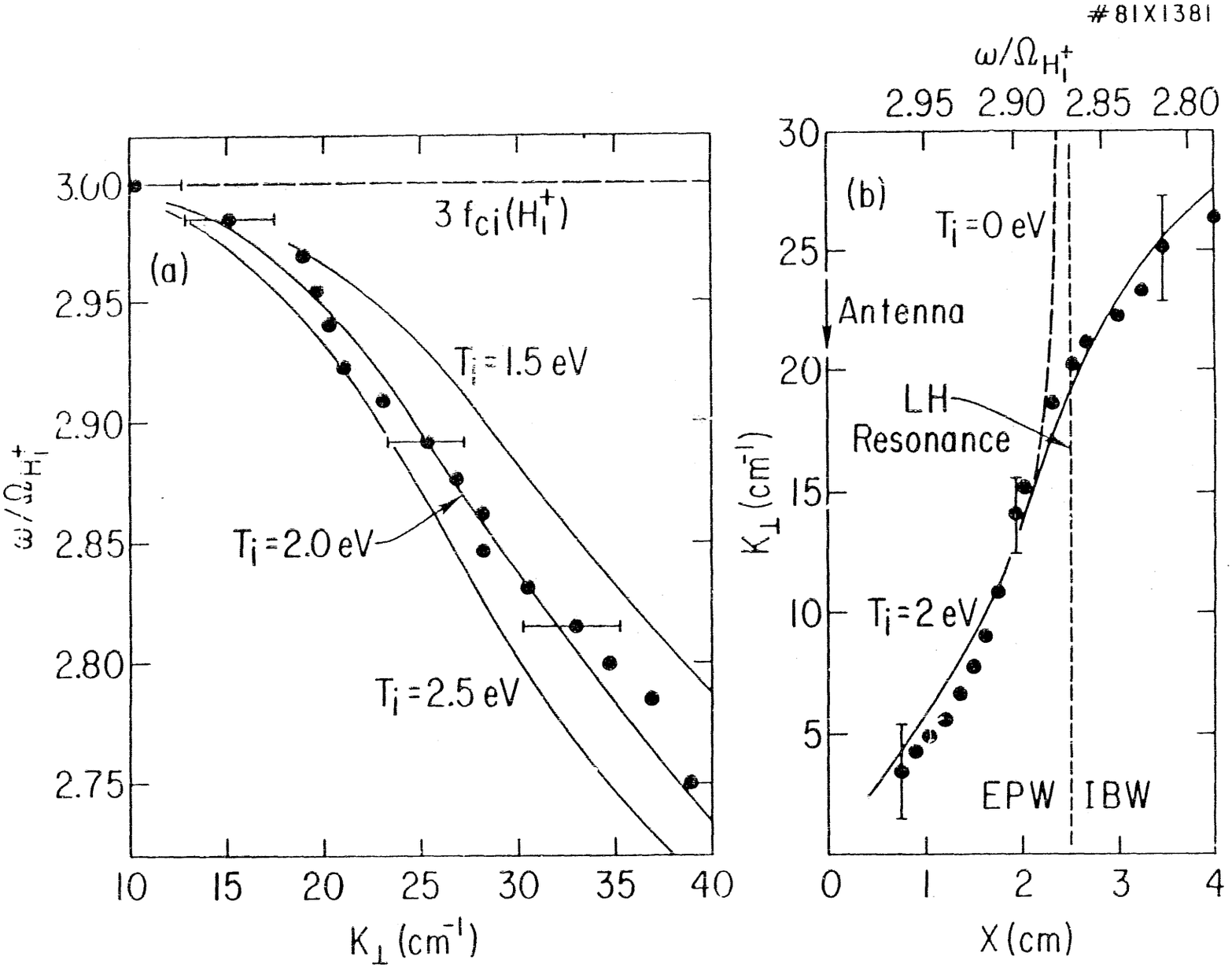
#81X1381
3 fci(H1+)
(a)
Ti = 1.5 eV
Ti = 2.0 eV
Ti = 2.5 eV
ω/Ω H1+
K⊥ (cm-1)
(b)
Ti = 0 eV
Antenna
LH
Resonance
Ti = 2 eV
EPW
IBW
X (cm)

Fig. 9

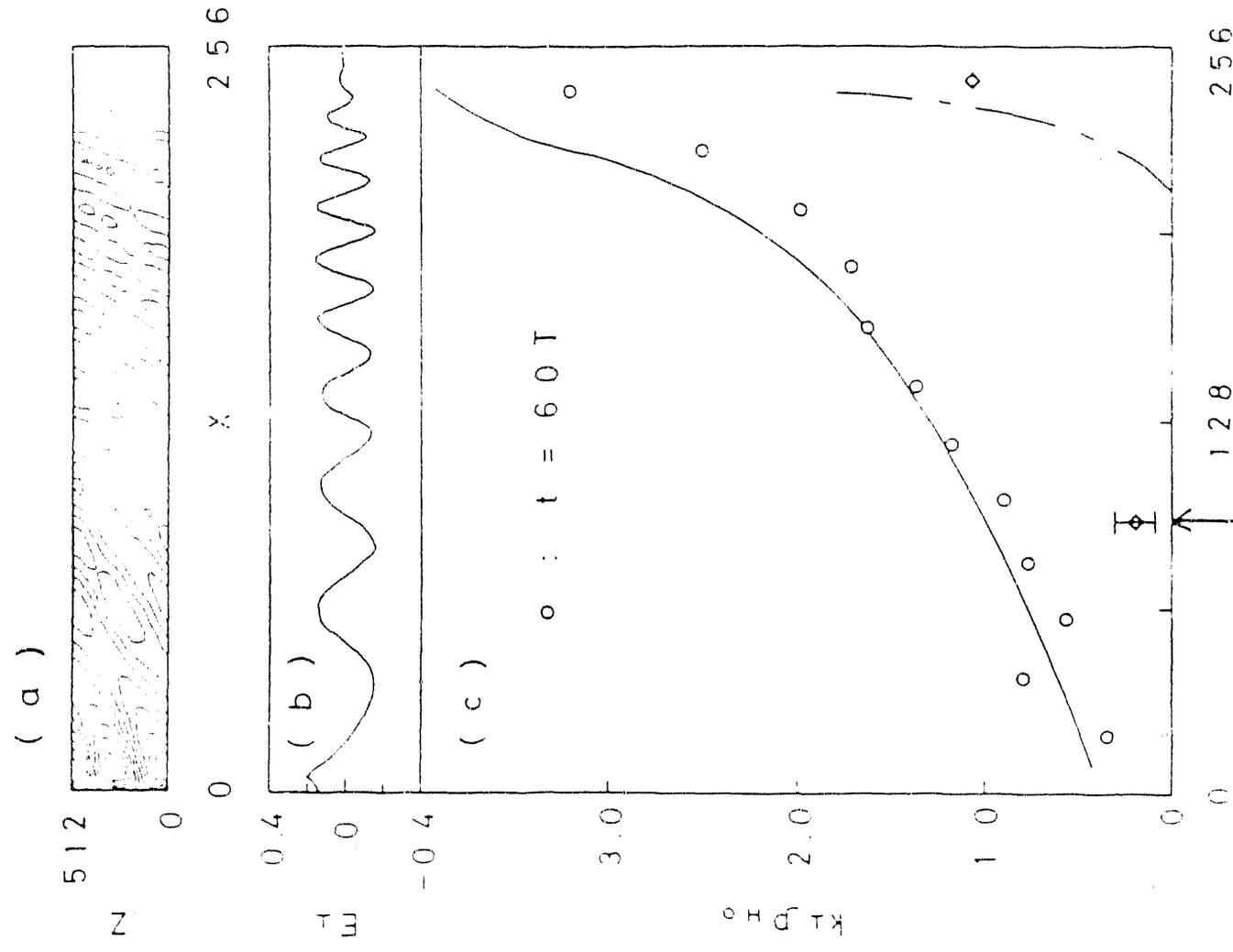

Fig.10

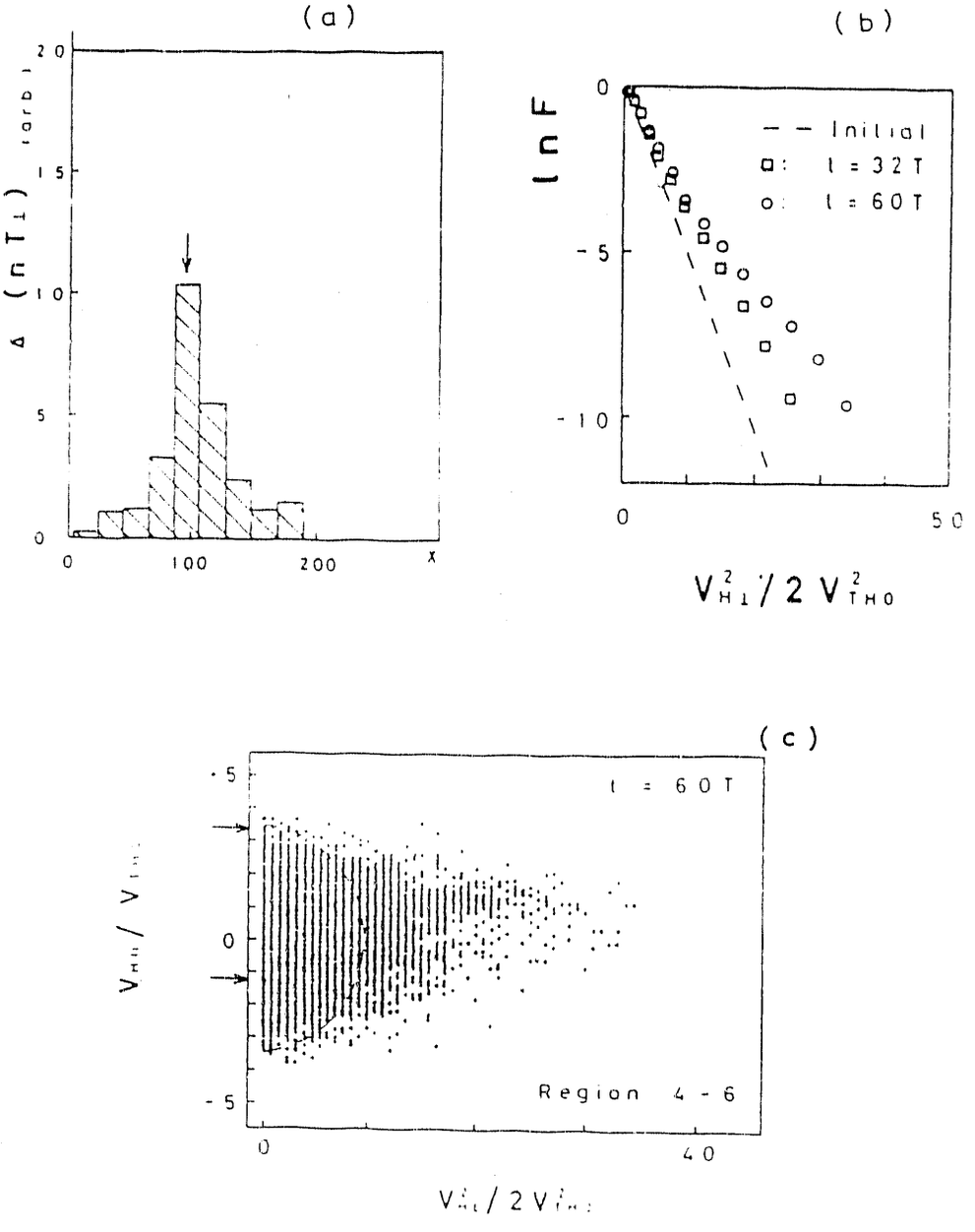

Fig.11

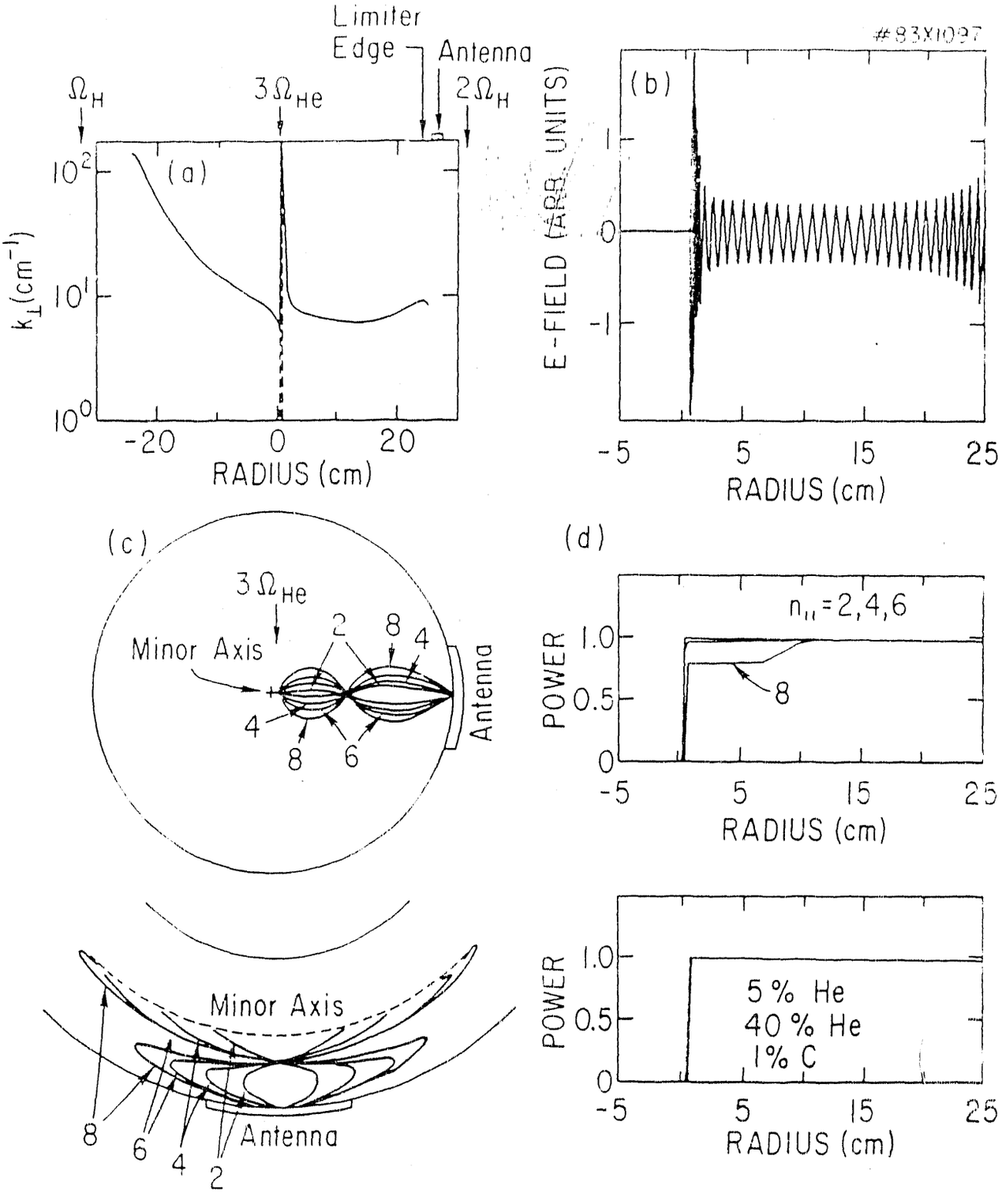
Limiter
Edge
Antenna
Ω_H
$3\Omega_{He}$
$2\Omega_H$
(a)
$k_\perp(cm^{-1})$
10^2
10^1
10^0
-20
0
20
RADIUS (cm)
#83X1097
(b)
E-FIELD (ARB. UNITS)
1
0
-1
-5
5
15
25
RADIUS (cm)
(c)
$3\Omega_{He}$
Minor Axis
2
8
4
Antenna
4
8
6
Minor Axis
8
6
4
2
Antenna
(d)
$n_{||}=2,4,6$
POWER
1.0
0.5
0
8
-5
5
15
25
RADIUS (cm)
5 % He
40 % He
1% C
POWER
1.0
0.5
0
-5
5
15
25
RADIUS (cm)

Fig. 12

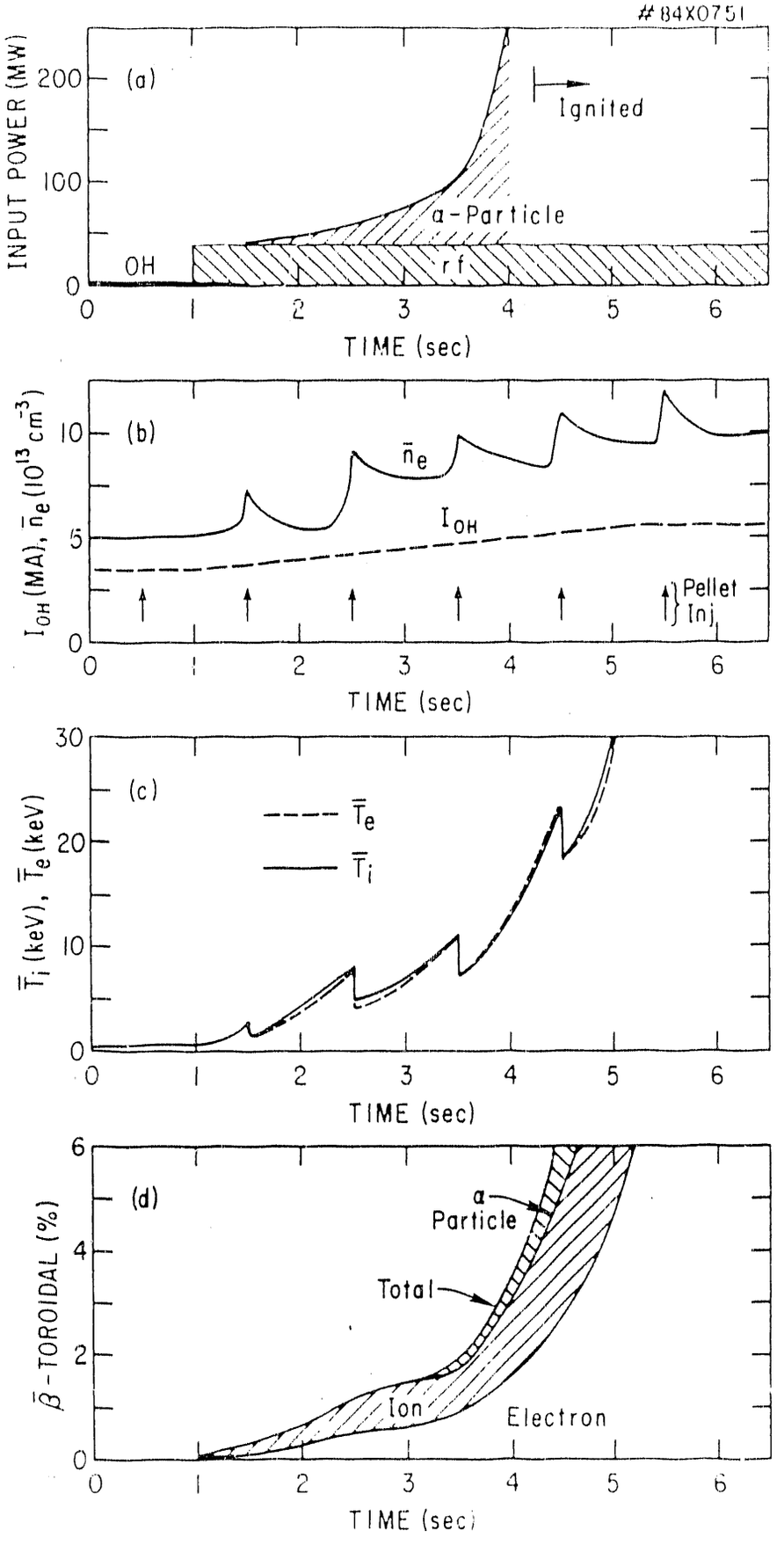
#84X0751
(a)
INPUT POWER (MW)
200
100
0
Ignited
α-Particle
OH
rf
0 1 2 3 4 5 6
TIME (sec)
(b)
I_{OH} (MA), $\bar{n}_e$ (10^{13} cm^{-3})
10
5
0
$\bar{n}_e$
I_{OH}
Pellet Inj
0 1 2 3 4 5 6
TIME (sec)
(c)
$\bar{T}_i$ (keV), $\bar{T}_e$ (keV)
30
20
10
0
$\bar{T}_e$
$\bar{T}_i$
0 1 2 3 4 5 6
TIME (sec)
(d)
$\bar{\beta}$-TOROIDAL (%)
6
4
2
0
α Particle
Total
Ion
Electron
0 1 2 3 4 5 6
TIME (sec)

Fig.13

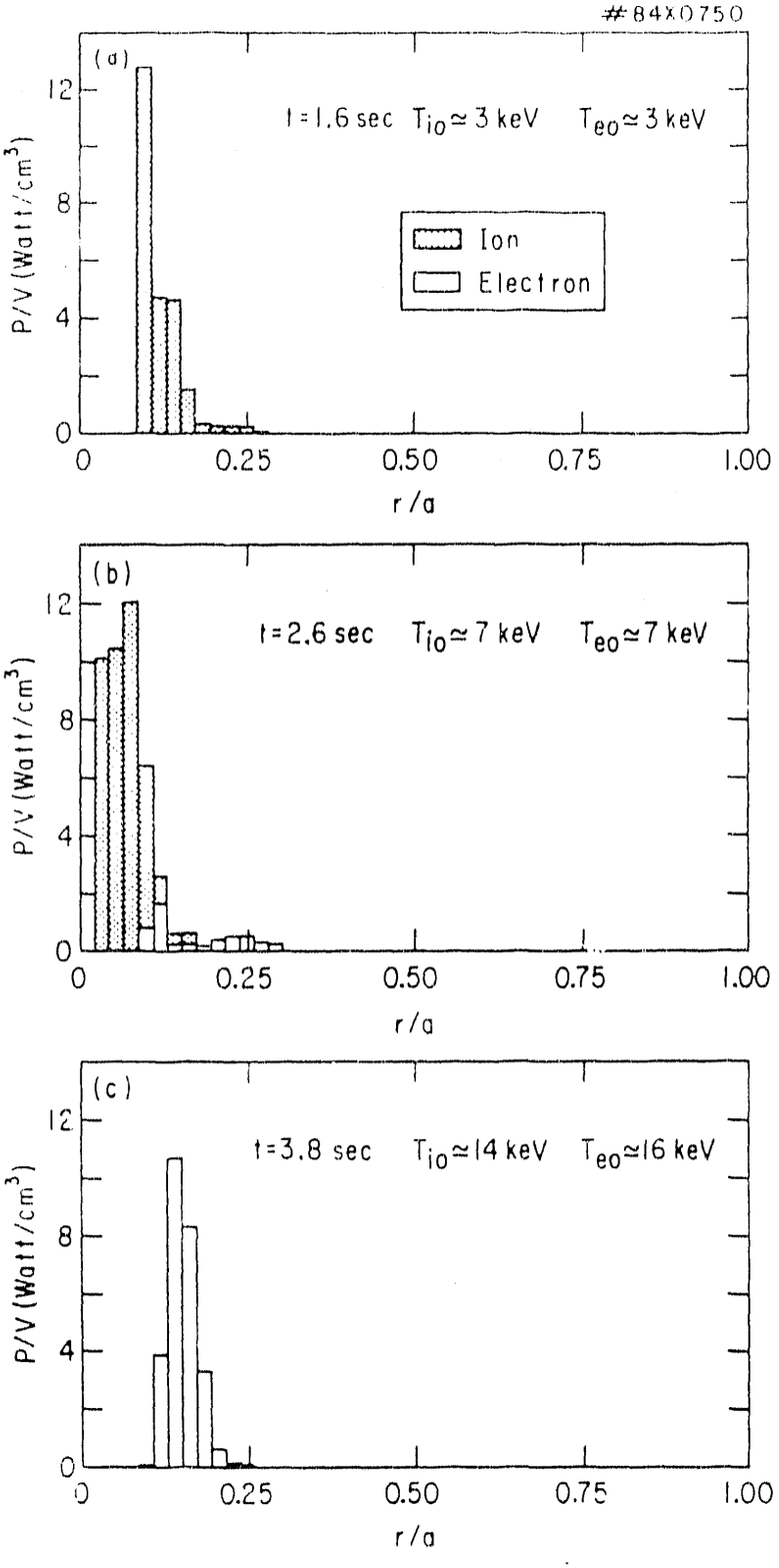
#84X0750
(a)
t=1.6 sec $T_{io}\simeq 3$ keV $T_{eo}\simeq 3$ keV
Ion
Electron
P/V (Watt/cm^3)
r/a
(b)
t=2.6 sec $T_{io}\simeq 7$ keV $T_{eo}\simeq 7$ keV
P/V (Watt/cm^3)
r/a
(c)
t=3.8 sec $T_{io}\simeq 14$ keV $T_{eo}\simeq 16$ keV
P/V (Watt/cm^3)
r/a

Fig. 14

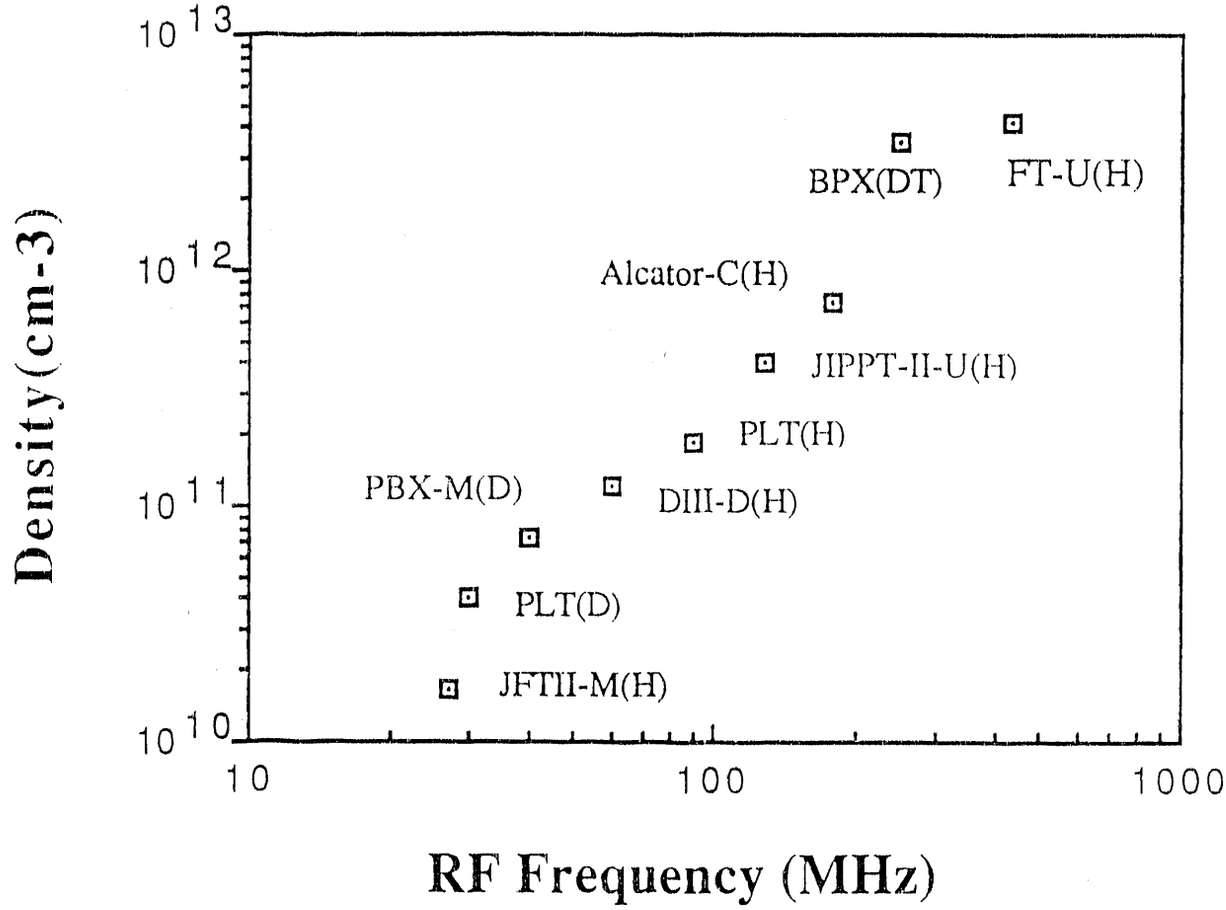
Density(cm-3)
10 13
10 12
10 11
10 10
10
100
1000
BPX(DT)
FT-U(H)
Alcator-C(H)
JIPPT-II-U(H)
PLT(H)
PBX-M(D)
DIII-D(H)
PLT(D)
JFTII-M(H)
RF Frequency (MHz)

Fig. 15

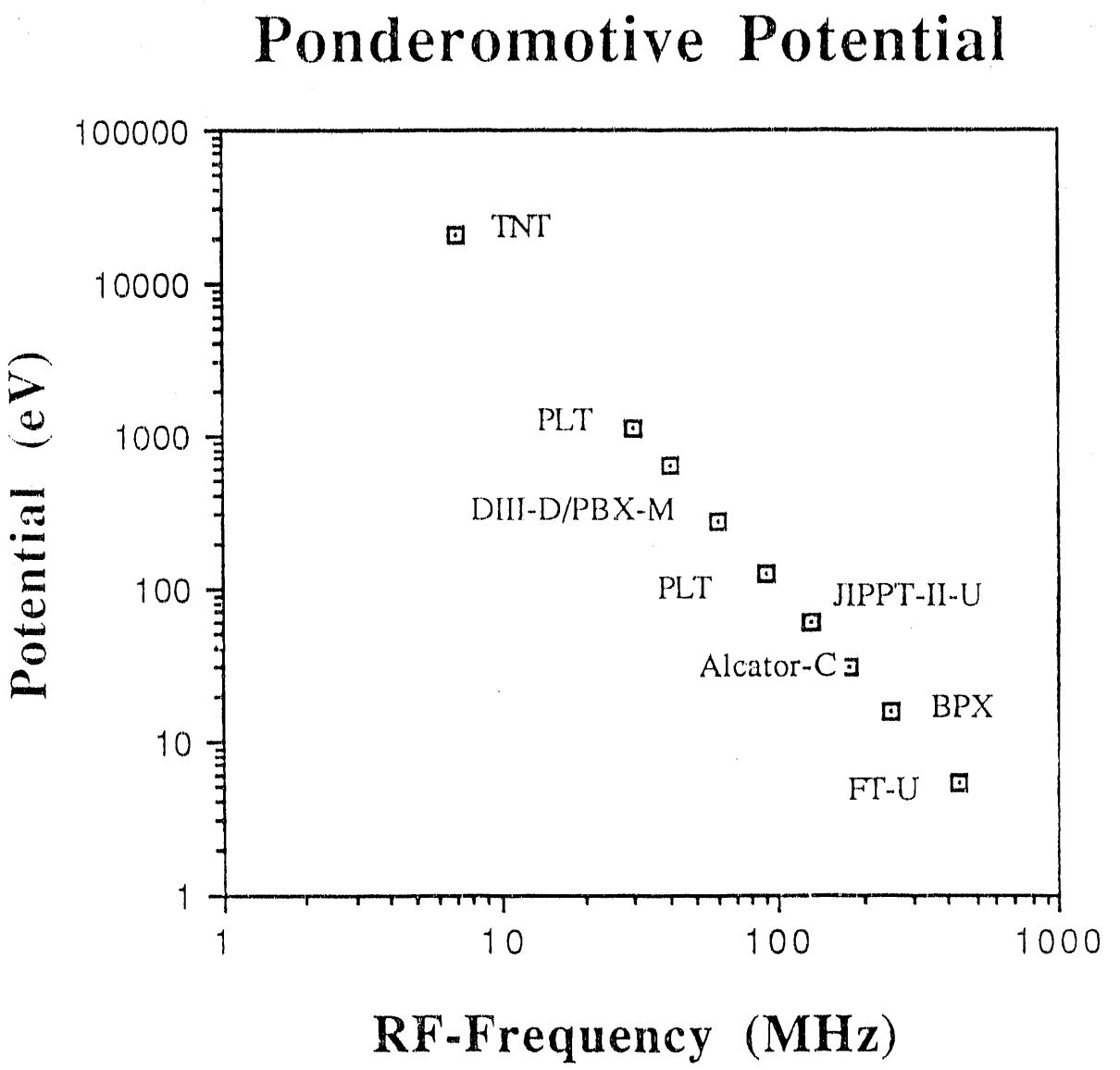
Ponderomotive Potential
100000
10000
1000
100
10
1
Potential (eV)
TNT
PLT
DIII-D/PBX-M
PLT
JIPPT-II-U
Alcator-C
BPX
FT-U
1
10
100
1000
RF-Frequency (MHz)

Fig. 16

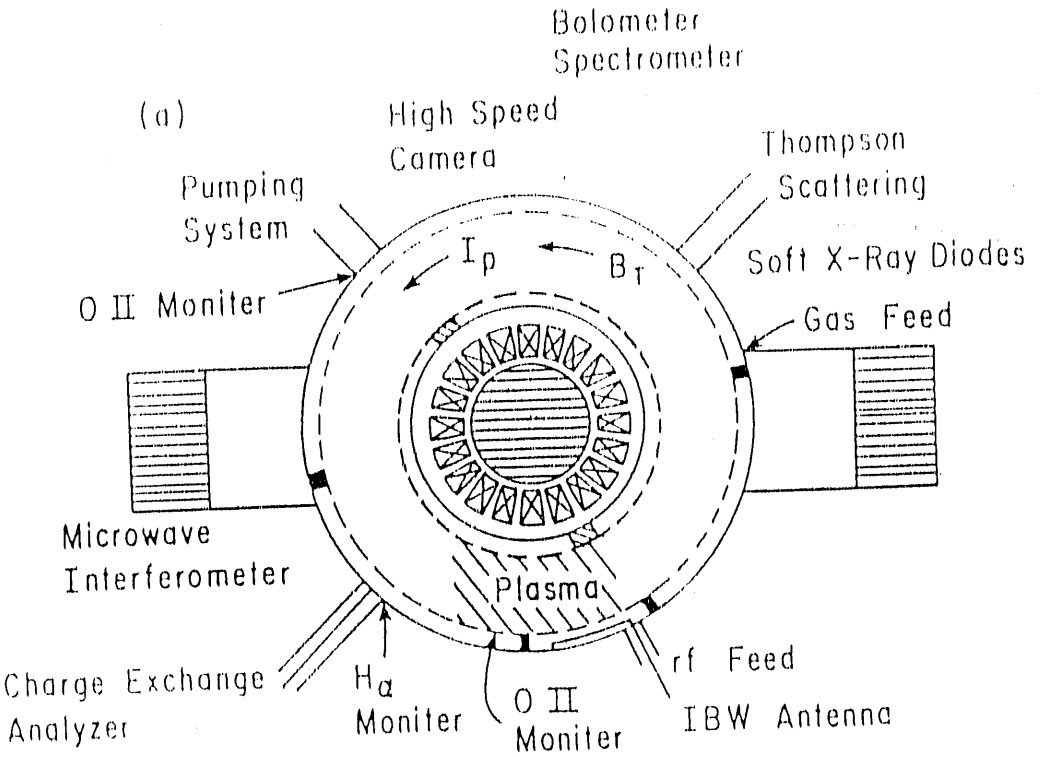

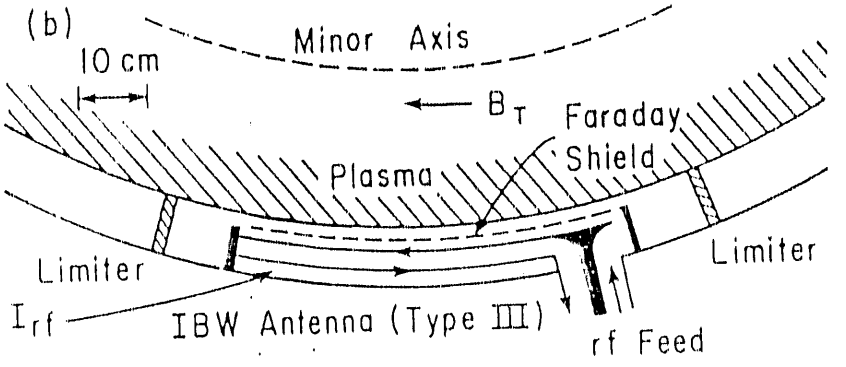

Fig. 17

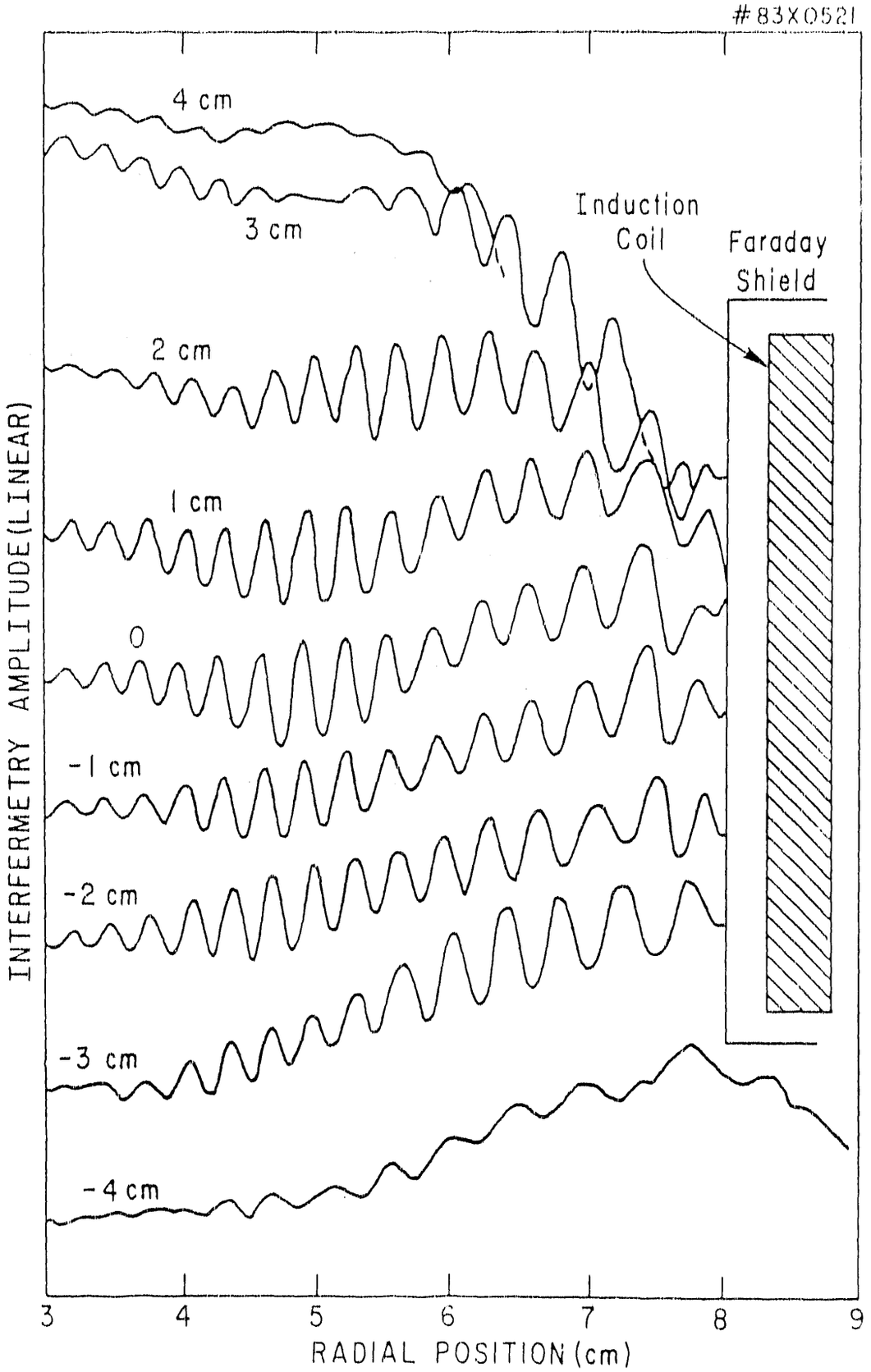
#83X0521
4 cm
3 cm
2 cm
1 cm
0
-1 cm
-2 cm
-3 cm
-4 cm
Induction Coil
Faraday Shield
INTERFERMETRY AMPLITUDE (LINEAR)
3
4
5
6
7
8
9
RADIAL POSITION (cm)

Fig. 18

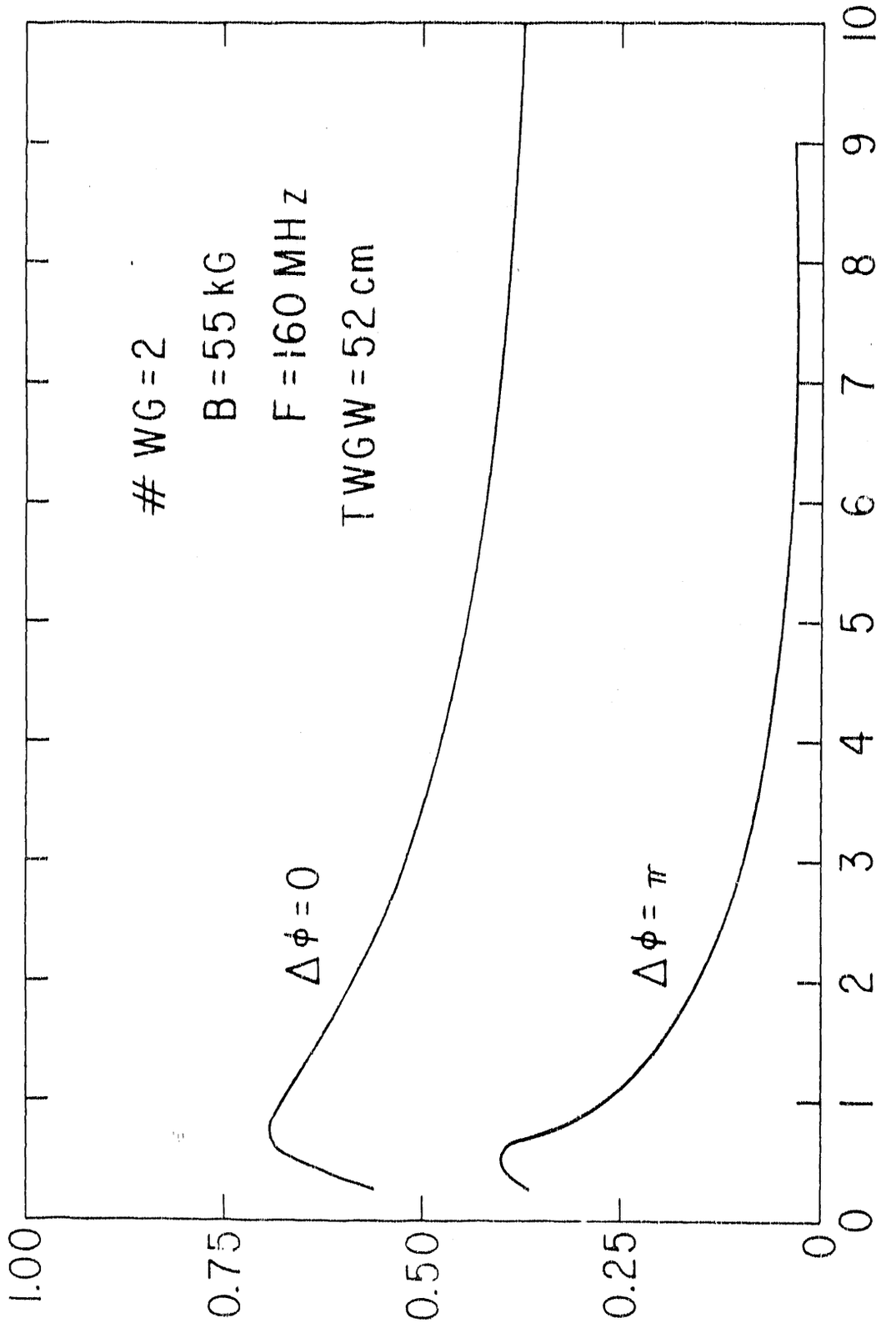
1.00
0.75
0.50
0.25
0
R
0
1
2
3
4
5
6
7
8
9
10
L (cm)
# WG = 2
B = 55 kG
F = 160 MHz
TWGW = 52 cm
Δφ = 0
Δφ = π

Fig. 19

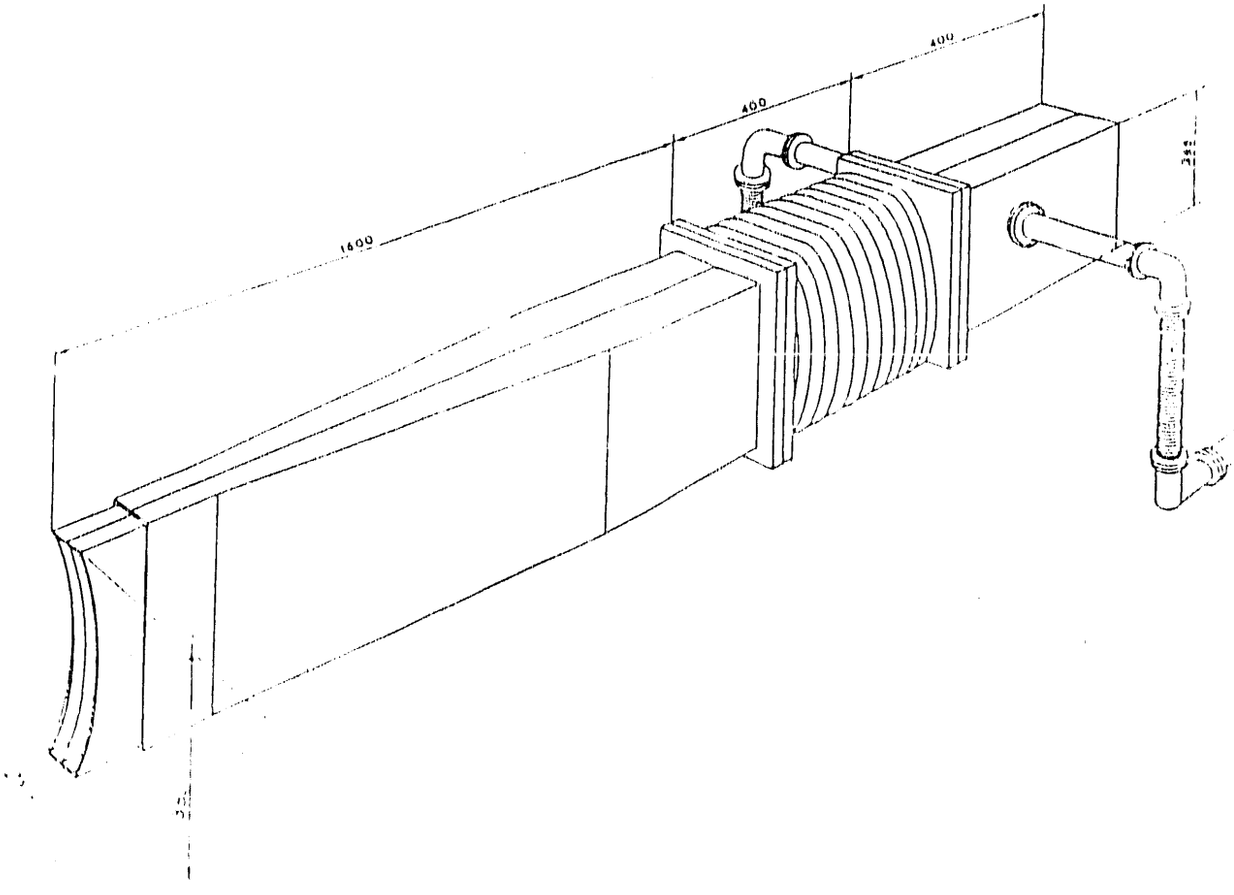

Fig. 20

Axial - Convective - Loss Model

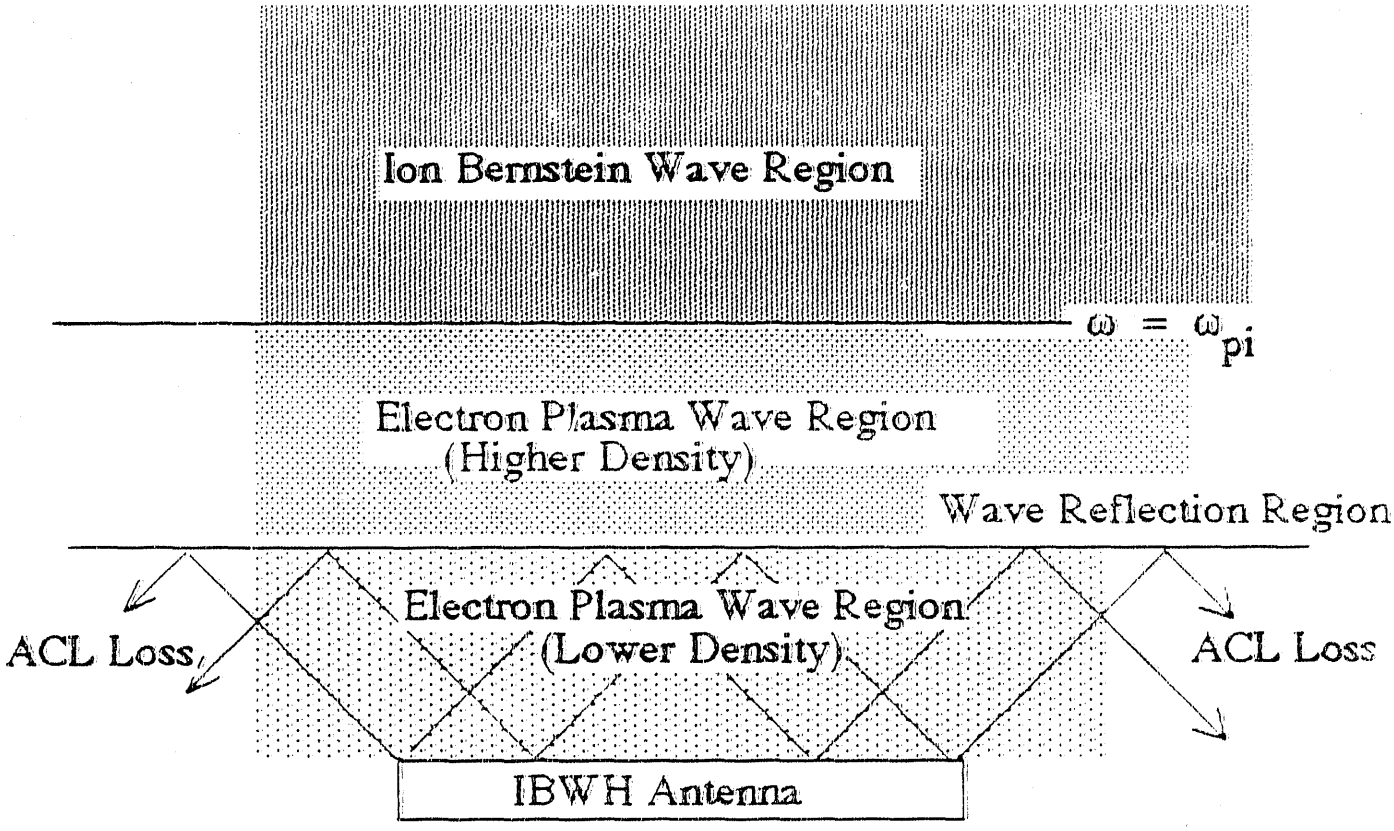

Fig. 21

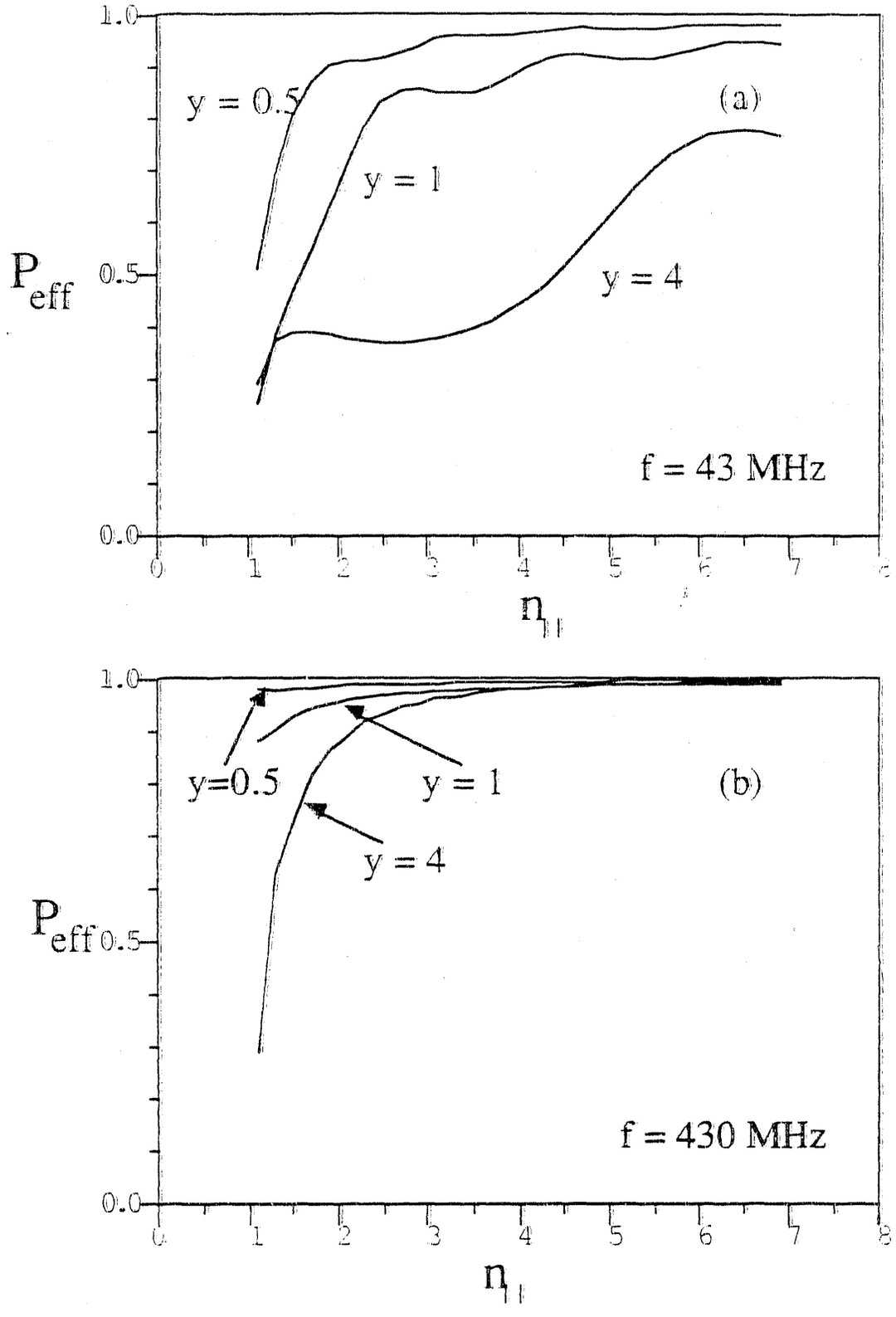
1.0
0.5
0.0
P_{eff}
y = 0.5
y = 1
y = 4
(a)
f = 43 MHz
0
1
2
3
4
5
6
7
$n_{||}$
1.0
0.5
0.0
P_{eff}
y=0.5
y = 1
y = 4
(b)
f = 430 MHz
0
1
2
3
4
5
6
7
8
$n_{||}$

Fig. 22

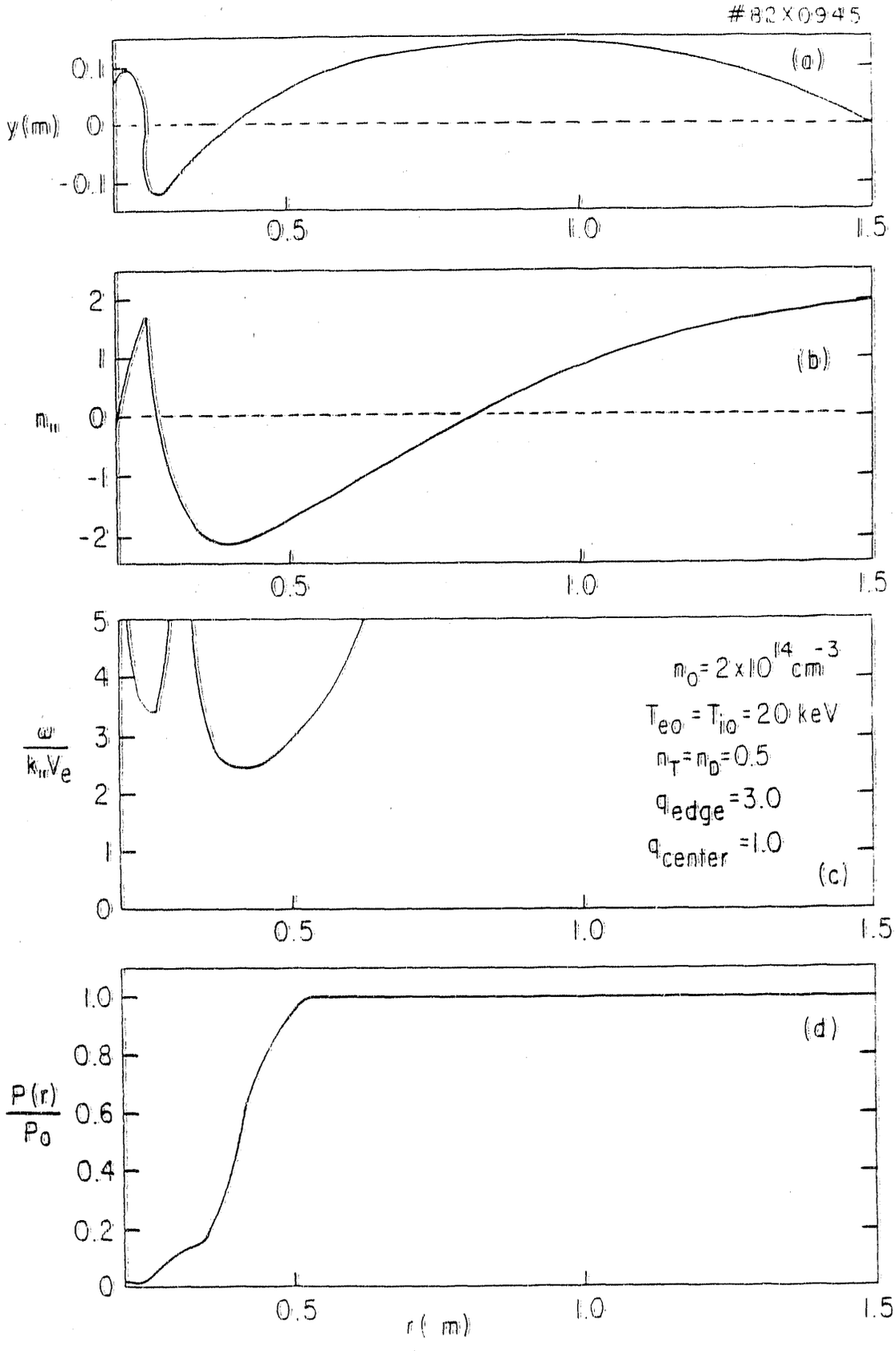
#82X0945
(a)
y(m)
0.1
0
-0.1
0.5
1.0
1.5
(b)
$n_{\parallel}$
2
1
0
-1
-2
0.5
1.0
1.5
(c)
$\frac{\omega}{k_{\parallel}V_e}$
5
4
3
2
1
0
$n_0 = 2 \times 10^{14}\ cm^{-3}$
$T_{eo} = T_{io} = 20\ keV$
$n_T = n_D = 0.5$
$q_{edge} = 3.0$
$q_{center} = 1.0$
0.5
1.0
1.5
(d)
$\frac{P(r)}{P_0}$
1.0
0.8
0.6
0.4
0.2
0
0.5
1.0
1.5
r(m)

Fig. 23

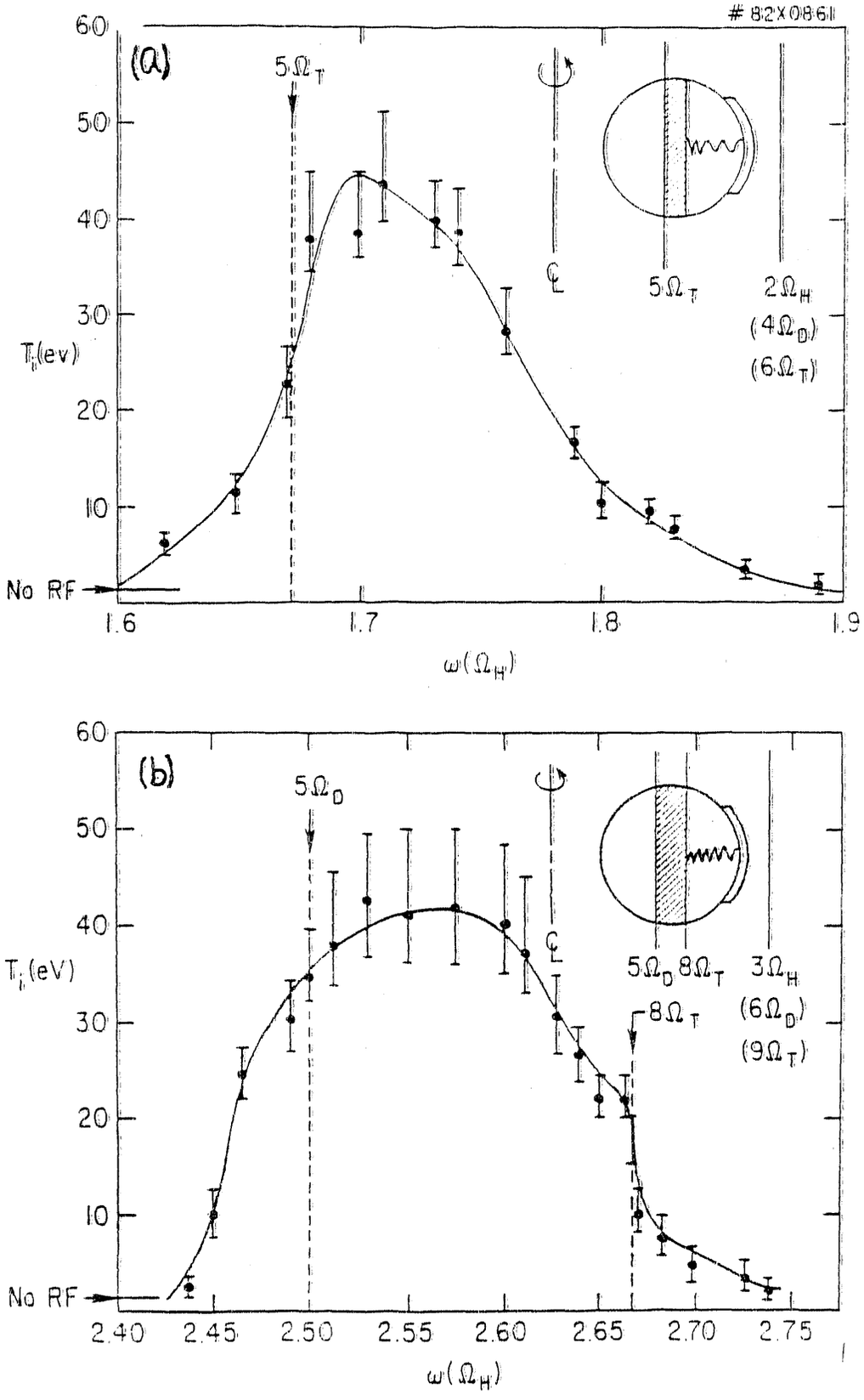
82X0861
(a)
$5\Omega_T$
T_i(ev)
No RF
$5\Omega_T$
$2\Omega_H$
$(4\Omega_D)$
$(6\Omega_T)$
$\omega(\Omega_H)$
(b)
$5\Omega_D$
T_i(eV)
No RF
$5\Omega_D$ $8\Omega_T$
$8\Omega_T$
$3\Omega_H$
$(6\Omega_D)$
$(9\Omega_T)$
$\omega(\Omega_H)$

Fig. 24

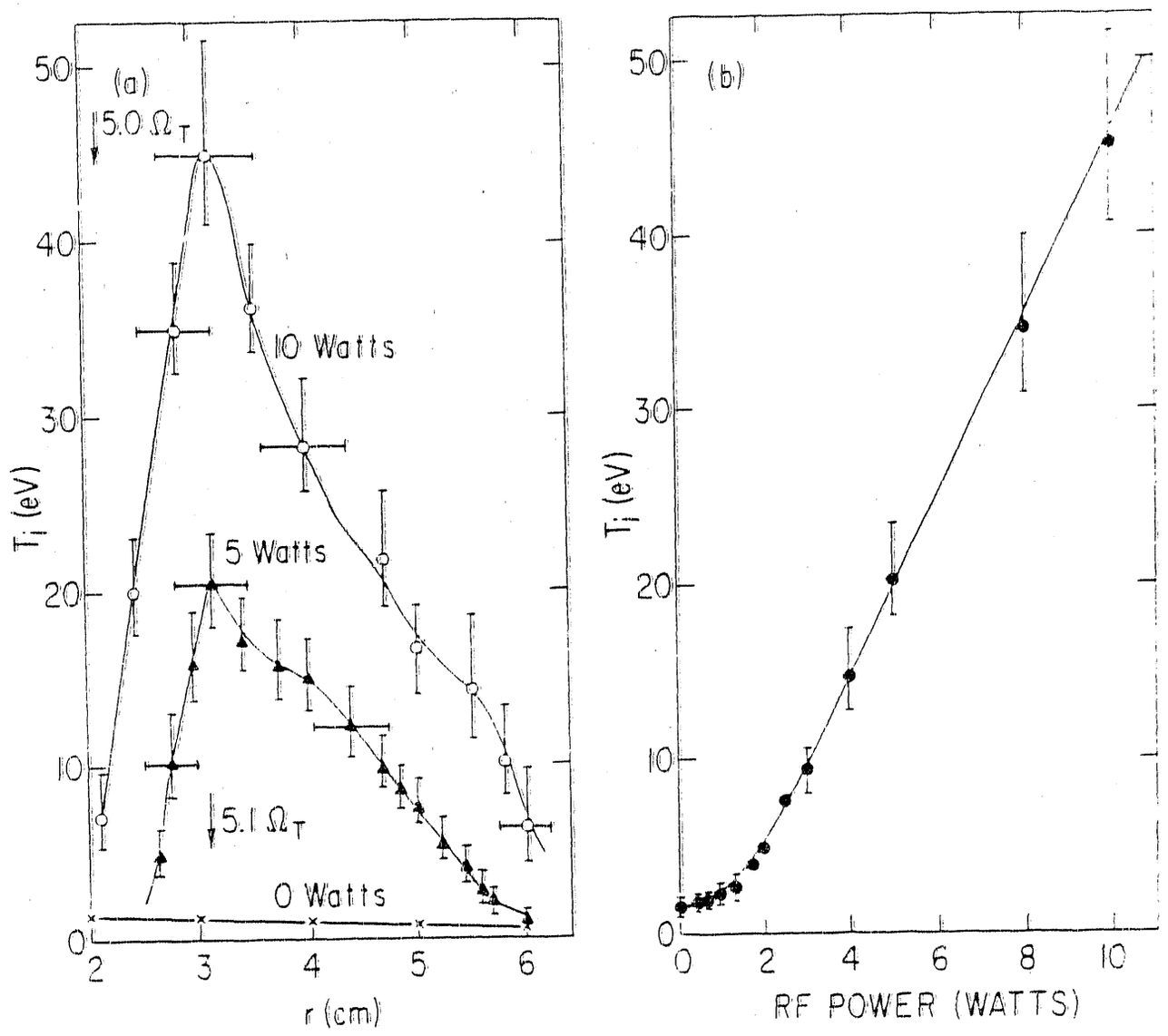
(a)
5.0 Ω_T
10 Watts
5 Watts
5.1 Ω_T
0 Watts
T_i (eV)
r (cm)
(b)
T_i (eV)
RF POWER (WATTS)

Fig. 25

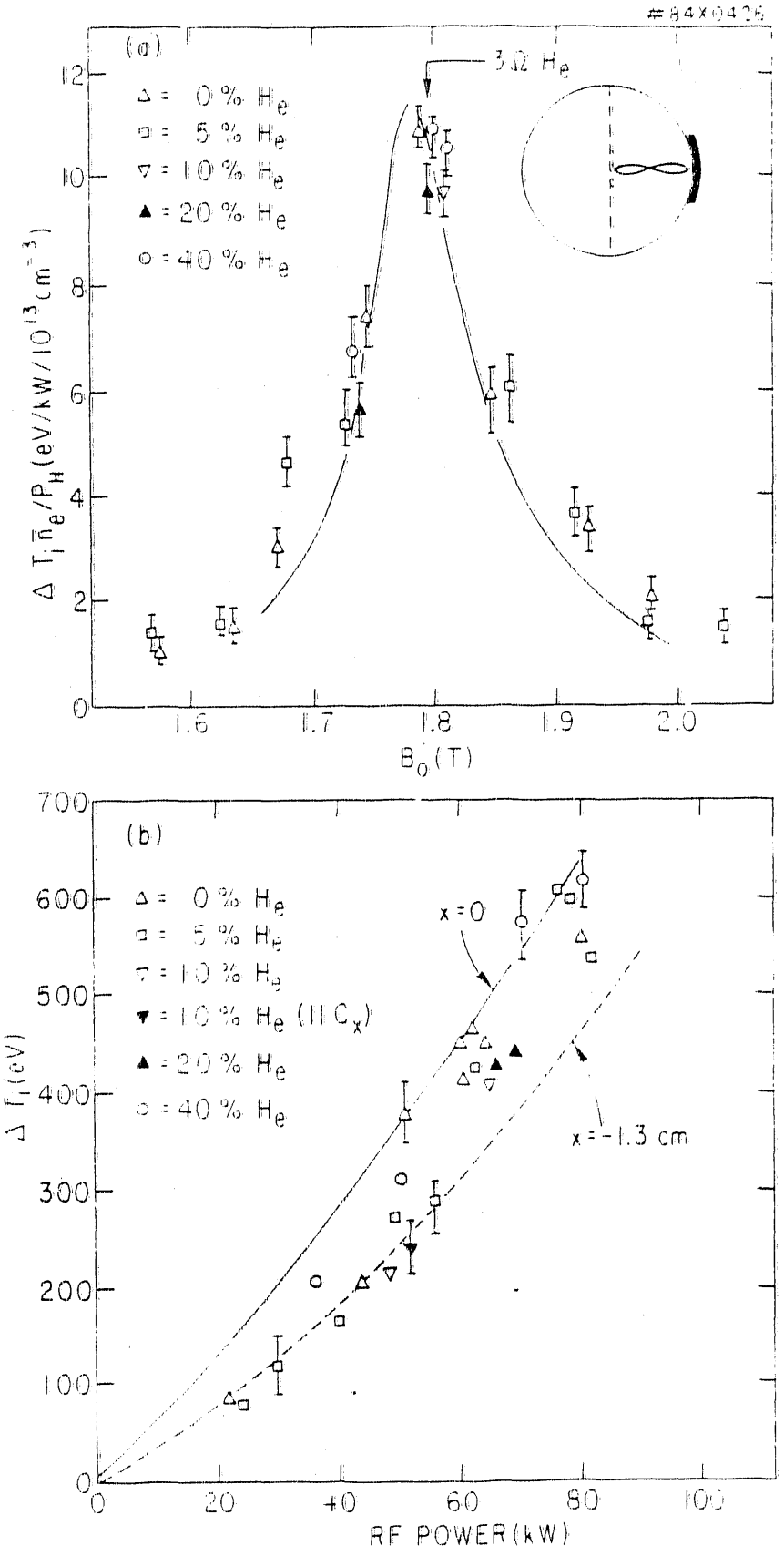
#84X0425
(a)
3Ω He
Δ = 0 % He
□ = 5 % He
▽ = 10 % He
▲ = 20 % He
○ = 40 % He
Δ T_i n̄_e/P_H (eV/kW/10^13 cm^-3)
B_0 (T)
(b)
Δ = 0 % He
□ = 5 % He
▽ = 10 % He
▼ = 10 % He (II C_x)
▲ = 20 % He
○ = 40 % He
x = 0
x = -1.3 cm
Δ T_i (eV)
RF POWER (kW)

Fig. 26

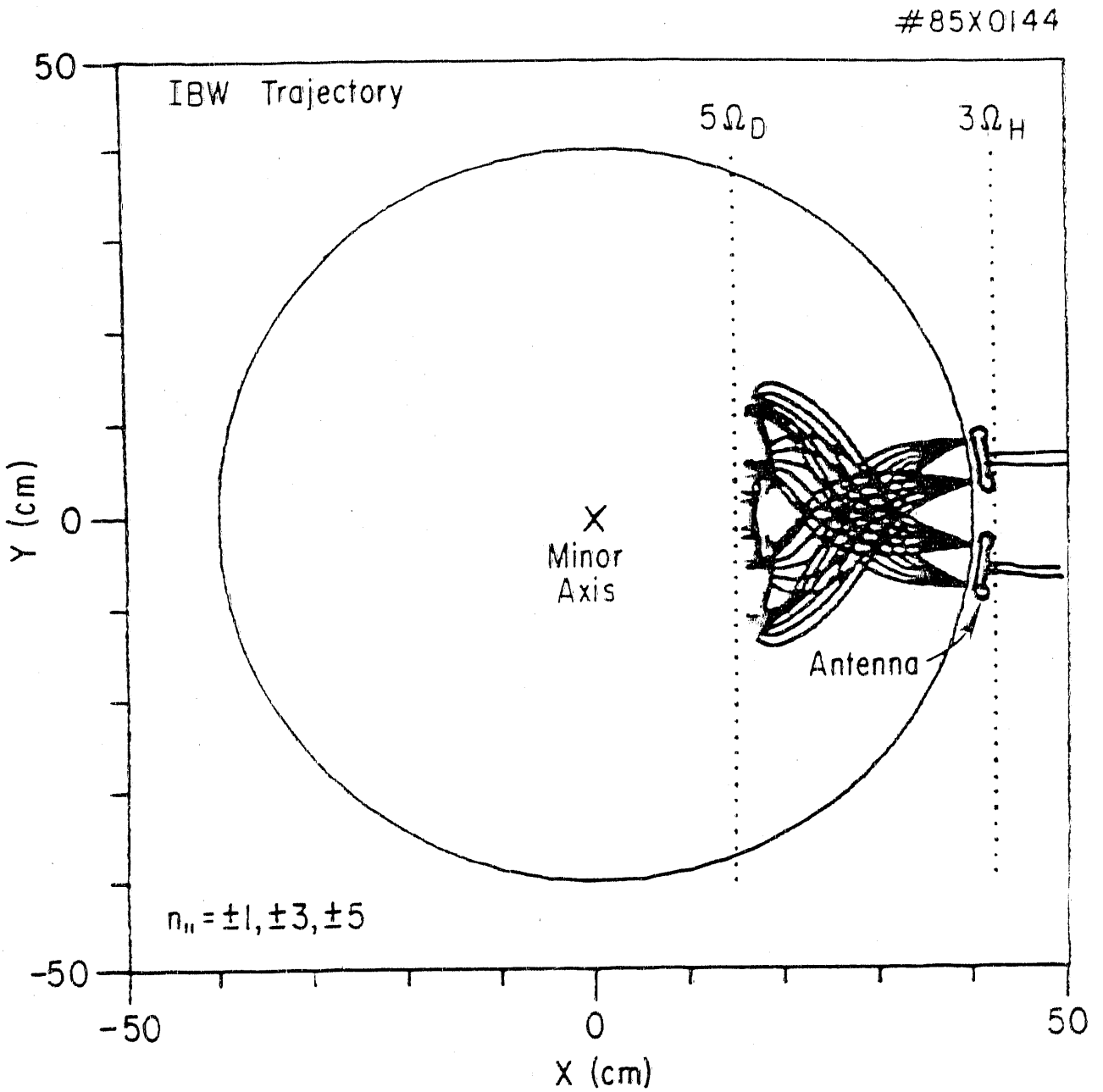
#85X0144
IBW Trajectory
5Ω_D
3Ω_H
X
Minor
Axis
Antenna
n_∥ = ±1, ±3, ±5
50
0
-50
Y (cm)
-50
0
50
X (cm)

Fig. 27

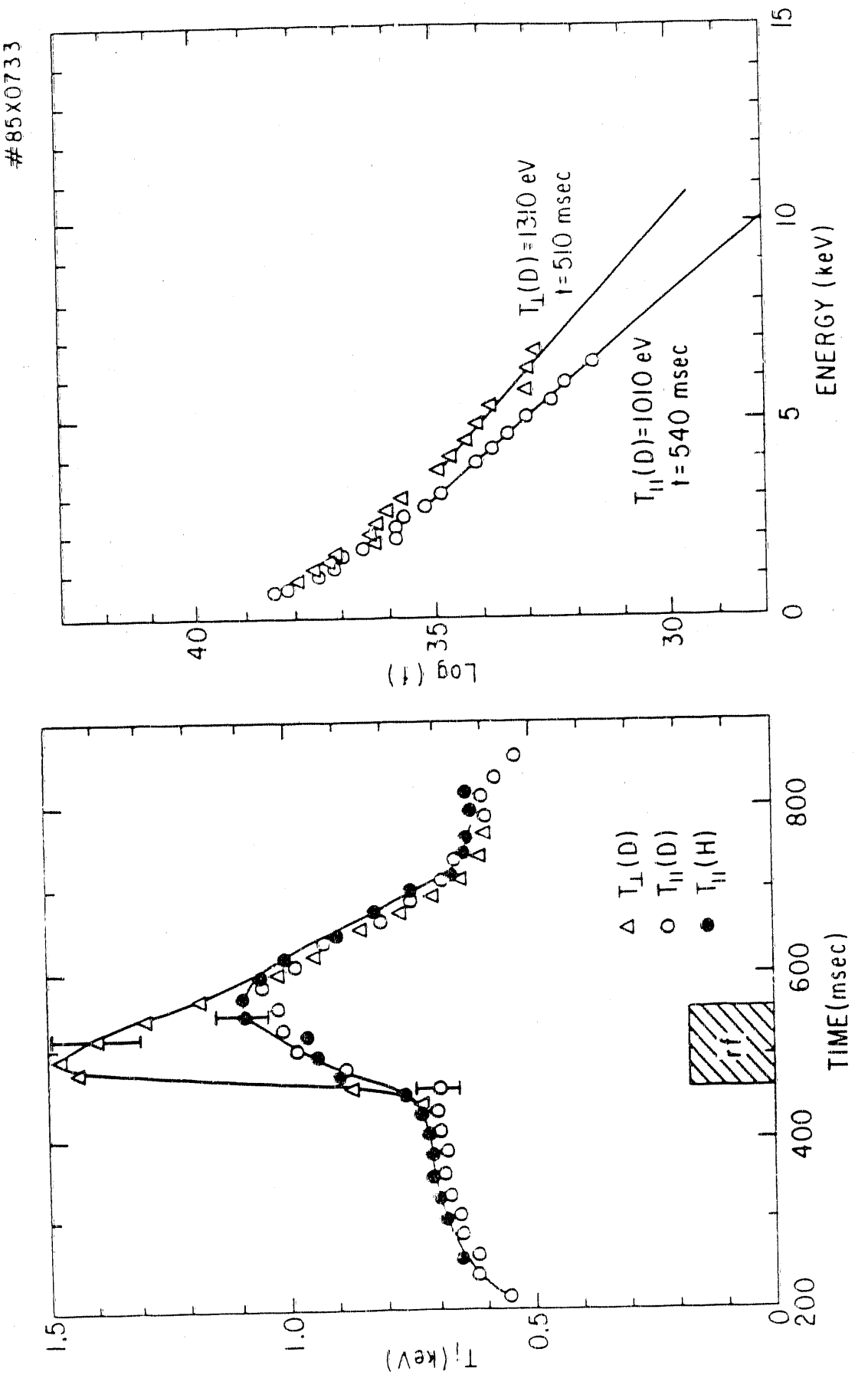
#85X0733
Log (↑)
40
35
30
0
5
10
15
ENERGY (keV)
$T_\perp(D)$=1310 eV
t=510 msec
$T_{||}(D)$=1010 eV
t=540 msec
T_i(keV)
1.5
1.0
0.5
0
200
400
600
800
TIME(msec)
$T_\perp(D)$
$T_{||}(D)$
$T_{||}(H)$
rf

Fig. 28

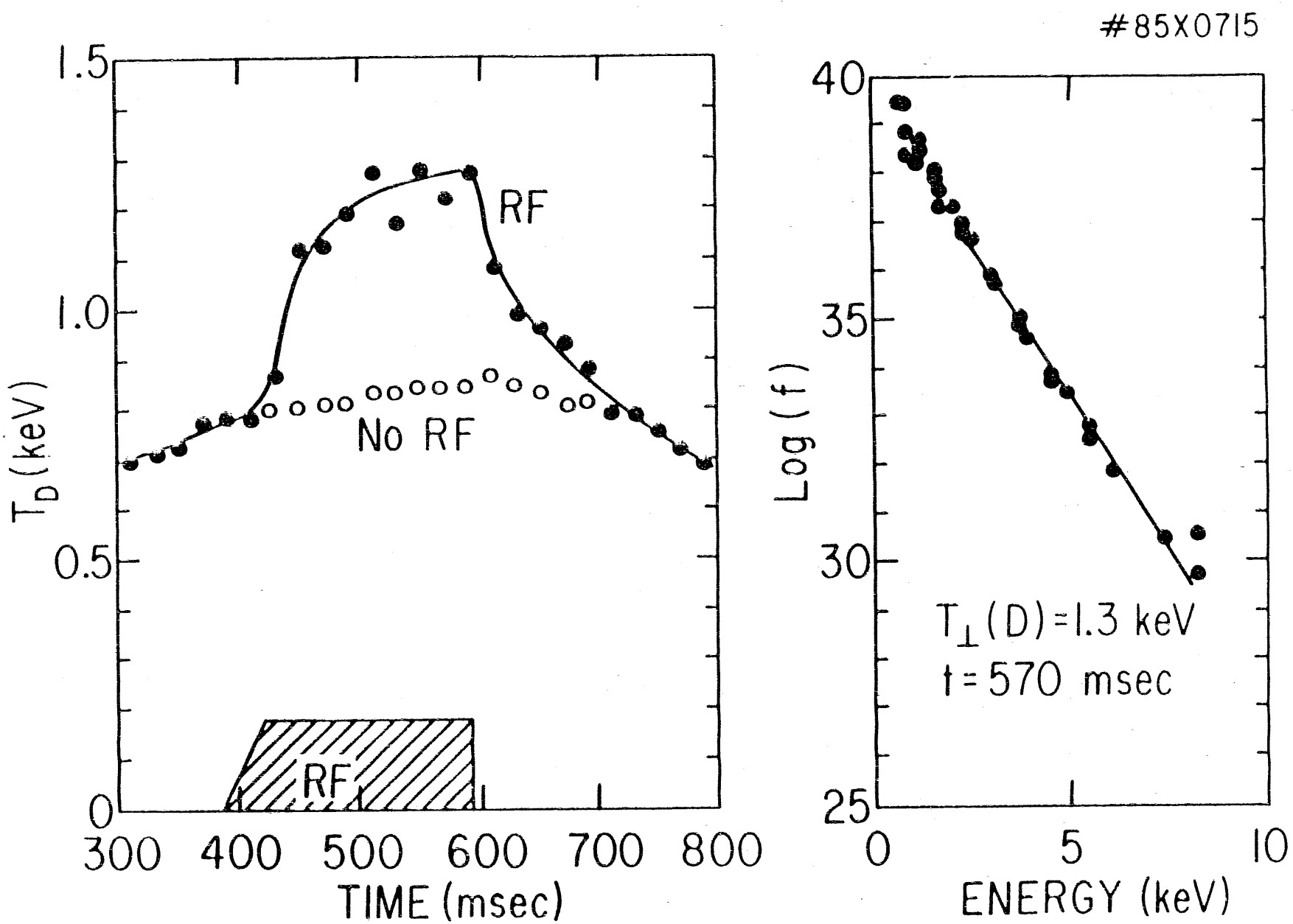
#85X0715
1.5
1.0
0.5
0
T_D (keV)
RF
No RF
RF
300
400
500
600
700
800
TIME (msec)
40
35
30
25
Log (f)
$T_\perp$ (D) = 1.3 keV
t = 570 msec
0
5
10
ENERGY (keV)

Fig. 29

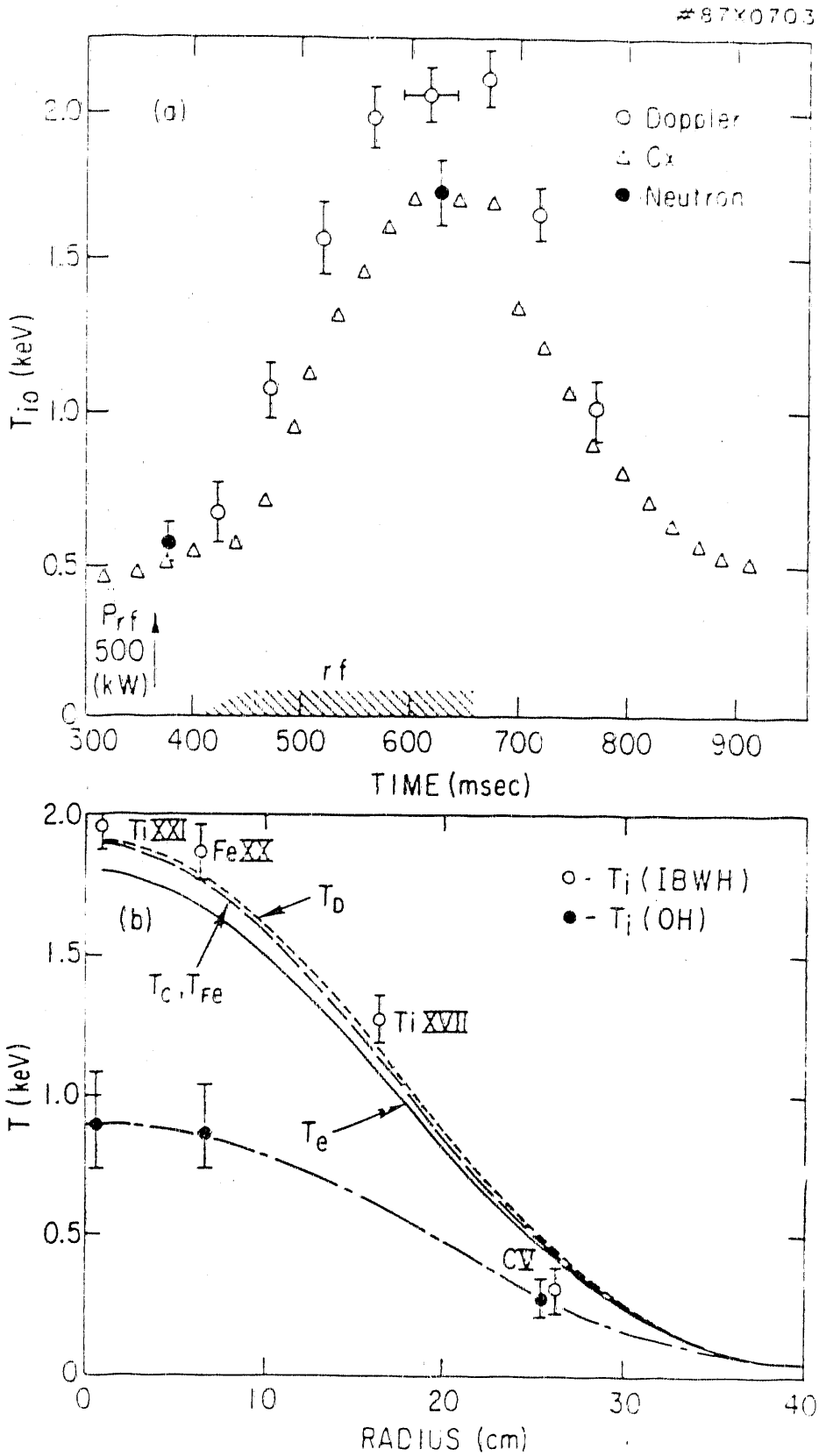
#87X0703
(a)
Doppler
Cx
Neutron
T_{io} (keV)
P_{rf}
500
(kW)
rf
TIME (msec)
(b)
Ti XXI
Fe XX
T_D
T_C, T_{Fe}
Ti XVII
T_e
C VI
T_i (IBWH)
T_i (OH)
T (keV)
RADIUS (cm)

Fig. 30

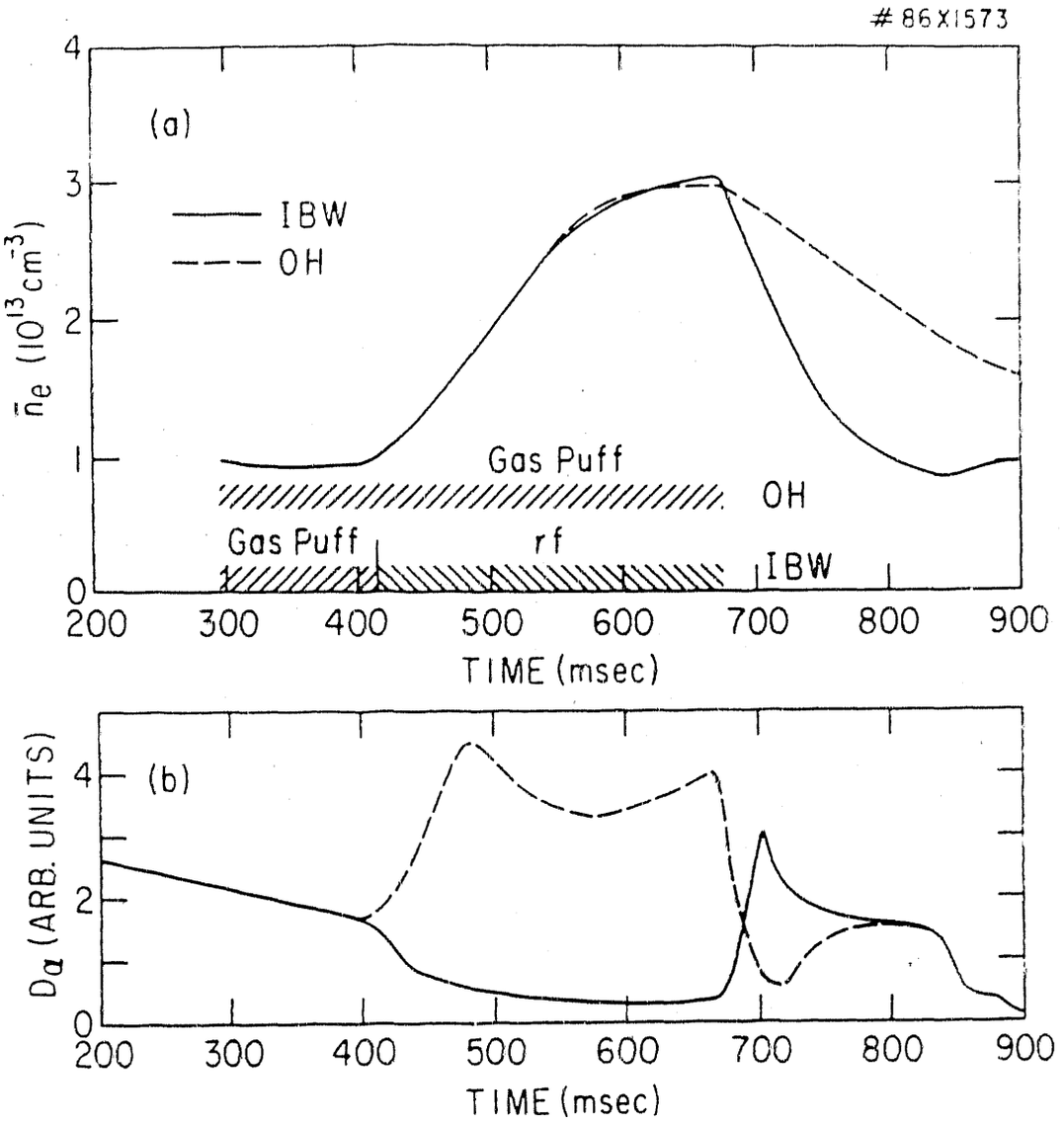
#86X1573
(a)
IBW
OH
$\bar{n}_e$ (10^{13}cm^{-3})
Gas Puff
OH
Gas Puff
rf
IBW
TIME (msec)
(b)
D_α (ARB. UNITS)
TIME (msec)

Fig.31

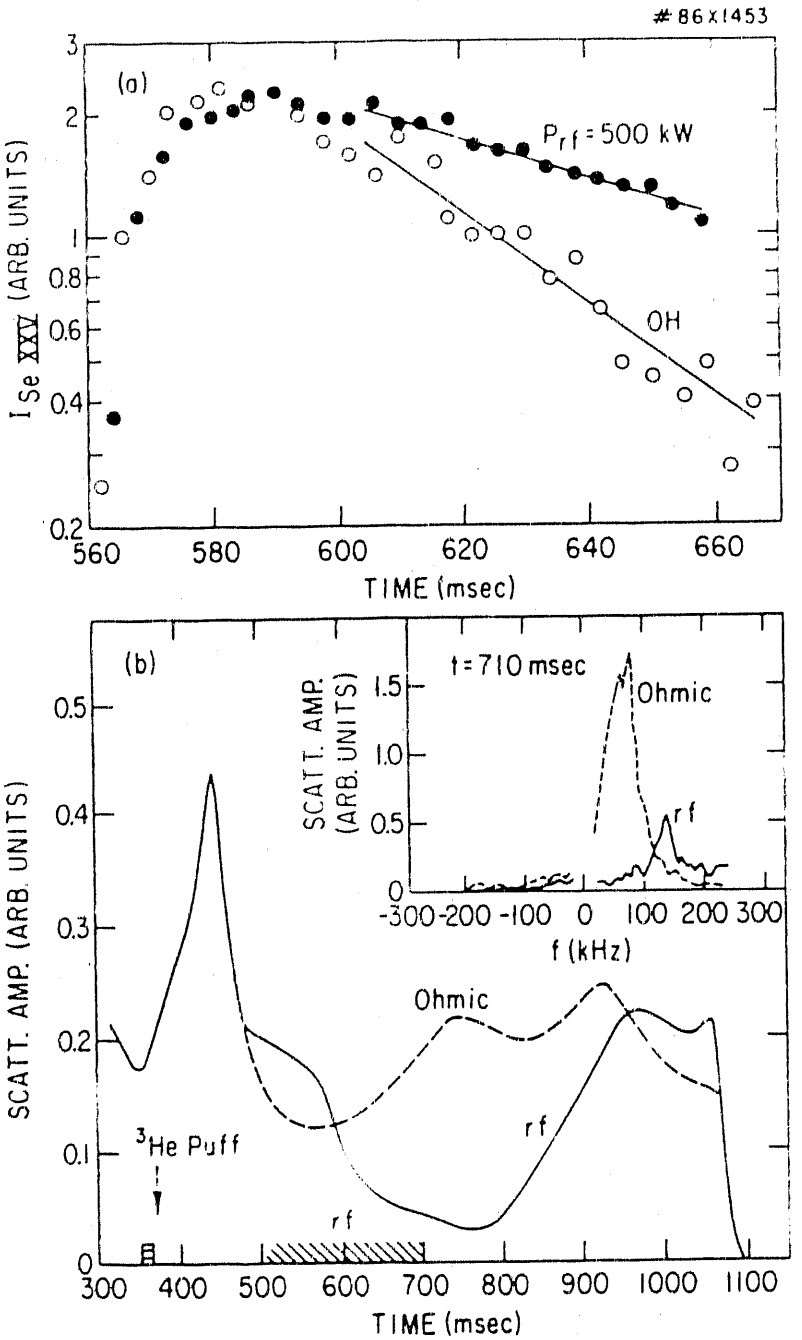
#86x1453
(a)
P_{rf} = 500 kW
OH
$I_{Se\ XXV}$ (ARB. UNITS)
TIME (msec)
(b)
t = 710 msec
Ohmic
rf
SCATT. AMP. (ARB. UNITS)
f (kHz)
Ohmic
rf
rf
^{3}He Puff
SCATT. AMP. (ARB. UNITS)
TIME (msec)

Fig.32

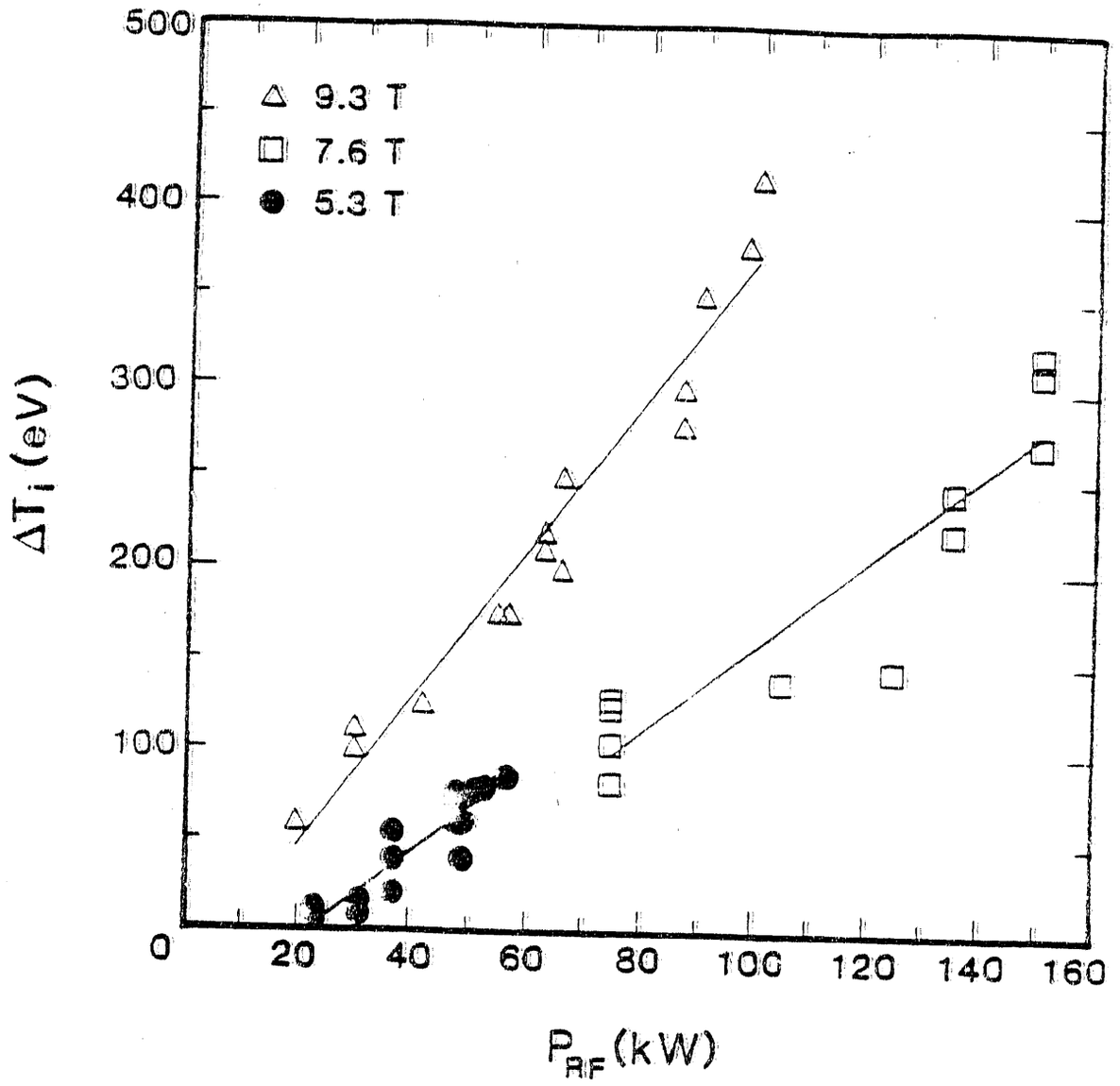
500
400
300
200
100
0
20
40
60
80
100
120
140
160
9.3 T
7.6 T
5.3 T
ΔTi (eV)
PRF (kW)

Fig.33

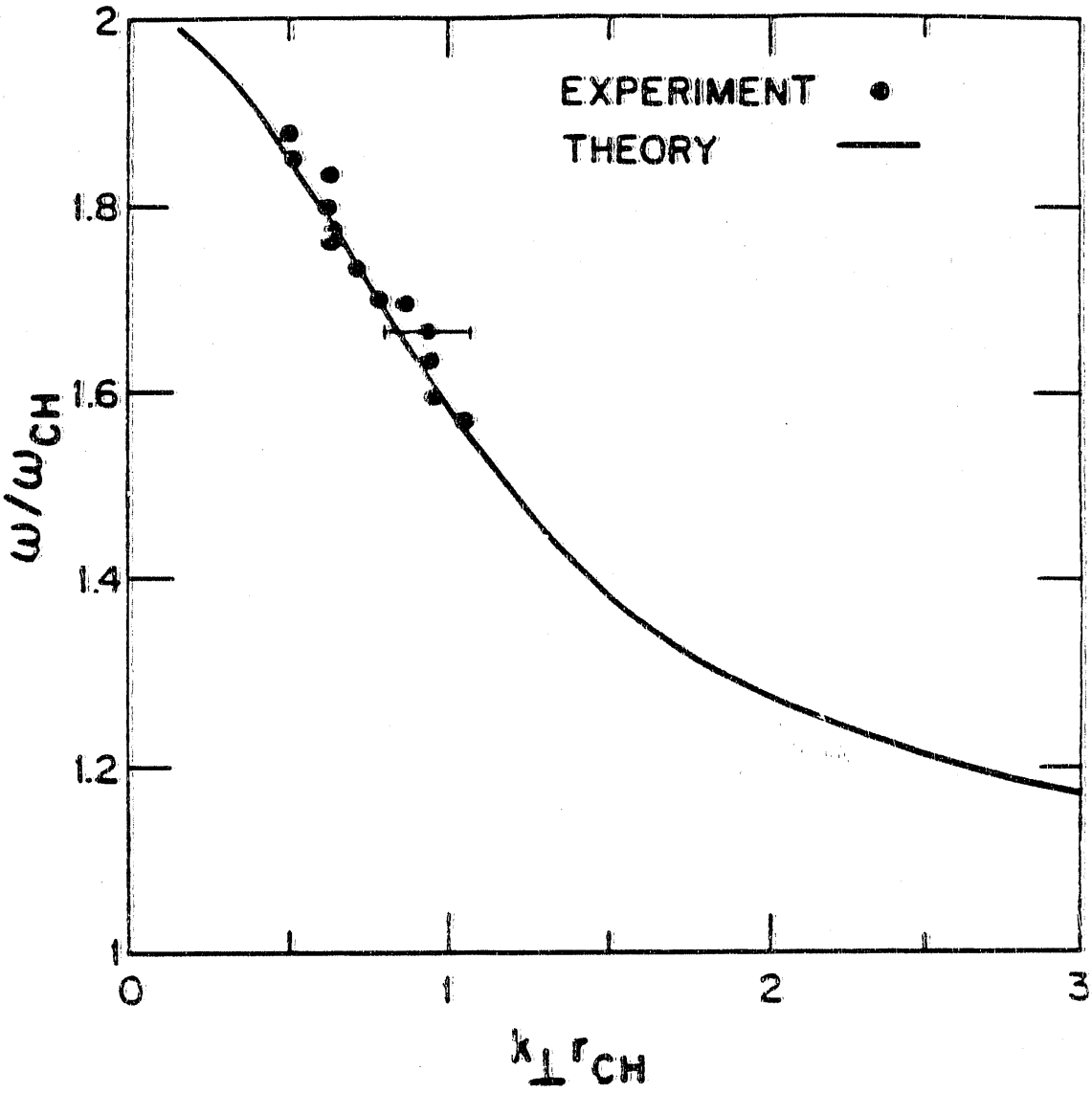

Fig. 34

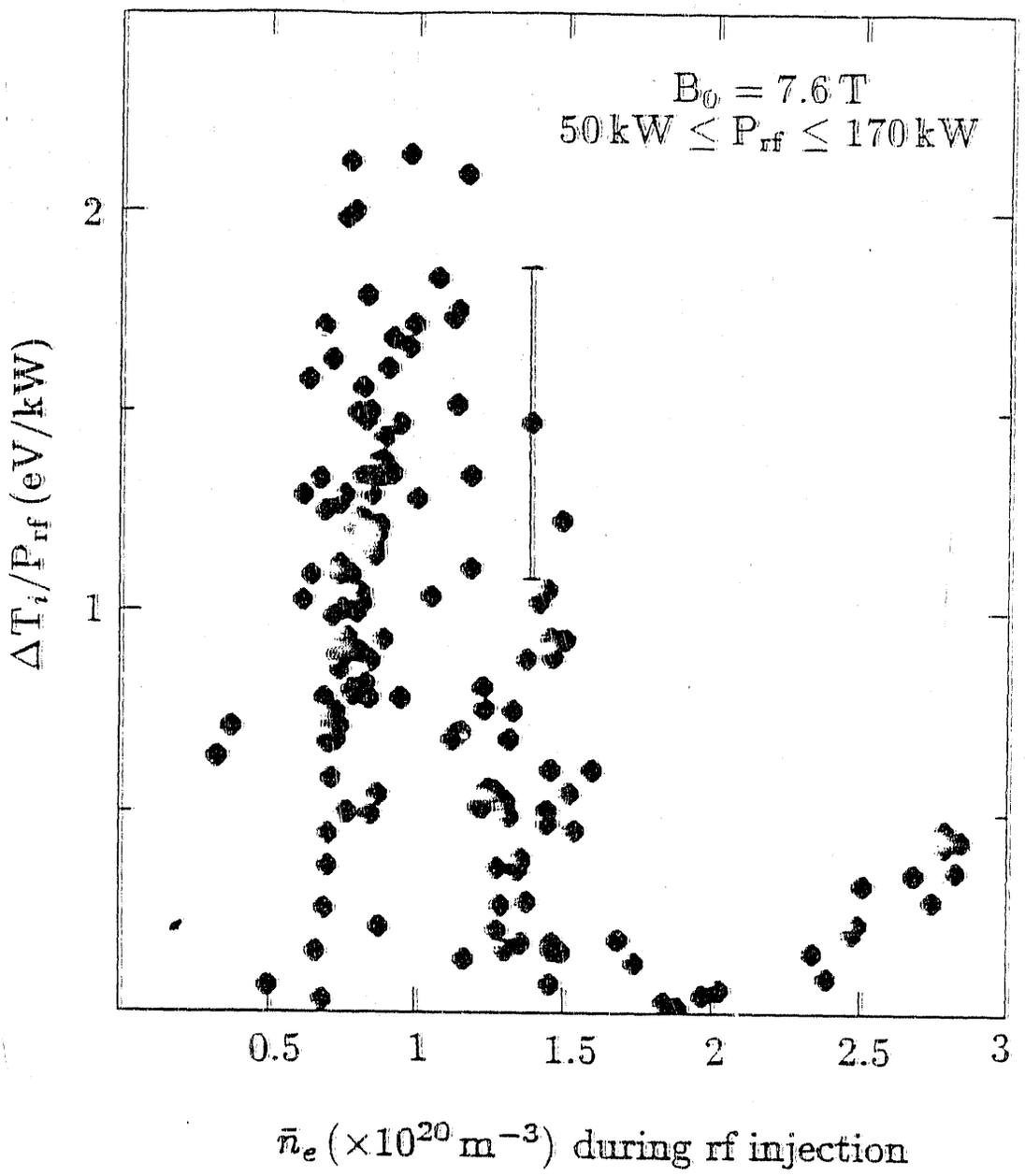
$B_0 = 7.6\,T$
$50\,kW \leq P_{rf} \leq 170\,kW$
$\Delta T_i/P_{rf}\,(eV/kW)$
2
1
0.5
1
1.5
2
2.5
3
$\bar{n}_e\,(\times 10^{20}\,m^{-3})$ during rf injection

Fig. 35

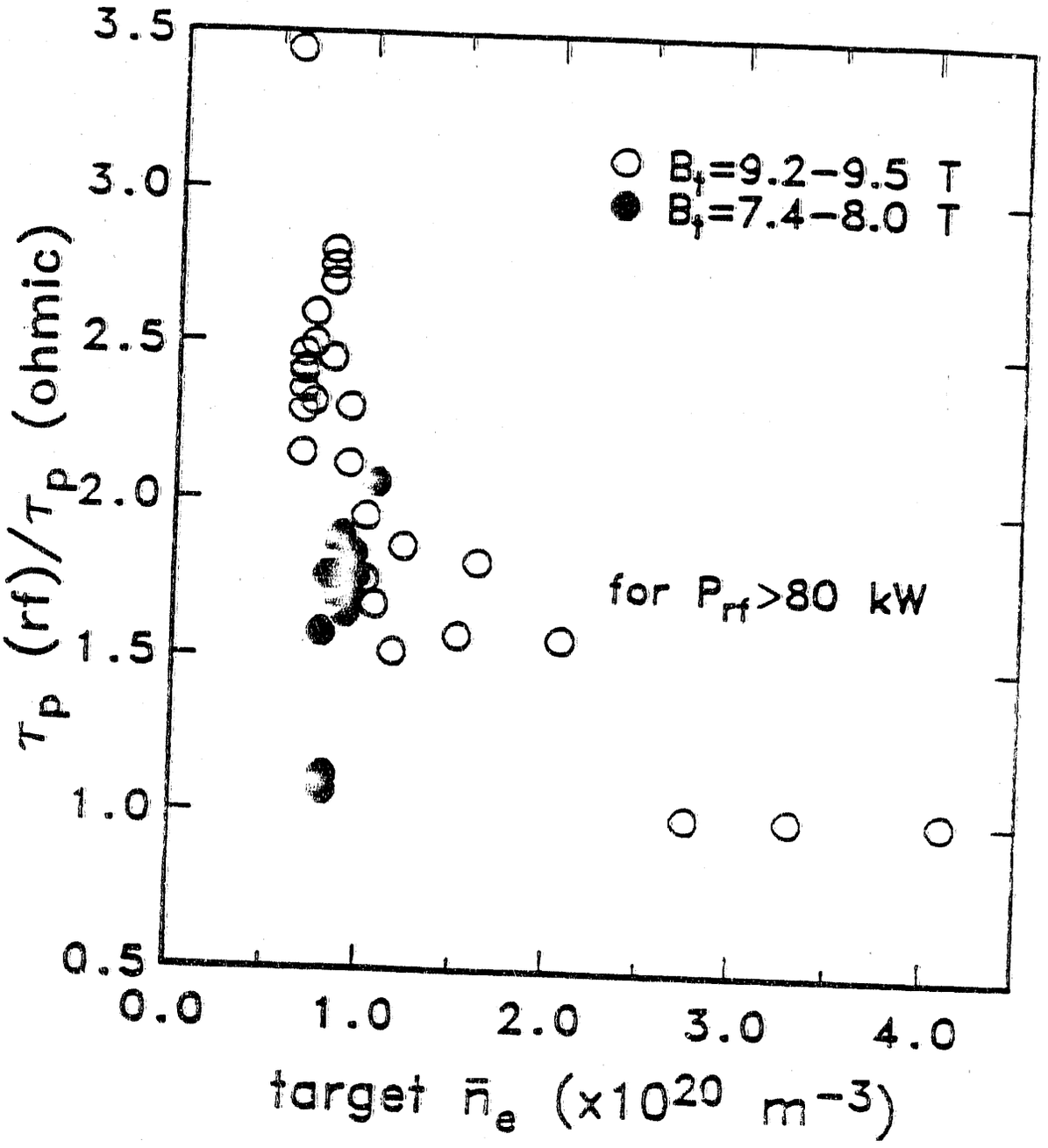
3.5
3.0
2.5
2.0
1.5
1.0
0.5
τ_p (rf)/τ_p (ohmic)
B_t=9.2–9.5 T
B_t=7.4–8.0 T
for P_{rf}>80 kW
0.0
1.0
2.0
3.0
4.0
target $\bar{n}_e$ (x10^{20} m^{-3})

Fig. 36

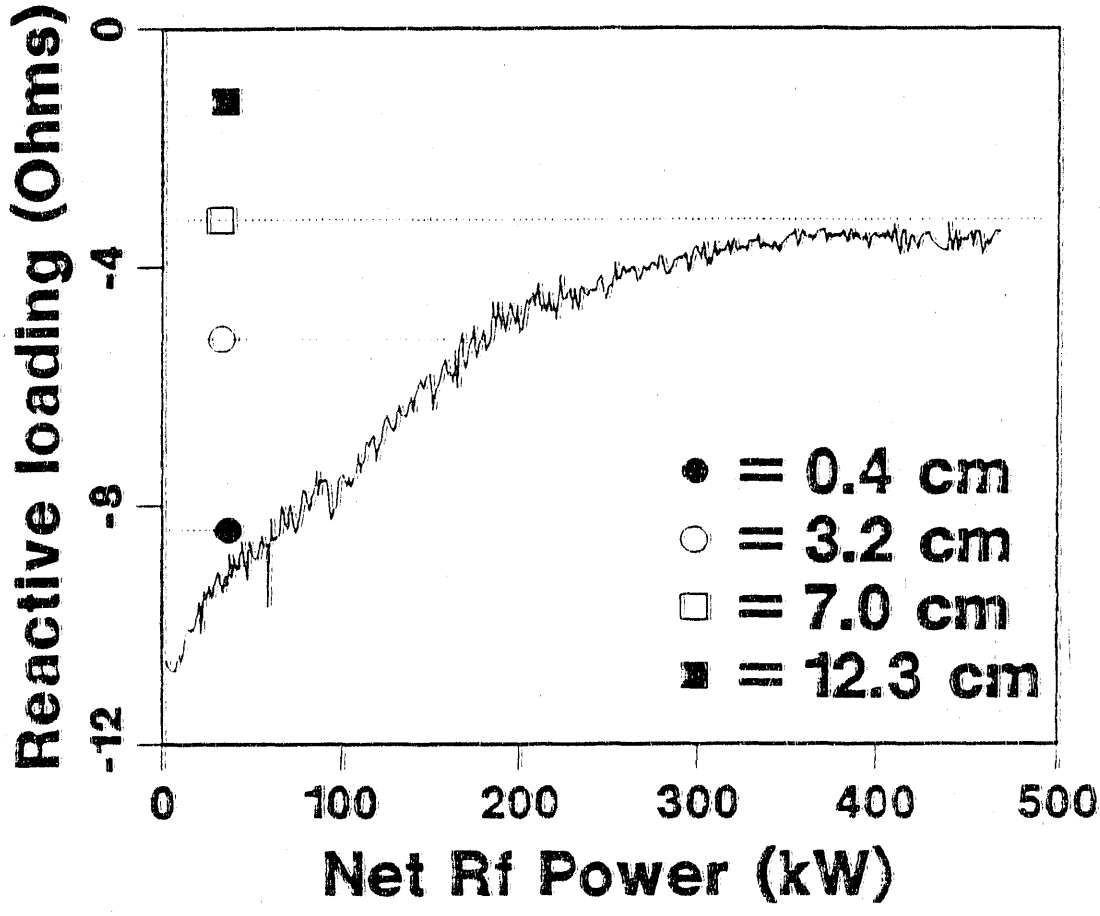
Reactive loading (Ohms)
0
-4
-8
-12
0
100
200
300
400
500
Net Rf Power (kW)
● = 0.4 cm
○ = 3.2 cm
□ = 7.0 cm
■ = 12.3 cm

Fig. 37

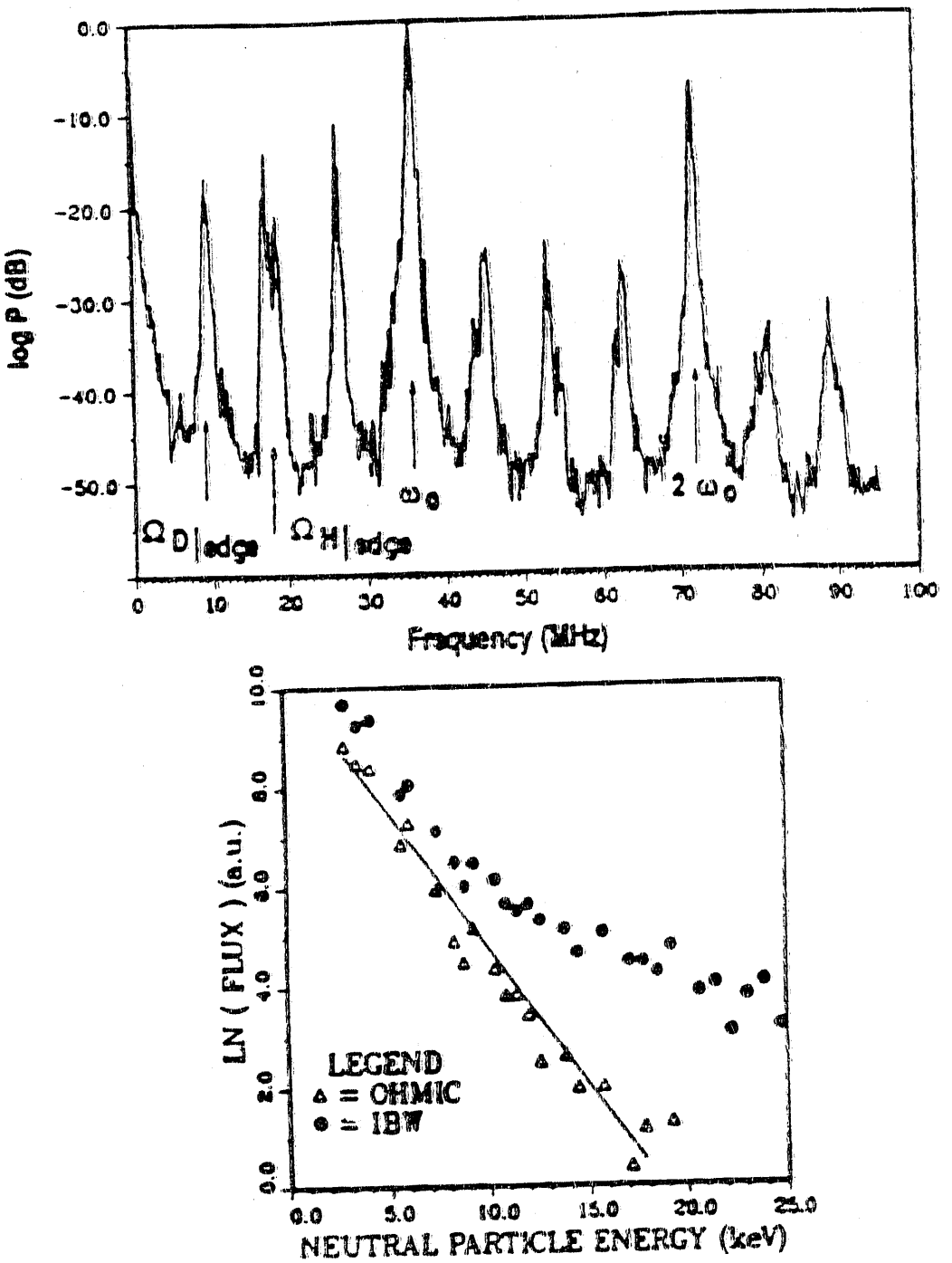
0.0
-10.0
-20.0
-30.0
-40.0
-50.0
log P (dB)
$\Omega_{D|edge}$
$\Omega_{H|edge}$
ω_0
$2\omega_0$
0
10
20
30
40
50
60
70
80
90
100
Frequency (MHz)
10.0
8.0
6.0
4.0
2.0
0.0
LN (FLUX) (a.u.)
LEGEND
△ = OHMIC
● = IBW
0.0
5.0
10.0
15.0
20.0
25.0
NEUTRAL PARTICLE ENERGY (keV)

Fig. 38

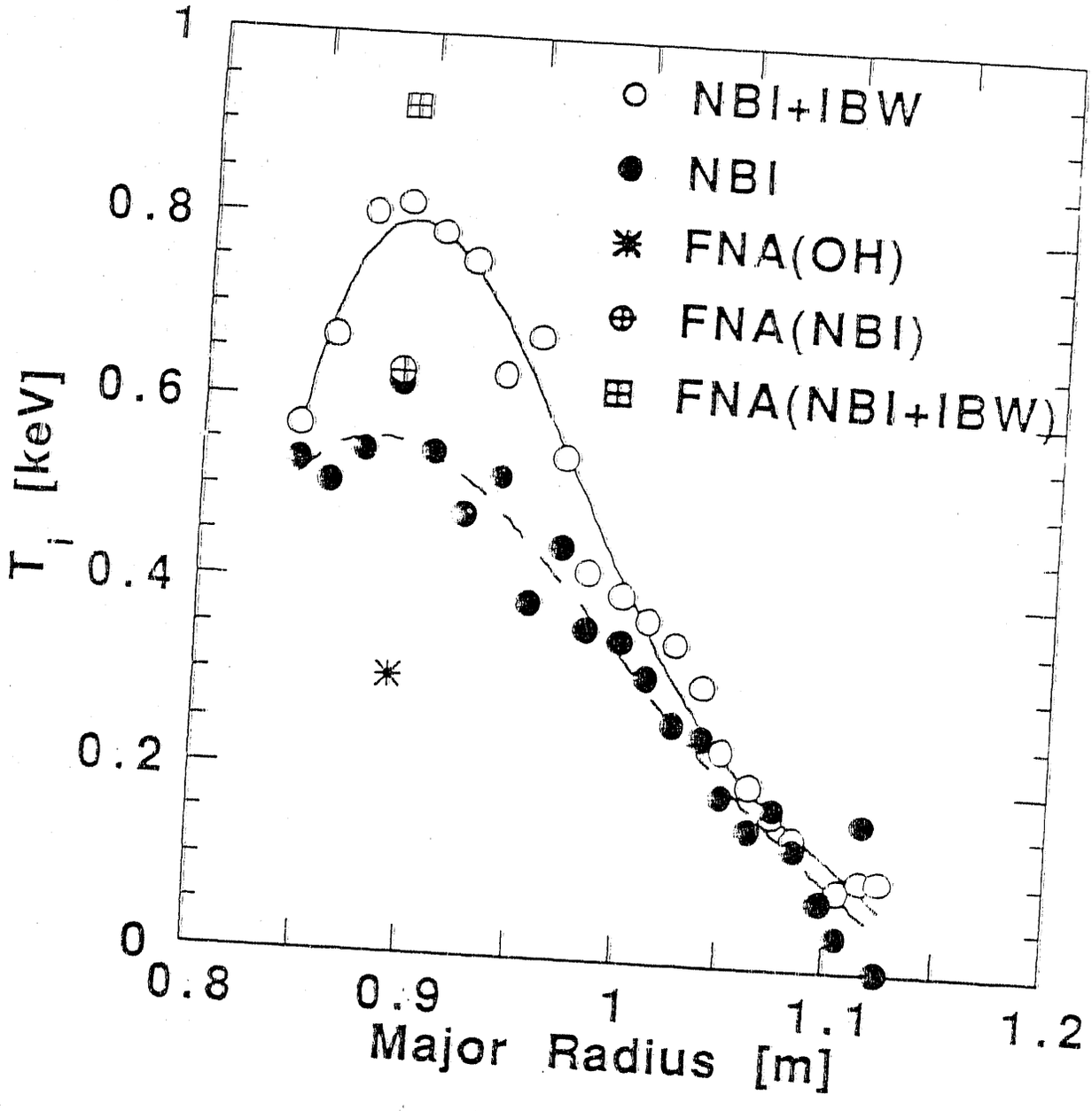
NBI+IBW
NBI
FNA(OH)
FNA(NBI)
FNA(NBI+IBW)
T_i [keV]
Major Radius [m]
0
0.2
0.4
0.6
0.8
1
0.8
0.9
1
1.1
1.2

Fig. 39

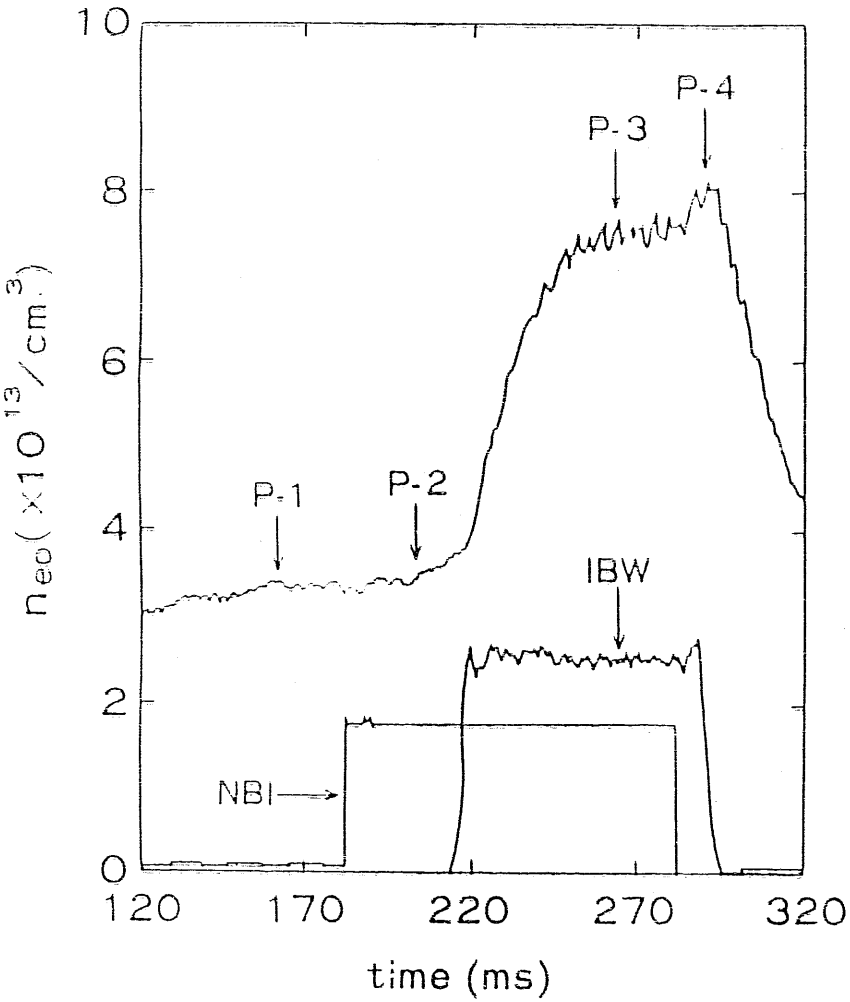
10
8
6
4
2
0
n_{eo} ($\times 10^{13}$/cm^3)
P-1
P-2
P-3
P-4
IBW
NBI
120
170
220
270
320
time (ms)

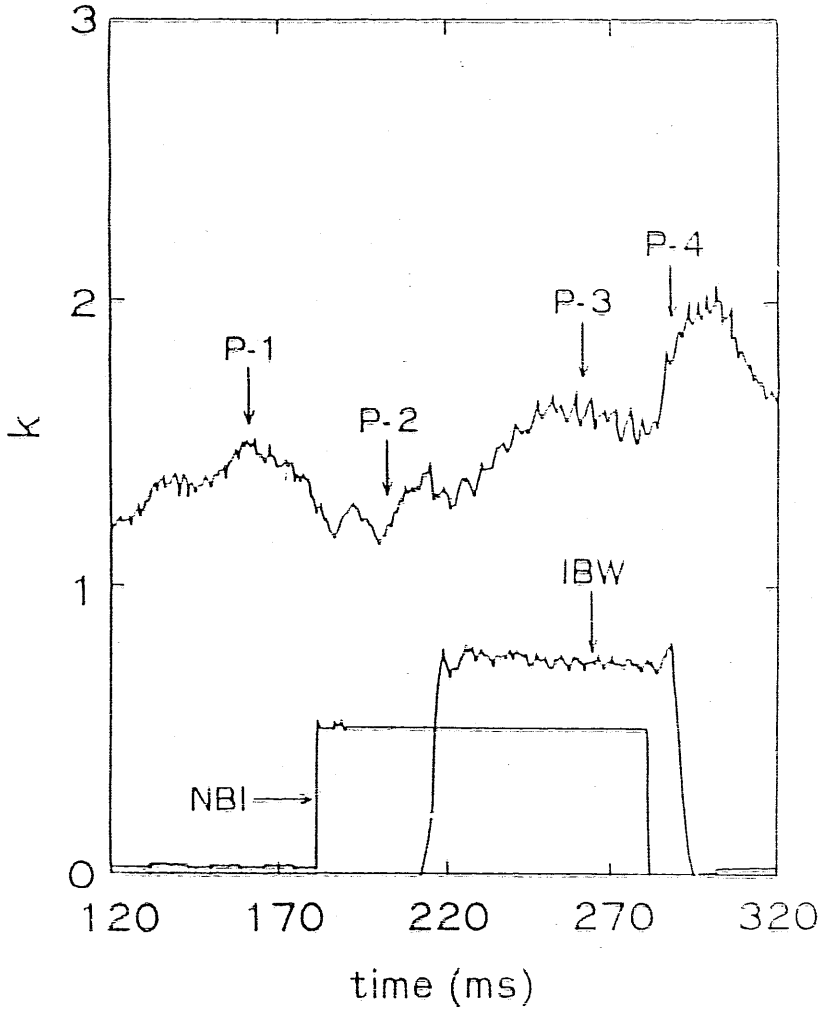
3
2
1
0
κ
P-1
P-2
P-3
P-4
IBW
NBI
120
170
220
270
320
time (ms)

Fig. 40

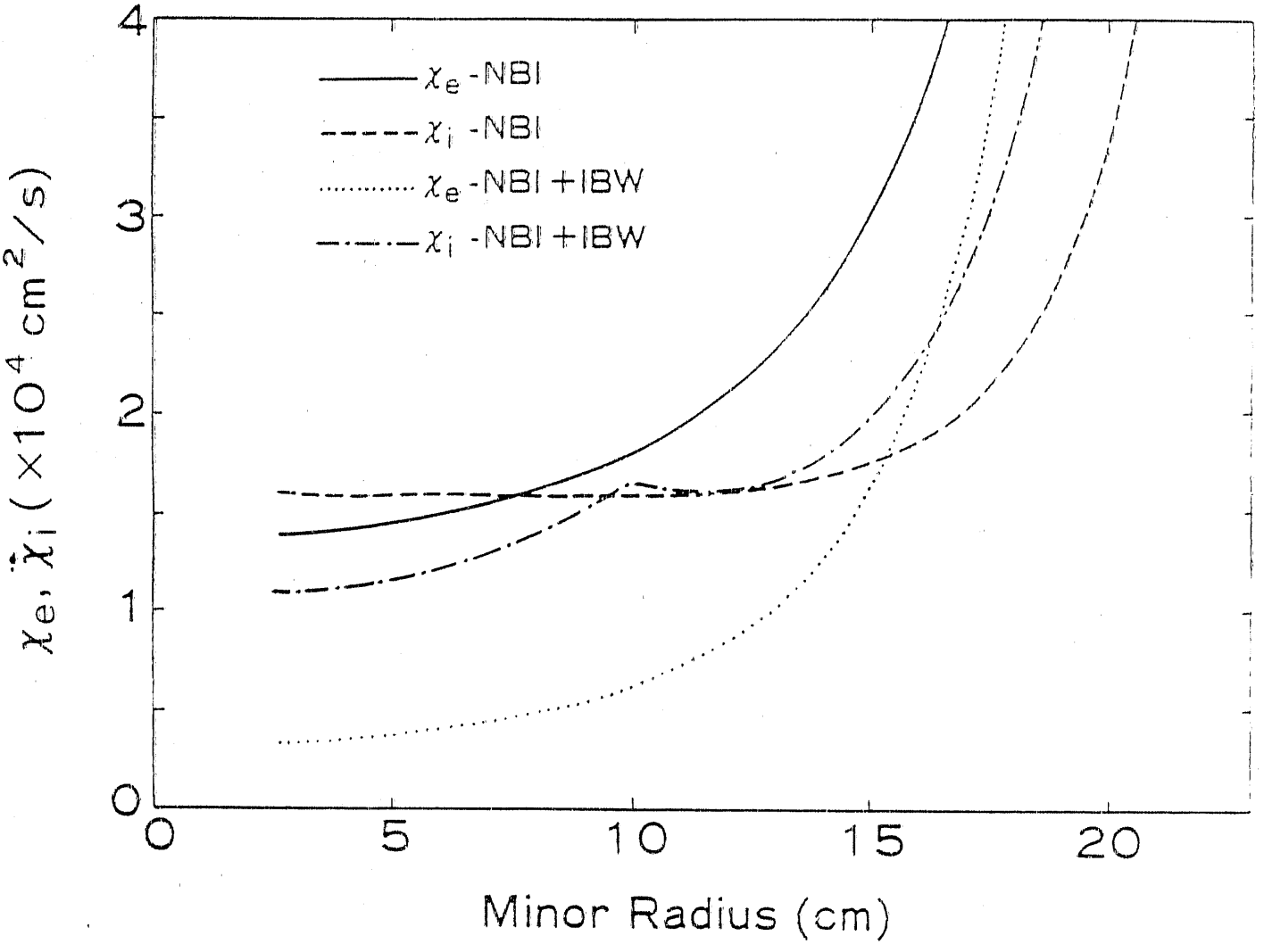
χ_e -NBI
χ_i -NBI
χ_e -NBI +IBW
χ_i -NBI +IBW
χ_e, χ_i ($\times 10^4$ cm^2/s)
0
1
2
3
4
0
5
10
15
20
Minor Radius (cm)

Fig. 41

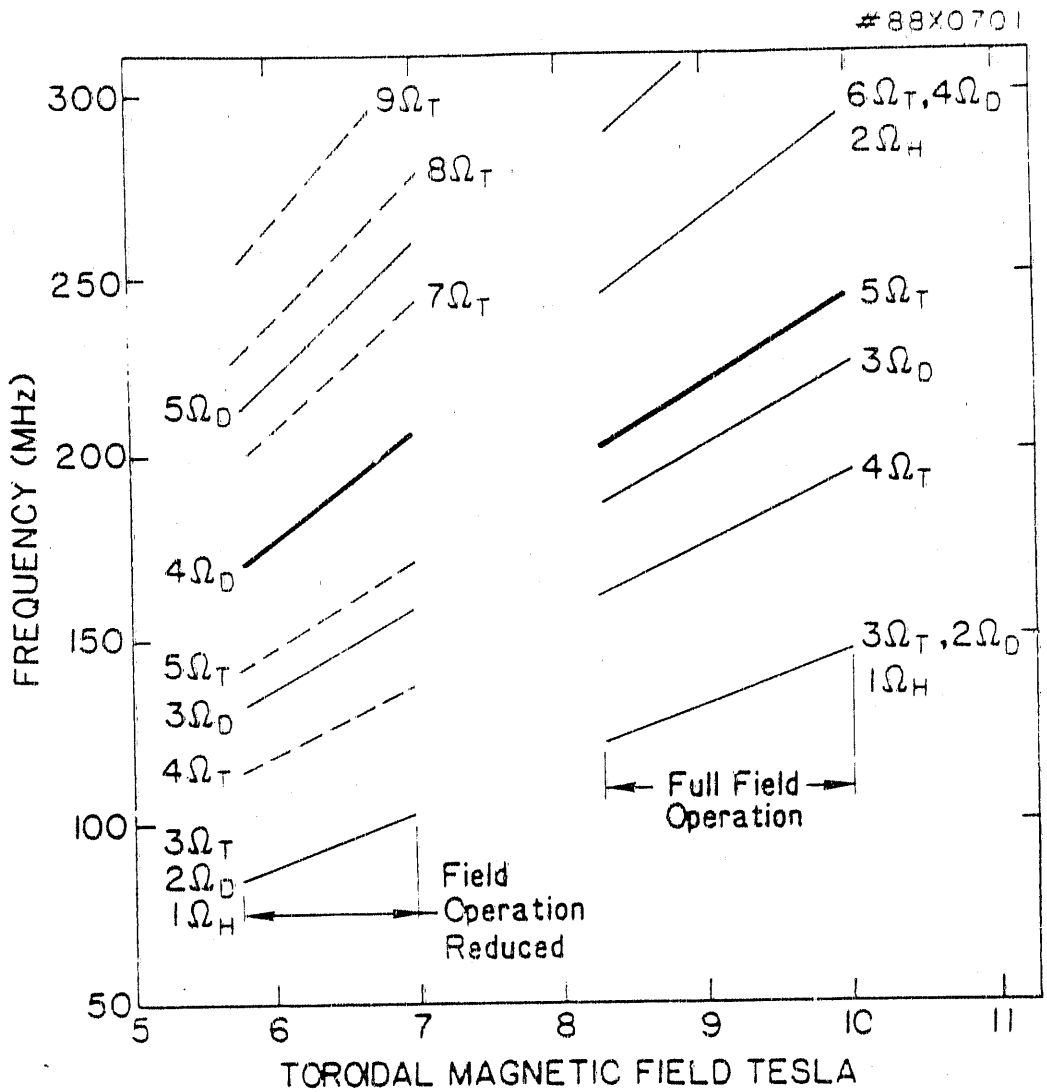
#88X0701
300
250
200
150
100
50
FREQUENCY (MHz)
9Ω_T
8Ω_T
7Ω_T
5Ω_D
4Ω_D
5Ω_T
3Ω_D
4Ω_T
3Ω_T
2Ω_D
1Ω_H
Field Operation Reduced
6Ω_T,4Ω_D
2Ω_H
5Ω_T
3Ω_D
4Ω_T
3Ω_T,2Ω_D
1Ω_H
Full Field Operation
5
6
7
8
9
10
11
TOROIDAL MAGNETIC FIELD TESLA

Fig. 42

EXTERNAL DISTRIBUTION IN ADDITION TO UC-420

Dr. F. Paoloni, Univ. of Wollongong, AUSTRALIA
Prof. M.H. Brennan, Univ. of Sydney, AUSTRALIA
Plasma Research Lab., Australian Nat. Univ., AUSTRALIA
Prof. I.R. Jones, Flinders Univ, AUSTRALIA
Prof. F. Cap, Inst. for Theoretical Physics, AUSTRIA
Prof. M. Heindler, Institut für Theoretische Physik, AUSTRIA
Prof. M. Goossens, Astronomisch Instituut, BELGIUM
Ecole Royale Militaire, Lab. de Phy. Plasmas, BELGIUM
Commission-European, DG. XII-Fusion Prog., BELGIUM
Prof. R. Boucique, Rijksuniversiteit Gent, BELGIUM
Dr. P.H. Sakanaka, Instituto Fisica, BRAZIL
Instituto Nacional De Pesquisas Espaciais-INPE, BRAZIL
Documents Office, Atomic Energy of Canada Ltd., CANADA
Dr. M.P. Bachynski, MPB Technologies, Inc., CANADA
Dr. H.M. Skarsgard, Univ. of Saskatchewan, CANADA
Prof. J. Teichmann, Univ. of Montreal, CANADA
Prof. S.R. Sreenivasan, Univ. of Calgary, CANADA
Prof. T.W. Johnston, INRS-Energie, CANADA
Dr. R. Bolton, Centre canadien de fusion magnétique, CANADA
Dr. C.R. James,, Univ. of Alberta, CANADA
Dr. P. Lukác, Komenského Universzita, CZECHO-SLOVAKIA
The Librarian, Culham Laboratory, ENGLAND
Library, R61, Rutherford Appleton Laboratory, ENGLAND
Mrs. S.A. Hutchinson, JET Library, ENGLAND
Dr. S.C. Sharma, Univ. of South Pacific, FIJI ISLANDS
P. Mähönen, Univ. of Helsinki, FINLAND
Prof. M.N. Bussac, Ecole Polytechnique,, FRANCE
C. Mouttet, Lab. de Physique des Milieux Ionisés, FRANCE
J. Radet, CEN/CADARACHE - Bat 506, FRANCE
Prof. E. Economou, Univ. of Crete, GREECE
Ms. C. Rinni, Univ. of Ioannina, GREECE
Dr. T. Mual, Academy Bibliographic Ser., HONG KONG
Preprint Library, Hungarian Academy of Sci., HUNGARY
Dr. B. DasGupta, Saha Inst. of Nuclear Physics, INDIA
Dr. P. Kaw, Inst. for Plasma Research, INDIA
Dr. P. Rosenau, Israel Inst. of Technology, ISRAEL
Librarian, International Center for Theo Physics, ITALY
Miss C. De Palo, Associazione EURATOM-ENEA , ITALY
Dr. G. Grosso, Istituto di Fisica del Plasma, ITALY
Prof. G. Rostangni, Istituto Gas Ionizzati Del Cnr, ITALY
Dr. H. Yamato, Toshiba Res & Devel Center, JAPAN
Prof. I. Kawakami, Hiroshima Univ., JAPAN
Prof. K. Nishikawa, Hiroshima Univ., JAPAN
Director, Japan Atomic Energy Research Inst., JAPAN
Prof. S. Itoh, Kyushu Univ., JAPAN
Research Info. Ctr., National Instit. for Fusion Science, JAPAN
Prof. S. Tanaka, Kyoto Univ., JAPAN
Library, Kyoto Univ., JAPAN
Prof. N. Inoue, Univ. of Tokyo, JAPAN
Secretary, Plasma Section, Electrotechnical Lab., JAPAN
S. Mori, Technical Advisor, JAERI, JAPAN
Dr. O. Mitarai, Kumamoto Inst. of Technology, JAPAN
J. Hyeon-Sook, Korea Atomic Energy Research Inst., KOREA
D.I. Choi, The Korea Adv. Inst. of Sci. & Tech , KOREA
Prof. B.S. Liley, Univ. of Waikato, NEW ZEALAND
Inst of Physics, Chinese Acad Sci PEOPLE'S REP. OF CHINA
Library, Inst. of Plasma Physics, PEOPLE'S REP. OF CHINA
Tsinghua Univ. Library, PEOPLE'S REPUBLIC OF CHINA
Z. Li, S.W. Inst Physics, PEOPLE'S REPUBLIC OF CHINA
Prof. J.A.C. Cabral, Instituto Superior Tecnico, PORTUGAL
Dr. O. Petrus, AL I CUZA Univ., ROMANIA
Dr. J. de Villiers, Fusion Studies, AEC, S. AFRICA
Prof. M.A. Hellberg, Univ. of Natal, S. AFRICA
Prof. D.E. Kim, Pohang Inst. of Sci. & Tech., SO. KOREA
Prof. C.I.E.M.A.T, Fusion Division Library, SPAIN
Dr. L. Stenflo, Univ. of UMEA, SWEDEN
Library, Royal Inst. of Technology, SWEDEN
Prof. H. Wilhelmson, Chalmers Univ. of Tech., SWEDEN
Centre Phys. Des Plasmas, Ecole Polytech, SWITZERLAND
Bibliotheek, Inst. Voor Plasma-Fysica, THE NETHERLANDS
Asst. Prof. Dr. S. Cakir, Middle East Tech. Univ., TURKEY
Dr. V.A. Glukhikh,Sci. Res. Inst. Electrophys.l Apparatus, USSR
Dr. D.D. Ryutov, Siberian Branch of Academy of Sci , USSR
Dr. G.A. Eliseev, I.V. Kurchatov Inst., USSR
Librarian, The Ukr.SSR Academy of Sciences, USSR
Dr. L.M. Kovrizhnykh, Inst. of General Physics, USSR
Kernforschungsanlage GmbH, Zentralbibliothek, W. GERMANY
Bibliothek, Inst. Für Plasmaforschung, W. GERMANY
Prof. K. Schindler, Ruhr-Universität Bochum, W. GERMANY
Dr. F. Wagner, (ASDEX), Max-Planck-Institut, W. GERMANY
Librarian, Max-Planck-Institut, W. GERMANY
Prof. R.K. Janev, Inst. of Physics, YUGOSLAVIA

END

DATE FILMED

4/30/92